Relay Feedback of Simple Systems

Holmberg, Ulf

1991

Document Version:
Publisher's PDF, also known as Version of record

Ulf Holmberg Relay Feedback of Simple Systems

Relay Feedback of Simple Systems

Ulf Holmberg

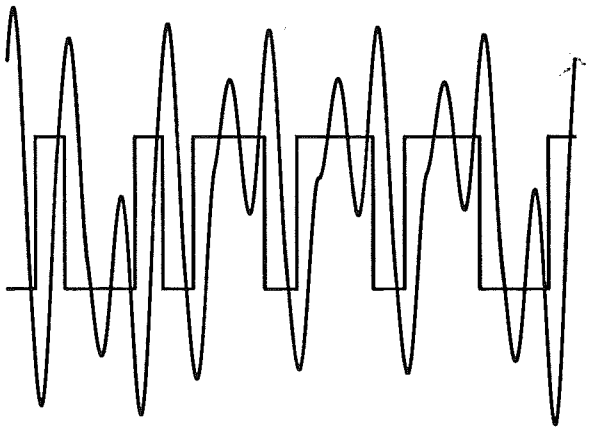

Department of Automatic Control, Lund Institute of Technology

CODEN: LUTFD2/(TFRT-1034)/1–150/(1991)

Digitalt exemplar

Relay Feedback of Simple Systems

av

Ulf Holmberg
Tekn. lic., Civ. ing.

Kristianstads Nation

Akademisk avhandling som för avläggande av teknisk doktorsexamen vid Tekniska fakulteten vid Universitetet i Lund kommer att offentligen försvaras i sal M:A, Maskinteknikhuset, Lunds Tekniska Högskola, fredagen den 4 oktober 1991, kl 10.15.

Relay Feedback of Simple Systems

Ulf Holmberg

Lund 1991

Department of Automatic Control
Lund Institute of Technology
Box 118
S-221 00 LUND
Sweden

Published 1991
Printed in Sweden
Studentlitteratur

Department of Automatic Control
Lund Institute of Technology
P.O. Box 118
S-221 00 Lund Sweden

Document name
DOCTORAL DISSERTATION

Date of issue
August 1991

Document Number
CODEN: LUTFD2/(TFRT-1034)/1-150/(1991)

Author(s)
Ulf Holmberg

Supervisor
Karl Johan Åström

Sponsoring organisation
STU Contract 86 – 3552 and 88 – 2110

Title and subtitle
Relay Feedback of Simple Systems

Abstract

In the fifties there was much work on relay systems because relays were commonly used as power amplifiers. Lately, there has been a renewed interest in systems with relay feedback. One of the reasons is the use of relay feedback for automatic tuning of PID controllers. Another reason is the renewed interest in the theory of dynamic systems and chaotic behaviour. However, systems with relay feedback may have very complex behaviour that is not fully understood. The goal of this thesis is to contribute to the understanding of such systems. This is done by a detailed analysis of first and second order systems with time delays. The main contribution is a thorough investigation of first order systems with time delays and a direct term. The direct term and the time delay makes this problem far from trivial. Different types of limit cycles are observed and classified. Their convergence regions are also specified and it is shown that the limit cycle can be reached already after one switch. The analysis of second order systems with relay feedback is not complete but aim to give an understanding of the convergence mechanisms. It is shown that the convergence is very fast for systems with real eigenvalues that are widely spread. These results explain the fast convergence of the relay auto-tuners that have been observed in practice. It is also shown how relay feedback can be used as excitation for parameter estimation. This idea is applied to the problem of determining dynamics of a biological reactor. The estimator has been simulated and tested in a full scale experiment at Malmö Sewage Works.

Key words
Relay feedback, Automatic tuning, Limit cycles, Chaos, Dissolved oxygen, Estimation, Oxygen transfer rate, Respiration rate, Activated sludge

Classification system and/or index terms (if any)

Supplementary bibliographical information

ISSN and key title

ISBN

Language
English

Number of pages
150

Recipient's notes

Security classification

(3)

Contents

Preface

This thesis is actually about two different subjects. The major part is about, as the title say, relay feedback of simple systems. Then there is one chapter in the end about identification of the dissolved oxygen concentration dynamics in a biological reactor. However, there is a relay feedback also involved in that context used in an unconventional way. The waste water research has been published at different conferences: Holmberg-Olsson (1985), Holmberg (1986), Holmberg *et al* (1988) and Holmberg (1990). From my very start at the Department the intention was to do research about control of waste water treatment plants. The above papers documents this. This research also led to a technical licentiate degree, Holmberg (1987). The intention was then to fill up with results in the same area to a PhD thesis. However, by accident I got the idea about the relay with phase adaptive hysteresis. A lot of people showed their interest, especially Prof. Karl Johan Åström who had formulated the problem some weeks before. I was asked to document the invention. However, in order to understand how a relay with variable hysteresis works I started to investigate usual relays with fix hysteresis. Suddenly, I found myself deep into another area of research—relay feedback systems. As time passed, the analysis of relay feedback systems took larger and larger part of the thesis. The waste water research now takes a smaller part. But since waste water was the topic of my last thesis, I don't have bad feeling about the new outline of the thesis.

Acknowledgements

First of all, I would like to thank my supervisor Professor Karl Johan Åström who encouraged me to fulfill my work about relay feedback systems. His enthusiasm and support was invaluable. I also would like to thank all my colleagues at the Department. I am particular grateful to Professor Gustaf Olsson who got me interested in the control of waste water treatment plants. He has continuously being a source of encouragement even after he left the Department. I am indebted to Professor Björn Wittenmark, Dr. Tore Hägglund and Dr. Mats Lilja who had many valuable comments on the manuscript. Dr. Per Hagander had a great influence on the presentation of Chapter 4. For this I am most greatful. Leif Andersson has written the TEXmacros which were used in the type-setting of the thesis. The experiments at Malmö Sewage Works would not have been possible without the support by Bengt Andersson and Claes Hansson. The research about waste water was partly supported by the National Swedish Board of Technical Development (STU contract 86 – 3552 and 88 – 2110).

1

Introduction

It don't mean a thing
if it ain't got that swing
—Duke Ellington

When a dynamical system is at equilibrium, measurements of its input and output can reveal only the static gain. To get information about its dynamical properties it is essential to excite the system with a nonstatic input. In this thesis, the excitation is introduced automatically by a relay feedback resulting in an oscillation.

Relay feedback is a classical configuration with many applications. The classical work by Tsypkin (1984) was motivated by relays that were used as power amplifiers. Examples given in Graham-McRuer (1961) are relay servos and modeling of Coulumb friction. Relay feedback has also been involved in different automatic control strategies, see Åström-Wittenmark (1989). The self-oscillating adaptive system (SOAS) uses a relay feedback to keep the gain high in the feedback loop. The response of the closed-loop system will be relatively insensitive to the variations in process dynamics because of the high loop gain. The idea originated in work at Honeywell on adaptive flight control in the late 1950s. The SOAS has also been applied in process control but has not found widespread use. The auto-tuner, on the other hand, has been more successful in process control applications where relay feedback is used to tune PID controllers, see Åström-Hägglund (1984a and b). The method is a modification of the Ziegler-Nichols closed-loop method, see Ziegler-Nichols (1942). The modification is the introduction of the relay feedback. All adaptive schemes require *a priori* information about the process dynamics. It is particularly important to know the time scales, which are

critical for determining suitable sampling intervals and filtering. The relay method is ideally suited as a pre-tuner for a more sophisticated adaptive controller. Thus, in parallel with the development of adaptive controllers and the auto-tuner there has been a renewed interest in the behaviour of relay feedback systems. In all the above applications the behaviour of the relay feedback is typically investigated by use of describing function analysis. Since this is an approximate method it is interesting to make a more careful analysis.

A brief introduction to classical describing function analysis is given in Chapter 2. In this context, the Tsypkin's necessary conditions for limit cycle oscillations are also given for comparison and interpretation. In Chapter 3 the relay hysteresis is allowed to vary adaptively. Describing function analysis is used here to show that the relay with adaptive hysteresis acts as a nonlinearity with a specific phase shift. One application can be a pre-tuner where the Nyquist curve is scanned in phase rather than in frequency as is the case in usual frequency analysis experiments. In the following chapters the describing function analysis is not used. In Chapter 4, relay feedback of first order systems with time delay is investigated. The first order system is allowed to be unstable. It also has a direct term and can therefore be thought of as being an approximation of a second order system with one fast and one slow mode. Necessary and sufficient conditions for convergence to and existence of limit cycles are given. Because of the direct term and the time delay, the system can have different types of limit cycles. These are investigated and classified. Some results for second order systems without a time delay are given in Chapter 5. Then in Chapter 6, feedback of an unstable second order system with time delay is investigated. It is demonstrated that such systems may have very complex behaviour with multi switch limit cycles and chaos. (One period of a 12-switch limit cycle is shown on the front page). It was shown by Cook (1985) that such systems can exhibit chaotic motions also without a time delay if a positive feedback is used. The limit cycle solutions were also shown to be unstable. The difference here when a time delay is introduced is that chaos can arise also with negative feedback. Another difference is that some limit cycle solutions appear to be stable. A nonconventional application of relay feedback is given in Chapter 7. The problem is to identify the dissolved oxygen concentration dynamics in a biological reactor. A relay feedback is used to excite the system to give identifiability. The relay amplitude is automatically adjusted to give a certain oscillation amplitude of the dissolved oxygen concentration. This gives a compromise between control and estimation. The idea is investigated by simulations and shown to work in a full scale experiment at Malmö Sewage Works in the south of Sweden. Chapter 8 contains some final conclusions.

2

Introduction to relay feedback systems

The interest for the relay feedback system as shown in Figure 2.1 has increased during the last years. One reason is the appearance of the so called *Autotuner* introduced by Åström-Hägglund (1984a). The autotuning idea is to use the information revealed by *self-excitation* during relay feedback to tune a PID controller. PID controllers are the most common used controllers in the process industry. They are very often poorly tuned. It is therefore easy to understand how appealing the autotuning idea is to a process engineer. However, the collection of information during the relay feedback experiment is based on describing function analysis — an approximate method. The information gathered can therefore be more or less accurate and sometimes inaccurate depending on the validity of the describing function analysis. This chapter will give a basic introduction to describing function analysis of relay feedback systems, its use and misuse.

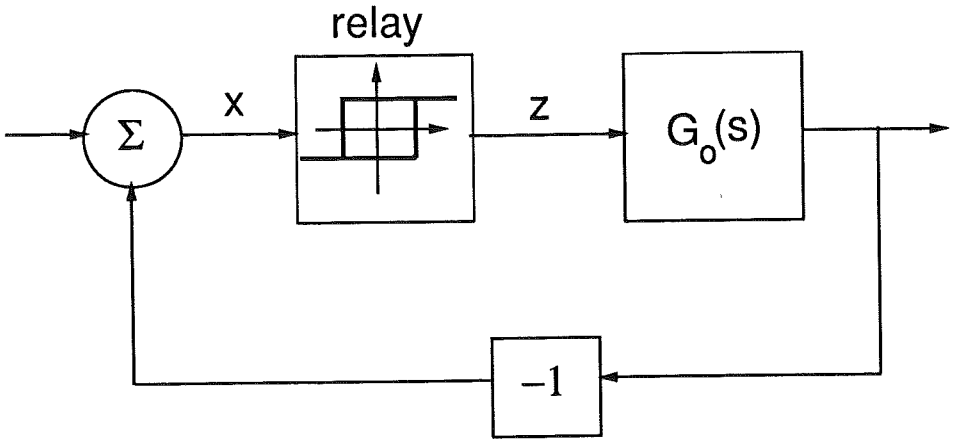

Figure 2.1 A relay feedback system.

2.1 Describing function analysis

The use of describing function analysis to investigate the relay feedback system in Figure 2.1 has been treated by many authors, see e.g. Atherton (1975), Tsypkin (1984). A brief introduction will be given here.

When analyzing a nonlinear system like that in Figure 2.1 the principle of superposition is not applicable. It is therefore important to specify the relay input. Since the purpose is to investigate conditions for self oscillation a sinusoidal relay input is *chosen*, such as

$$x(t) = A\sin(\omega t)$$

The relay output, $z(t)$ in Figure 2.1, can be partitioned into two parts, one sinusoidal signal which amplitude and phase is depending on the relay input amplitude, plus one error signal, i.e.

$$z(t) = A \cdot K(A)\sin(\omega t + \Phi(A)) + e(t)$$

We want to determine $K(A)$, an equivalent gain dependent on the relay input amplitude A, and $\Phi(A)$, an equivalent phase shift also dependent on A. The appropriate choice should be done such that $e(t)$ is made small in some sense. We *choose* the least squares sense, i.e. minimize

$$I = \int_0^T e^2(t)dt \qquad \text{where} \qquad T = 2\pi/\omega$$

It then follows from the construction of a Fourier series expansion of the T-periodic $z(t)$ that $K(A)$ and $\Phi(A)$ can be expressed in the Fourier coefficients associated with the first harmonics, i.e.

$$\begin{cases} K(A) = c_1/A = \sqrt{a_1^2 + b_1^2}/A \\ \Phi(A) = \Phi_1 = \arctan(a_1/b_1) \end{cases}$$

where the Fourier series of $z(t)$ is defined as

$$\begin{aligned} z_{\mathcal{F}}(t) &= \frac{a_0}{2} + \sum_{n=1}^{\infty}(a_n \cos(n\omega t) + b_n \sin(n\omega t)) = \\ &= \frac{a_0}{2} + \sum_{n=1}^{\infty} c_n \sin(n\omega t + \Phi_n) \end{aligned}$$

where

$$\begin{cases} a_n = \dfrac{2}{T}\displaystyle\int_0^T z(t)\cos(n\omega t)dt & n = 0, 1, \ldots \\ b_n = \dfrac{2}{T}\displaystyle\int_0^T z(t)\sin(n\omega t)dt & n = 1, 2, \ldots \end{cases}$$

$$\begin{cases} \Phi_n = \arctan(a_n/b_n) \\ c_n = \sqrt{a_n^2 + b_n^2} \end{cases}$$

DEFINITION 2.1—The describing function
The describing function $Y_N(A)$ of the nonlinear relay system in Figure 2.1 is defined as

$$Y_N(A) \stackrel{\text{def}}{=} c_1 e^{i\Phi_1}/A = (b_1 + ia_1)/A$$

where a_1, b_1, (c_1 and Φ_1) are the coefficients in the Fourier series expansion of $z(t)$ when the input is $x(t) = A\sin(\omega t)$ □

The describing function can be interpreted as an amplitude dependent transfer function from a sinusoidal input to the first harmonic of the periodic output. It specifies the change in amplitude and phase of the first harmonic of the output with respect to the sinusoidal input. The equivalent amplification, $K(A)$, and phase, $\Phi(A)$, are represented as a complex function, $Y_N(A) = K(A)e^{i\Phi(A)}$.

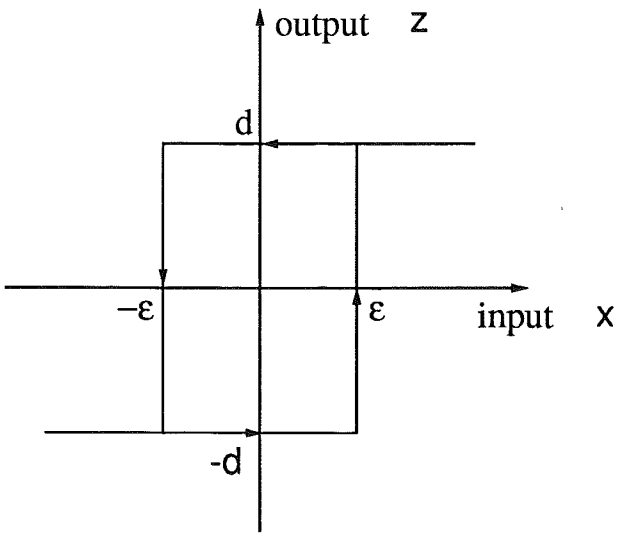

Figure 2.2 Characteristics for a relay with hysteresis.

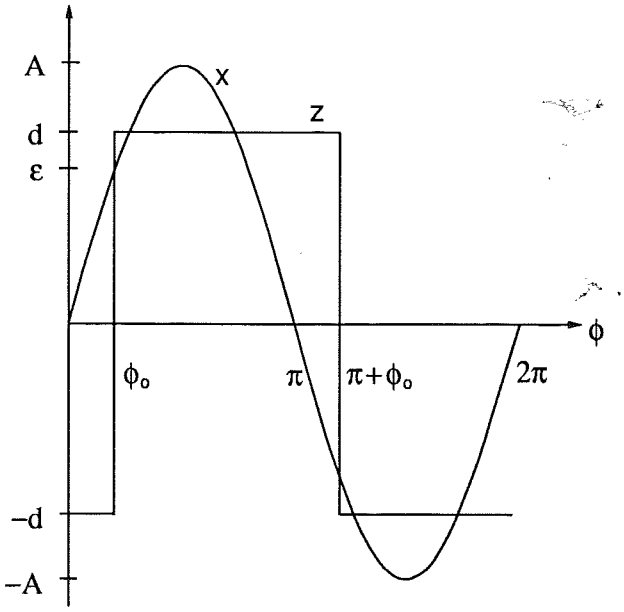

Figure 2.3 Relay input, x, and output, z.

DEFINITION 2.2—Relay characteristics

The characteristics of a relay with hysteresis ε and gain d is defined in Figure 2.2. □

The sinusoidal relay input $x(t) = A\sin(\omega t) = A\sin(\Phi)$ gives the relay output, z, shown in Figure 2.3. According to the figure the relay output becomes

$$z(\Phi) = \begin{cases} -d & 0 < \Phi < \Phi_0 \\ d & \Phi_0 < \Phi < \pi + \Phi_0 \\ -d & \pi + \Phi_0 < \Phi < 2\pi \end{cases}$$

where $\Phi_0 = \arcsin(\varepsilon/A)$. Then the Fourier coefficients are

$$\begin{aligned} a_1 &= \frac{1}{\pi}\int_0^{2\pi} z(\Phi)\cos(\Phi)d\Phi = \frac{1}{\pi}\int_0^{\Phi_0}(-d)\cos(\Phi)d\Phi + \\ &+ \frac{1}{\pi}\int_{\Phi_0}^{\pi+\Phi_0} d\cos(\Phi)d\Phi + \frac{1}{\pi}\int_{\pi+\Phi_0}^{2\pi}(-d)\cos(\Phi)d\Phi = -\frac{4d}{\pi}\sin(\Phi_0) \\ b_1 &= \frac{1}{\pi}\int_0^{2\pi} z(\Phi)\sin(\Phi)d\Phi = \ldots = \frac{4d}{\pi}\cos(\Phi_0) \end{aligned}$$

Thus the describing function for a relay with hysteresis is

$$Y_N(A) = \frac{4d}{\pi A}(\cos(\Phi_0) - i\sin(\Phi_0)) = \frac{4d}{\pi A}e^{-i\Phi_0} \qquad (A > \varepsilon)$$

Negative hysteresis There is a problem with the definition of a relay having a negative hysteresis. The problem arises when the relay input doesn't pass outside the hysteresis before it changes direction. In such a case we may never pass the hysteresis. Thus, the behaviour of a relay with negative hysteresis is highly dependent on the relay input behaviour. This doesn't need to be a severe problem for our purposes, though. As long as we check that the relay is working as we expect. The behaviour is illustrated in Figure 2.4 where the relay switches at time $t = t_1$ and $t = t_2$.

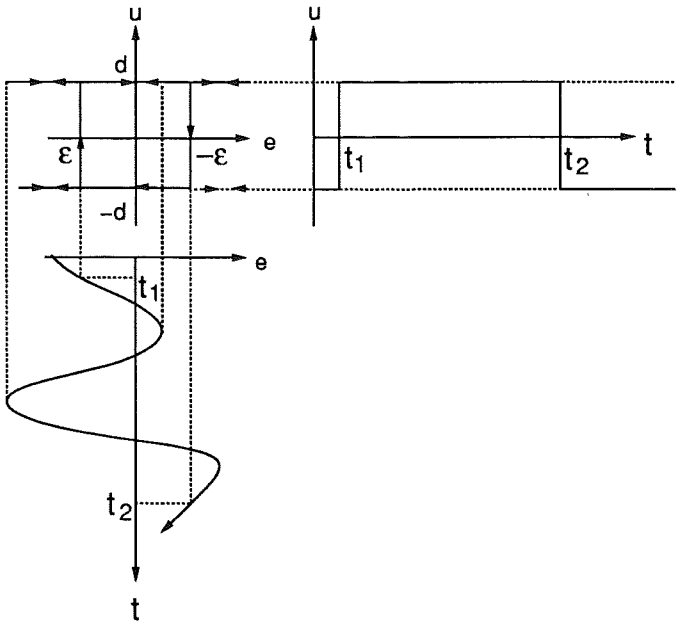

Figure 2.4 There are problems with the definition of negative hysteresis. The relay input must have been outside the hysteresis before a switch can occur. In this example the relay switches at $t = t_1$ and at $t = t_2$.

Nyquist criterion analogy

Consider the feedback system in Figure 2.5 with the constant gain K of the P-regulator.

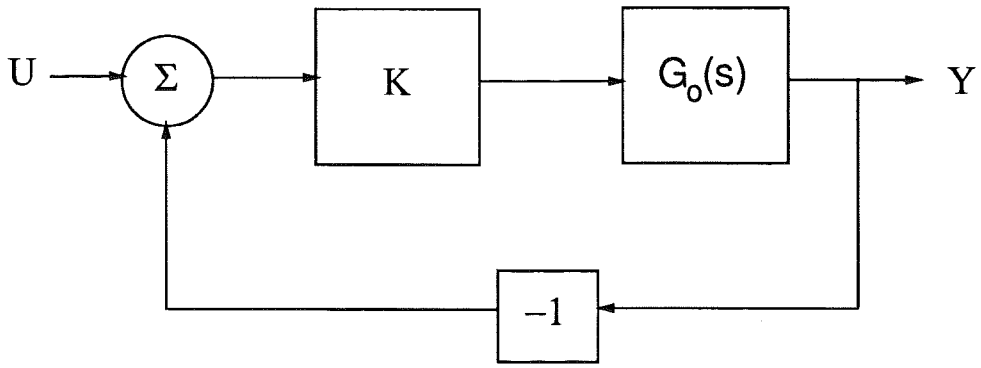

Figure 2.5 Block diagram for a simple feedback system.

The closed loop system transfer function is

$$\frac{Y}{U} = \frac{KG_0}{1 + KG_0} = \frac{G_0}{1/K + G_0}$$

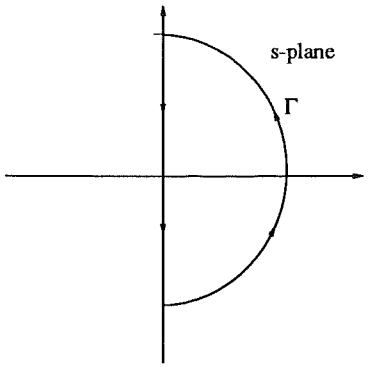

Figure 2.6 Contour Γ used in the formulation of the Nyquist criterion.

and the characteristic equation is

$$G_0(s) + 1/K = 0$$

Assume that $G_0(s)$ has no poles in the area encircled by Γ in the Figure 2.6, i.e. in the right half plane. It follows from Nyquist's theorem that the characteristic equation has all roots in the left half plane (outside Γ) if the map of Γ in the G_0-plane does not encircle the point $-1/K$,

The relay feedback system: Describing function analysis assumes there is a limit cycle in the feedback system. Also, $G_0(s)$ is assumed to be low pass such that all harmonics of high frequencies can be neglected. The relay input can then be approximated by $x(t) = A\sin(\omega t)$. Under these assumptions the relay acts as a variable gain, $Y_N(A)$, depending only on the relay input sinusoidal amplitude. An approximate equivalent feedback system is shown in Figure 2.7.

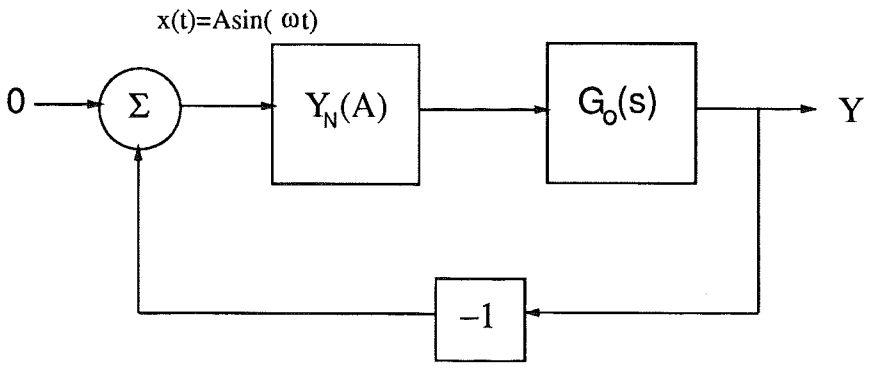

Figure 2.7 Approximate relay feedback system near the limit cycle. The relay acts as a variable gain.

The approximate characteristic equation is

$$G_0(s) + 1/Y_N(A) = 0$$

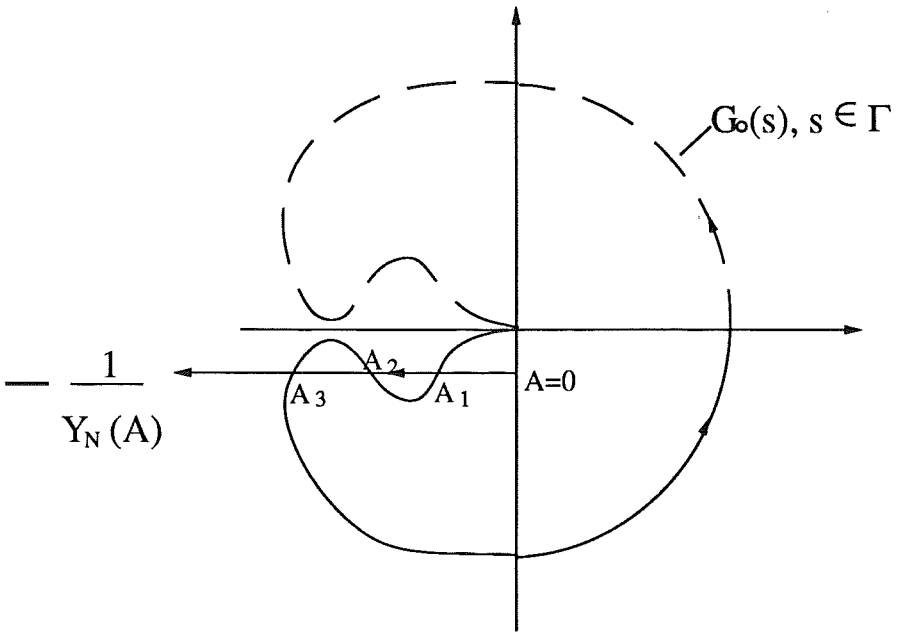

Figure 2.8 Illustration of how describing function analysis expects 3 limit cycle solutions. By Nyquist criterion analogy the solutions $A = A_1$ and $A = A_3$ are stable while $A = A_2$ is unstable.

In analogy with the Nyquist criterion the system can be expected to be stable if the map of Γ in the G_0-plane does not encircle $-1/Y_N(A)$. However, since there is a limit cycle by assumption the system is at the stability limit and $G_0(s) = -1/Y_N(A)$, $s \in \Gamma$. The Nyquist criterion is here used to investigate the stability of a limit cycle. If there is an encirclement when the amplitude A is reduced the instability of the system will increase the amplitude again toward the limit cycle solution. In Figure 2.8 describing function analysis expects 3 limit cycle solutions at the 3 intersections where $G_0(s) = -1/Y_N(A)$, $s \in \Gamma$. By Nyquist criterion analogy the solutions, $A = A_1$ and $A = A_3$ are stable while $A = A_2$ is unstable.

For a relay with hysteresis the curve $-1/Y_N(A)$ is a straight line with a constant imaginary part. Since $\Phi_0 = \arcsin \varepsilon/A = \arccos \sqrt{1-(\varepsilon/A)^2}$ we get

$$-\frac{1}{Y_N(A)} = -\frac{\pi A}{4d} e^{i\Phi_0} = -\frac{\pi A}{4d}(\cos\Phi_0 + i\sin\Phi_0)$$
$$= -\frac{\pi}{4d}(\sqrt{A^2-\varepsilon^2} + i\varepsilon)$$

Notice that if $d > 0$ the line $-1/Y_N(A)$ is in the left half plane while it is in the right half plane if $d < 0$. Thus with proper choices of relay gain, d, and hysteresis, ε, the line $-1/Y_N(A)$ can be positioned in either of the four quadrants, as shown in Figure 2.9.

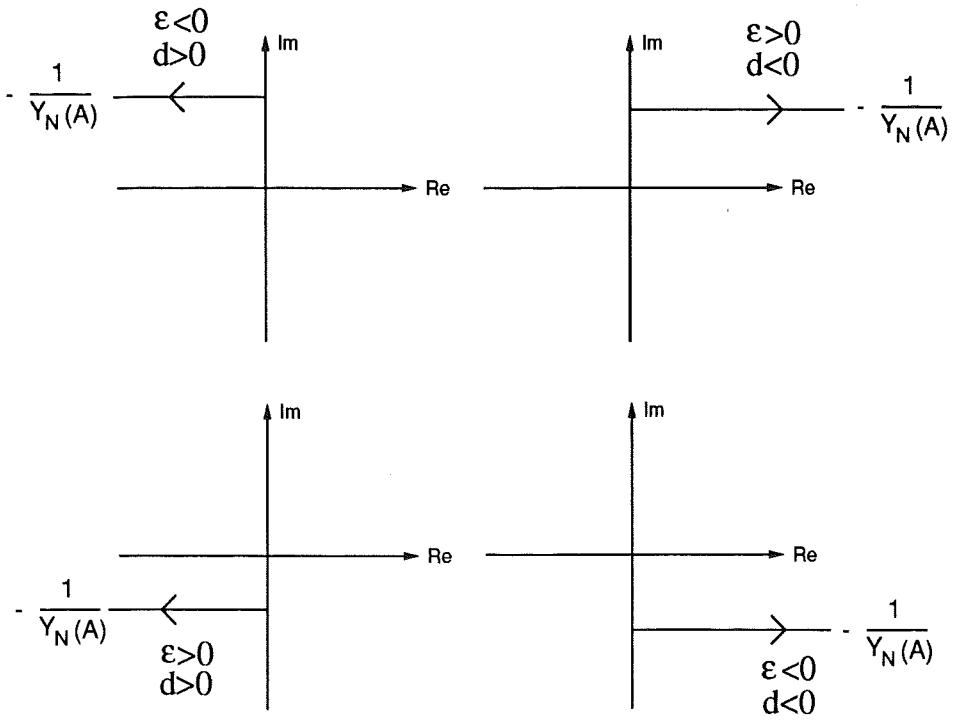

Figure 2.9 Position of the line $-1/Y_N(A)$ depending of the sign choices of the relay gain, d, and hysteresis, ε.

2.2 Use and misuse of describing function analysis

The describing function is an approximation introduced to simplify analysis of nonlinear feedback system. It is therefore important to be aware of the limitations of this approximation. The approximate method assumes the system output to be sinusoidal. Distortion, $\mathcal{D}$, is a common measure of how well a function is approximated by a sinusoid. A formal definition will be given later. According to Atherton (1975), $\mathcal{D}$ can be used to justify the use of describing function analysis, DF, by the following rule of thumb:

> *DF results for values of $\mathcal{D}$ much greater than* 0.1 *are probably unreliable whilst for values of $\mathcal{D}$ less than* 0.1 *they should be adequate for engineering purposes with errors probably no greater than* 10 *per cent.*

We are interesting in two DF results: Estimation of the transfer function at the limit cycle frequency, $\widehat{G}_0(i\omega)$, and prediction of the limit cycle period, $\widehat{T}$. Examples will show that $\mathcal{D}$ is not always a reliable measure of the DF accuracy, i.e. it may happen that the accuracy is bad when $\mathcal{D} < 10\%$ and vice versa, opposed to Atherton's rule of thumb. It is interesting to notice that the chosen examples are low pass systems. They might therefore be expected to be well suited for describing function analysis. However, the question is if they are *low pass enough*. The distortion, $\mathcal{D}$, defined in the following,

is a crude measure. It is wise to remember that. The rule of thumb is a suggestion, not a justification of describing function analysis.

Describing function estimates

The DF estimate $\widehat{G}_0(i\omega)$ is calculated from measurements of the limit cycle amplitude A and period T, as

$$\widehat{G}_0(i\omega) = -\frac{1}{Y_N(A)} \quad ; \quad \omega = 2\pi/T$$

The DF predicted limit cycle period $\widehat{T}$ is calculated from the presumed known system, i.e. by solving the equation

$$\mathrm{Im}\{G_0(i\widehat{\omega})\} = \mathrm{Im}\{-\frac{1}{Y_N}\} = -\frac{\pi\epsilon}{4d} \qquad \Rightarrow \widehat{T} = 2\pi/\widehat{\omega}$$

In the following, DF estimates of $G_0(s)$ and limit cycle period T will be given together with the distortion. The purpose is to show the importance of checking the validity of DF before conclusions about $G_0(s)$ and T are drawn. Also, to get some feeling for the accuracy of the results.

In order to investigate the influence from higher harmonics we express the signals in Fourier series. During the limit cycle, which is assumed to be symmetric, the relay output is the square wave

$$u(t) = \sum_{k=0}^{\infty} a_{2k+1} \sin[(2k+1)\omega t] \quad ; \quad a_k = \frac{4d}{\pi k}$$

and the system output is

$$y(t) = \sum_{k=0}^{\infty} b_{2k+1} \sin[(2k+1)\omega t + \varphi_{2k+1}] \quad ; \quad \begin{cases} b_k = a_k|G_0(ik\omega)| \\ \varphi_k = \arg[G_0(ik\omega)] \end{cases}$$

DEFINITION 2.3—Distortion
If the first harmonic of y is denoted, $\tilde{y}_1$, the distortion, $\mathcal{D}$, is defined as

$$\mathcal{D} = \frac{\sqrt{\frac{1}{T}\int_0^T [y(t) - \tilde{y}_1(t)]^2 dt}}{\sqrt{\frac{1}{T}\int_0^T \tilde{y}_1^2(t) dt}} \quad ; \quad T = \frac{2\pi}{\omega}$$

i.e. the r.m.s. (root mean square) value of the higher harmonics divided by the r.m.s. of the first harmonic. □

The first order system $G_0(s) = 1/(1+s)$ has distortion $\mathcal{D}(\omega) > 10\%$ for all ω. Thus, following Atherton's rule of thumb, the DF method should be unappropriate. Notice that distortion remains the same for fixed ω if a time delay is introduced in the system. But DF results such as the predicted limit cycle period, $\widehat{T}$, and the estimated transfer function, $\widehat{G}_0(s)$, depend on time delays. It is therefore interesting to see how the accuracy of the DF results change with the time delay.

EXAMPLE 2.1—First order system with time delay
DF results for the system family $G_0(s) = e^{-\tau s}/(s+1)$ for different τ values will be given. First we choose the hysteresis $\varepsilon = 0$. For a given τ we can then calculate the DF estimates $\widehat{G}_0(i\omega)$ and $\widehat{T}$. Their respective relative errors are shown in Figure 2.10 together with $\mathcal{D}$, all as a function of the time delay τ.

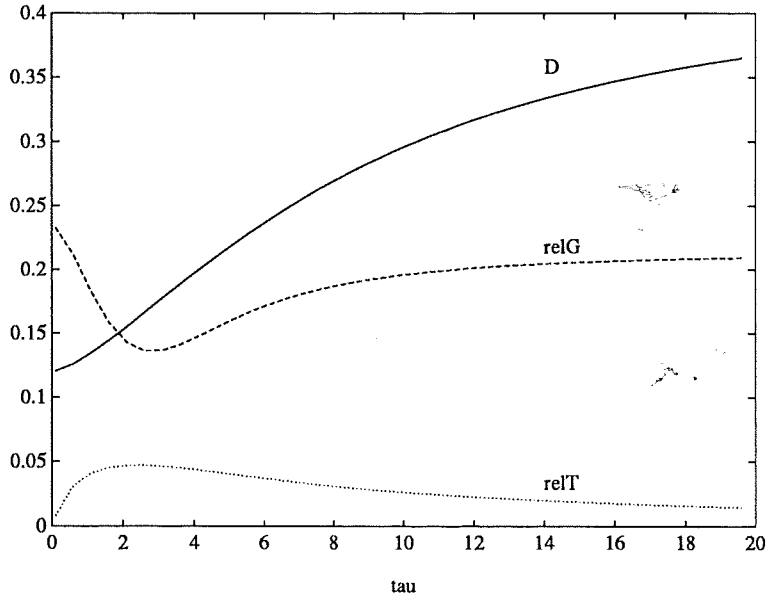

Figure 2.10 The distortion, $\mathcal{D}$ (solid curve), and the relative errors $|\frac{\widehat{G}_0 - G_0}{G_0}|$ (dashed curve) and $\frac{\widehat{T}-T}{T}$ (dotted curve) as a function of the time delay τ for the system family $G_0(s) = \frac{1}{s+1}e^{-s\tau}$ and relay parameters $d = 1$ and $\varepsilon = 0$.

The example shows that even though $\mathcal{D}$ is too large ($> 10\%$) DF results are occasionally surprisingly accurate. The relative period error is smaller than 5%. The largest errors occur when the relative transfer function error is 13%, at about $\tau = 2.5$. It is evidently possible to get quite accurate DF estimates even if $\mathcal{D} > 10\%$. However, this fact doesn't justify a noncritic use of the DF method when $\mathcal{D} > 10\%$. The distortion is a rather crude measure that simply doesn't tell the whole story about the DF results accuracy. It is even so, for an opposite situation when $\mathcal{D} < 10\%$, the DF results errors can

be substantial, opposed to Atherton's rule of thumb. This will be shown in a later example. But first we will show DF estimates $\widehat{G}_0$ for three cases. One corresponding to $\tau = 0.3$; another with $\tau = 2.5$, which according to Figure 2.10 will give quite accurate $\widehat{G}_0(i\omega)$ when $\varepsilon = 0$; and yet another with $\tau = 4$.

First order systems with a time delay will be thoroughly investigated in Chapter 4. Now we will just show the use of the DF method and its accuracy for the systems, $G_0(s) = e^{-\tau s}/(s+1)$, $\tau = 0.3, 2.5, 4$. It can be shown, (see chapter 4), that for these examples there can be limit cycles for hysteresis values ε such that

$$-\frac{1-e^{-\tau}}{1+e^{-\tau}} < \varepsilon < 1 \tag{2.1}$$

when $d = 1$ and τ is the time delay. The corresponding limit cycle period T will be

$$T = 2\ln\left(\frac{2-(1-\varepsilon)e^{-\tau}}{1-\varepsilon}\right) + 2\tau$$

The corresponding true $G_0(i2\pi/T)$ can therefore be calculated for comparison. The resulting amplitude will be $A = \varepsilon e^{-\tau} + G_0(0)d(1-e^{-\tau})$. The DF estimated transfer function can therefore be calculated directly from $\widehat{G}_0(i2\pi/T) = -1/Y_N(A)$. The DF estimated $\widehat{G}_0(i\omega)$ and the true $G_0(i\omega)$ are shown in Figure 2.11 for the time delay $\tau = 0.3$.

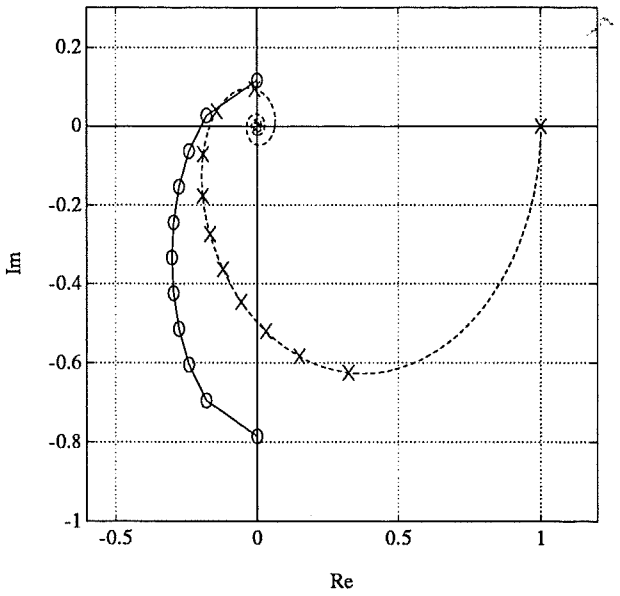

Figure 2.11 Consider the system $G_0(s) = e^{-0.3s}/(s+1)$. Eleven equidistant values of ε in the interval given by (2.1) are chosen to generate the DF estimate $\widehat{G}_0(i\omega)$. The resulting points are marked with 'o' on the solid curve. The corresponding true $G_0(i\omega)$ are marked with 'x' on the dashed curve.

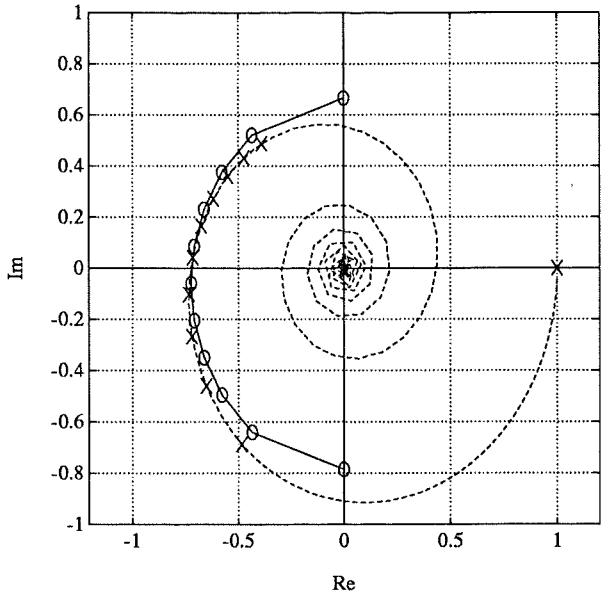

Figure 2.12 Consider the system $G_0(s) = e^{-2.5s}/(s+1)$. Eleven equidistant values of ε in the interval given by (2.1) are chosen to generate the DF estimate $\widehat{G}_0(i\omega)$. The resulting points are marked with 'o' on the solid curve. The corresponding true $G_0(i\omega)$ are marked with 'x' on the dashed curve.

The DF estimated $\widehat{G}_0(i\omega)$ and the true $G_0(i\omega)$ are shown in Figure 2.12 for the time delay $\tau = 2.5$. Note the good accuracy for ε near 0. That is in agreement with Figure 2.10. The DF estimated $\widehat{G}_0(i\omega)$ and the true $G_0(i\omega)$ are shown in Figure 2.13 for the time delay $\tau = 4$. It is interesting to see that in this case the amplitude margin is overestimated. If a controller were constructed by use of the DF estimated Nyquist curve the resulting closed loop system might be unstable due to this critical model error. □

EXAMPLE 2.2—Third order system

Consider the system $G_0(s) = 1/(s+1)^3$ in a relay feedback loop. DF estimated points on the Nyquist curve is shown in Figure 2.14 as 'o' on a solid line while the true Nyquist curve is dashed and corresponding points are marked with 'x'. (Also, there are spectral analysis estimates marked with triangles. See the following section about spectral analysis). The relative transfer function error $|(\widehat{G} - G)/G|$ is presented together with the distortion $\mathcal{D}$ in Figure 2.15. Note that $|(\widehat{G} - G)/G|$ is as large as 50% even though $\mathcal{D} \approx 10\%$, violating Atherton's rule of thumb. Above the break frequency $\omega_b = 1$, however, the relative error is less than 10%. □

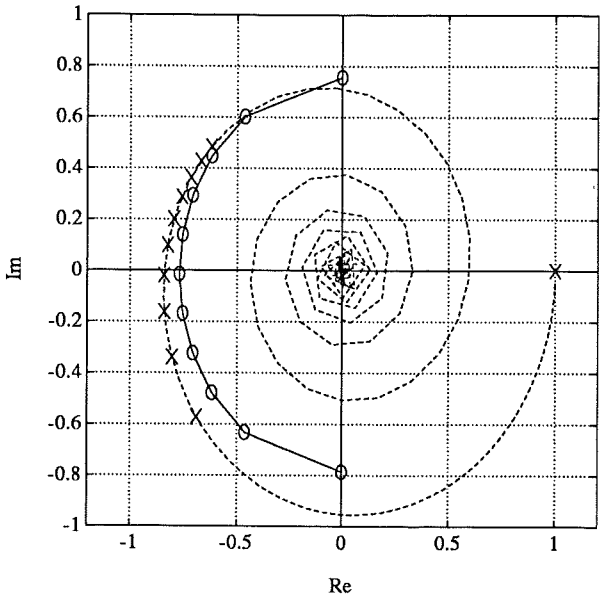

Figure 2.13 Consider the system $G_0(s) = e^{-4s}/(s+1)$. Eleven equidistant values of ε in the interval given by (2.1) are chosen to generate the DF estimate $\widehat{G}_0(i\omega)$. The resulting points are marked with 'o' on the solid curve. The corresponding true $G_0(i\omega)$ are marked with 'x' on the dashed curve. Note that the amplitude margin is overestimated by the DF method!

EXAMPLE 2.3—Filtering to improve distortion $\mathcal{D}$ at low frequencies
In the above example the accuracy of the DF estimate $\widehat{G}_0(i\omega)$ was more dependent on whether ω was larger than the break frequency or not, than it was dependent on whether $\mathcal{D}$ was less than 10% or not. The example showed that it is not enough to require the system to be low pass to get accurate DF estimate. It should be low pass at the frequency ω, i.e. ω should not be far below the break frequency of the system. To be able to identify points on the Nyquist curve, $G_0(i\omega)$, below the break frequency, a relay experiment can instead be performed on a compensated system, $G_f G_0$, where G_f is a known low pass filter that is changing its break frequency. Use e.g. the filter

$$G_f(s) = \frac{b^2}{(s+b)^2}$$

and adjust the parameter b to the limit cycle frequency ω. Since the limit cycle frequency ω is unknown when the experiment starts, an initial large value of b is chosen. Then ω is measured, b updated to ω, a new ω is found, b updated again, and so on. From the DF estimated filtered system $G_f G_0$ the system $G_0(i\omega)$ is extracted since $G_f(i\omega)$ is known. The result is shown in Figure 2.16, where the Nyquist curve is passing through the fourth quadrant. Compare with previous figures how the DF estimation of $G_0(s) = 1/(s+1)^3$ has improved at low frequencies! □

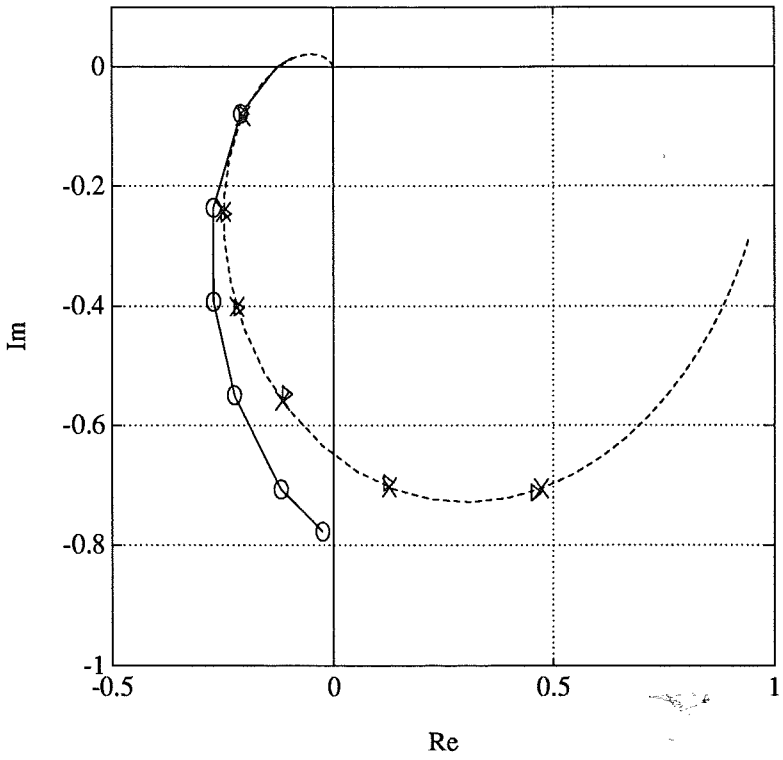

Figure 2.14 The DF estimated $\widehat{G}_0(i\omega)$ marked with 'o' on the solid curve. The true $G_0(i\omega) = 1/(i\omega + 1)^3$ marked with 'x' on the dashed curve. Also, there are spectral analysis estimates marked with triangles.

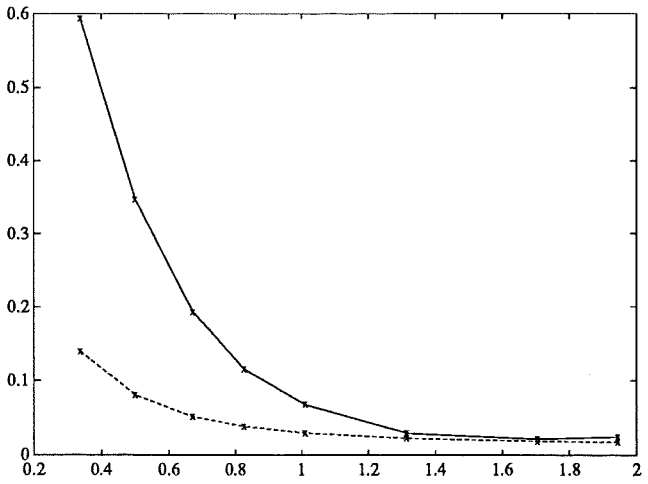

Figure 2.15 The relative transfer function error $|(\widehat{G}_0(i\omega) - G_0(i\omega))/G_0(i\omega)|$ (solid curve) and the distortion $\mathcal{D}(\omega)$ (dashed curve) for the third order system $G_0(s) = 1/(s + 1)^3$. Note that the relative error is about 50% when $\mathcal{D} \approx 10\%$.

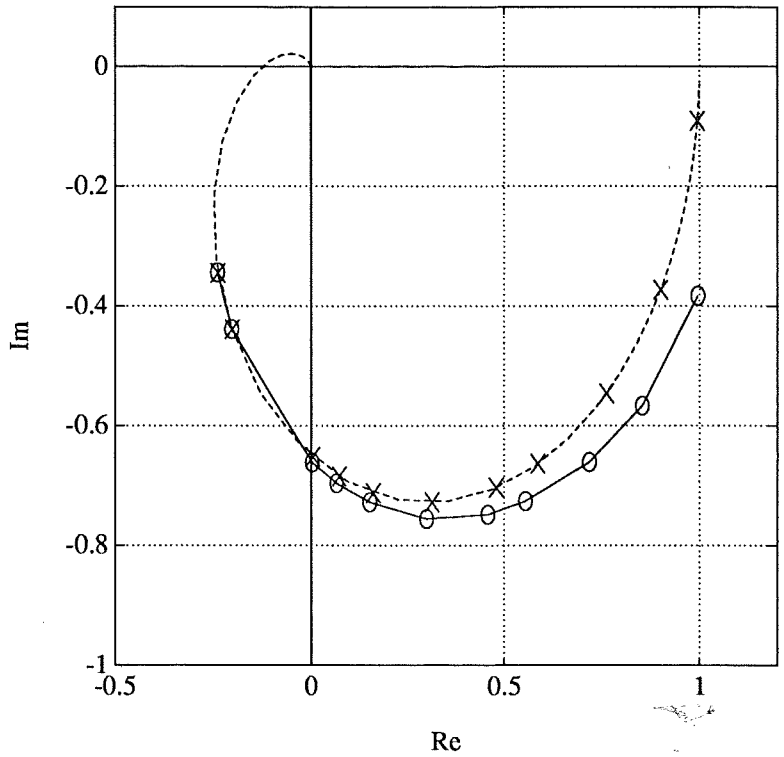

Figure 2.16 When $\mathcal{D} > 10\%$ below a break frequency ω_b the DF estimated $\widehat{G}_0$ is inaccurate. By use of an adaptive low pass filter $G_f(s) = b^2/(s+b)^2$, the $\mathcal{D}$ can be reduced to improve $\widehat{G}_0$ (solid curve) at lower frequencies. The true system is $G_0(s) = 1/(s+1)^3$ (dashed curve).

The examples above have illustrated the importance of the low pass condition. The last example showed how the accuracy of the DF estimates can be improved by making a system more low pass by use of a prefilter. However, the procedure was quite awkward and was meant as an illustration rather than a recommendation. Actually, there is no reason why only information from the first harmonic should be used, as is the case with the DF method. Instead, all information from the relay excitation can be used in a spectral analysis, see Figure 2.14. Then the low pass condition is not needed anymore.

Spectral analysis

The error introduced by the DF method is caused by the approximation of the relay output square wave as a sinusoid of the first harmonic. The only reason to make this approximation is to be able to use the DF method which is simple and gives insight. By proper choices of the relay gain and hysteresis we can then scan the interesting parts of the Nyquist diagram without need

of knowing the interesting frequency scale. However, when the introduced error is large (large $\mathcal{D}$) it is *misuse* to use the DF method. Instead we can use the square wave relay output and the nonsinusoidal output from G_0 to provide a *spectral analysis* estimate of $G_0(i\omega)$. In Figure 2.14 the spectral analysis estimate of $G_0(i\omega)$ is marked with triangles. The accuracy is seen by comparing with the true $G_0(i\omega)$ marked with 'x' on the dashed curve. The `Matlab` identification toolbox function **spa** (SPectral Analysis) has been used. This is using standard signal processing techniques to produce the estimate of $G_0(i\omega)$, see Ljung (1987) or Ljung (1988).

EXAMPLE 2.4—Another misuse of the DF method
The DF method is typically inaccurate to use below the break frequency of low pass systems as indicated earlier. Very often the systematic error is conservative in the sense that the stability margins are underestimated, however, not always, as has been demonstrated. It is illustrative to show how bad the DF results are when used on a system with poorly damped zeroes, i.e. a system where $\mathcal{D} \gg 10\%$. The Nyquist curve of the system $G_0(s) = (s^2+0.2s+1)/(0.1s+1)^3$ is shown in Figure 2.17. The DF estimated Nyquist curve is marked with 'o' on the solid curve and corresponding frequency points for the true system are marked with 'x' on the dashed curve. The spectral analysis estimates are marked with triangles.

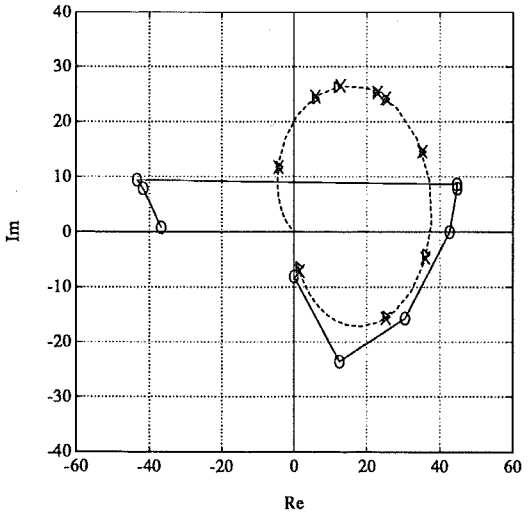

Figure 2.17 The DF estimated Nyquist curve for the system $G_0(s) = (s^2 + 0.2s + 1)/(0.1s + 1)^3$ is marked with 'o' on the solid curve and corresponding frequency points for the true system are marked with 'x' on the dashed curve. The spectral analysis estimates are marked with triangles.

2.3 Limit cycle periods

It has been shown that the DF method can predict limit cycle periods. The DF predicted period $\widehat{T}$ corresponds to the intersection of the presumed known Nyquist curve $G_0(i\widehat{\omega})$, $\widehat{\omega} = 2\pi/\widehat{T}$ with the line $-1/Y_N(A)$. Due to approximation errors of the DF method the estimate $\widehat{T}$ will deviate from the true limit cycle period T. Exact results about T are given here.

THEOREM 2.1—Necessary condition for symmetrical limit cycles
Assume that the relay feedback system defined in Figure 2.1 has a symmetrical limit cycle solution with the period T. Let $H_1(z,h)$ and $\widehat{H}_1(z,h)$ be the zero order hold sampled systems corresponding to $G_1(s)$ and $sG_1(s)$ respectively, where $G_0(s) = G_1(s) + G_0(\infty)$ and the sampling period is $h = T/2$. Then it follows

$$(i) \qquad [\widehat{H}_1(-1,h) - 2\lim_{s\to\infty} sG_1(s)] \cdot d < 0$$

$$(ii) \qquad H_1(-1,h) - G_0(\infty) = -\frac{\varepsilon}{d}$$

Proof: This is a reformulation of Tsypkin's conditions, see Årzén (1987). ∎

The condition (i) means that the derivative of the output should be such that the hysteresis is passed in right direction at the switch occasion. The condition (ii) means simply that the output is $-\varepsilon$ when the relay is switching from $-d$ to d. Since the theorem only considers conditions for the sampled system and is not taking into account the behaviour of the output between samples, there are sometimes solutions to (i) and (ii) that are not corresponding to limit cycle solutions. Extensions of the theorem to overcome this were made in Årzén, but only for finite dimensional systems. We will here, however, just consider the above theorem and make comparisons with the describing function analysis. The theorem gives the *existence* of symmetrical limit cycle solutions and the exact period time T for such a solution (or solutions). The following example will illustrate the correspondence between the exact solutions, T, given by the theorem and the approximate solutions, $\widehat{T}$, given by the DF method.

EXAMPLE 2.5—Limit cycle solutions where $h < \tau$
Consider the system $G_0(s) = e^{-s}/(s^2 + s + 1)$ in a relay feedback loop with relay gain, d, and hysteresis, ε. The choice $\varepsilon/d = 0.005$ gives 5 symmetrical solutions, h, to Theorem 2.1, see Figure 2.18. The solutions, that are numbered from 1 to 5 in growing frequency order, are also shown in the Nyquist diagram in Figure 2.19 and a magnified curve in Figure 2.20. The exact limit cycle frequencies from Figure 2.18 are marked with 'x' on the Nyquist

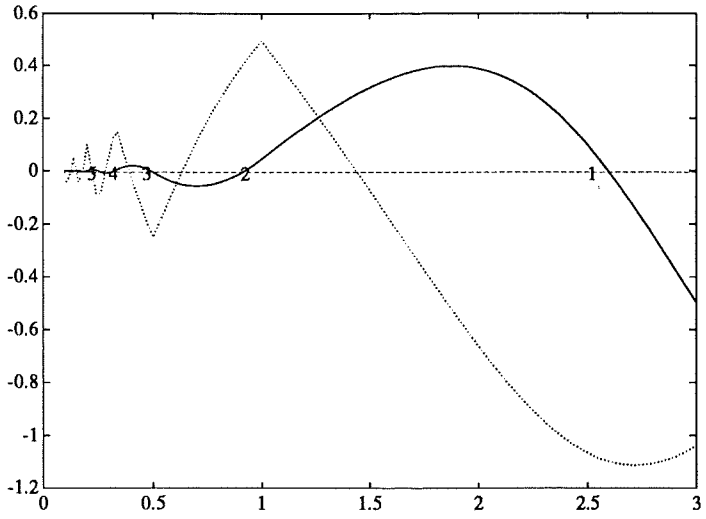

Figure 2.18 The function $H_1(-1,h)$ (solid curve) and $-\varepsilon/d = -0.005$ (dashed line) and $\widehat{H}_1(-1,h)$ (dotted curve) as functions of $h = T/2$ (half limit cycle period). The system is $G_0(s) = e^{-s}/(s^2+s+1)$. According to Theorem 2.1, the condition (ii) gives 5 solutions at the intersections of the solid and the dashed curve. These solutions are marked in growing frequency order. Condition (i) gives the sign of the relay gain d, i.e. when the dotted curve is positive the relay gain should be negative and vise versa. Therefore the solutions (1), (3) and (5) correspond to $d > 0$ while (2) and (4) correspond to $d < 0$.

curve. For the choice $d = 1$ and $\varepsilon = 0.005$ the line $-1/Y_N(A)$ is emerging leftwards in the third quadrant (dashed curve) passing through the solutions (5),(3),(1). For the choice $d = -1$ and $\varepsilon = -0.005$ the line $-1/Y_N(A)$ is emerging rightwards in the fourth quadrant (dash-dotted curve) passing through the solutions (4) and (2). Thus, the DF method automatically gives the signs of the relay gains. These are in well agreement with the results from Theorem 2.1, see Figure 2.18. Notice, that the DF method actually predicts yet another solution to the right of solution (2) in the fourth quadrant. This should correspond to a very low frequency. However, at such a low frequency the system is not low pass anymore and the DF method is not applicable. The solution does not exist and the DF method fails. This is a typical example showing that it is not enough to require G_0 to be low pass. It should be low pass at the limit cycle frequency! The true different relay feedback systems with $d, \varepsilon > 0$ and $d, \varepsilon < 0$ respectively are shown in block diagrams in Figure 2.21.

The solution (1) is predicted by the DF method to be locally stable. Also, it is the only solution that has the half period larger than the time delay, i.e. $h = 2.6 > \tau = 1$. The other cases, solutions number (2) to (5), correspond to $h < \tau$. This peculiar fact means that the cases (2) – (5) must

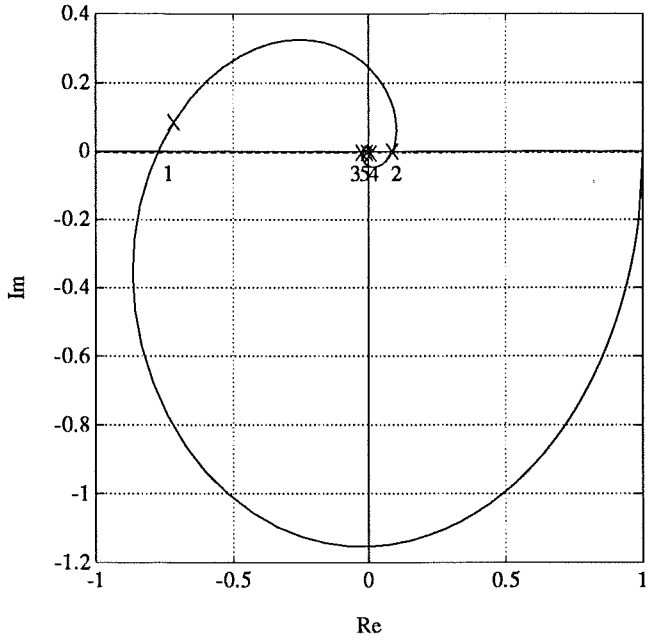

Figure 2.19 Nyquist curve for the system $G_0(s) = e^{-s}/(s^2 + s + 1)$ and the line $-1/Y_N(A)$ for $d = 1$, $\varepsilon = 0.005$ (dashed curve) and for $d = -1$, $\varepsilon = -0.005$ (dash-dotted curve). The theoretical exact limit cycle frequencies are marked with 'x' and numbered in growing order.

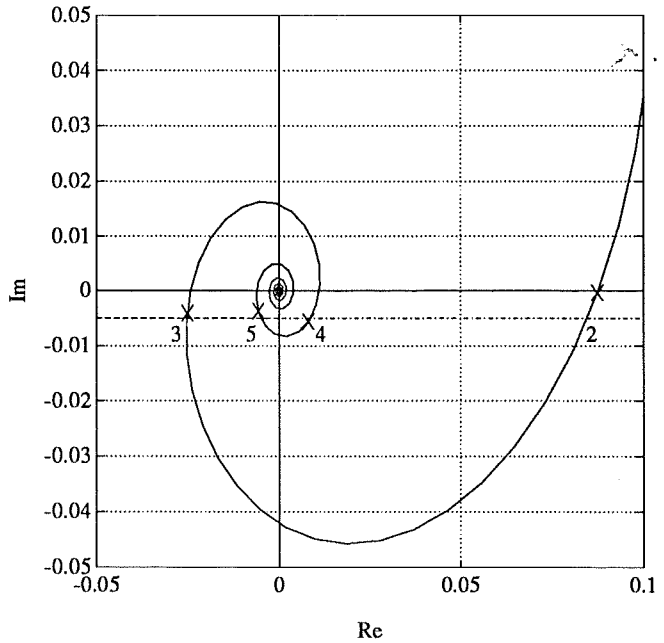

Figure 2.20 Magnified part of Figure 2.19. Compare the DF estimated frequencies, marked with 'x' and numbered in growing order.

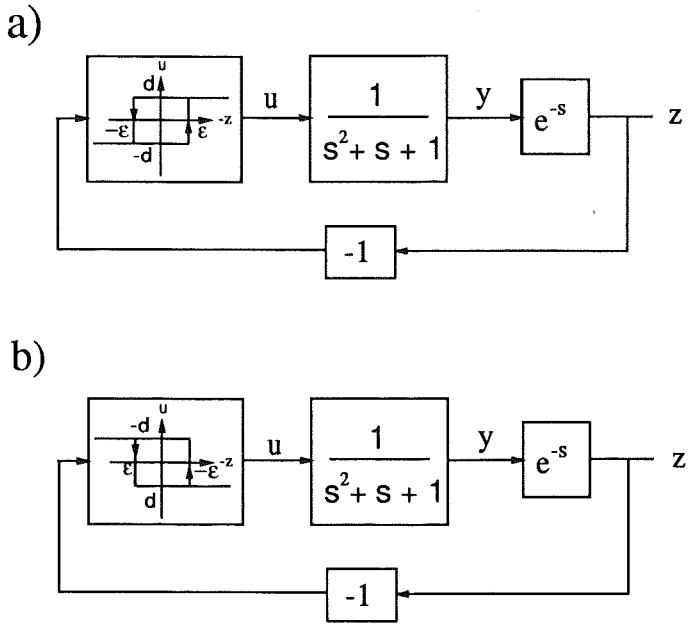

Figure 2.21 Block diagram of example 1.4 showing relay gain and hysteresis both being *a*) positive ($d, \varepsilon > 0$) and *b*) negative ($d, \varepsilon < 0$).

be initialized with a time history, $y(t)$, $t \in \{-\tau, 0\}$ that passes the hysteresis. The definition of y is shown in Figure 2.21. It is illustrated in Figure 2.22 how $y(t)$ is passing the negative hysteresis at $t = -\tau$ and $t = h - \tau$ in order to start up the infinite dimensional relay feedback system near the limit cycle solution number (2) ($d = -1$, $\varepsilon = -0.005$). Compare Figure 2.22 to Figure 2.21*b* to easier realize the behaviour of the negative d and ε.

The solution number (3) is easy to initialize. The reason is since $T = \tau$ the corresponding finite dimensional system without the time delay will have the same limit cycle solution. Therefore choose $d = 1$, $\varepsilon = 0.005$, and simulate the system from $t = -\tau$ to $t = 0$ without the time delay, such that $y(t)$ passes the hysteresis three times; at $t = -\tau = -2h$, $t = h - \tau = -h$ and at $t = 2h - \tau = 0$. Then introduce the time delay $\tau = 1$ and the solution number (3) is started up in the limit cycle, see Figure 2.23. Compare Figure 2.23 to Figure 2.21a to confirm the behaviour for positive d and ε. □

EXAMPLE 2.6—Solutions that are not limit cycles

Not all solutions given by Theorem 2.1 correspond to relay feedback solutions. The relay should switch the first time the hysteresis is passed correctly. This condition is not covered by the conditions (*i*) and (*ii*) in Theorem 2.1. To clarify the situation the Figure 2.18 is replotted for larger h in Figure 2.24. Here, $-\varepsilon/d = -1$ (dashed curve) indicates a lot of possible solutions, h. However, only two of them correspond to relay feedback solutions. To realize

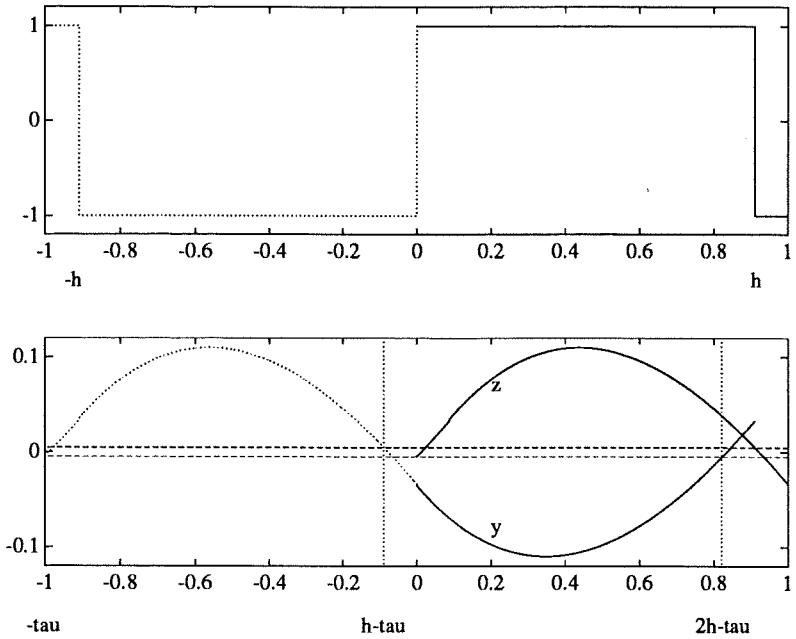

Figure 2.22 Start up of the limit cycle solution number (2) having $h = (T/2) = 0.91$. The solution corresponds to negative relay gain, $d = -1$, and negative relay hysteresis, $\varepsilon = -0.005$. Above is the relay output u and below are y and z shown. These are defined in Figure 2.21b.

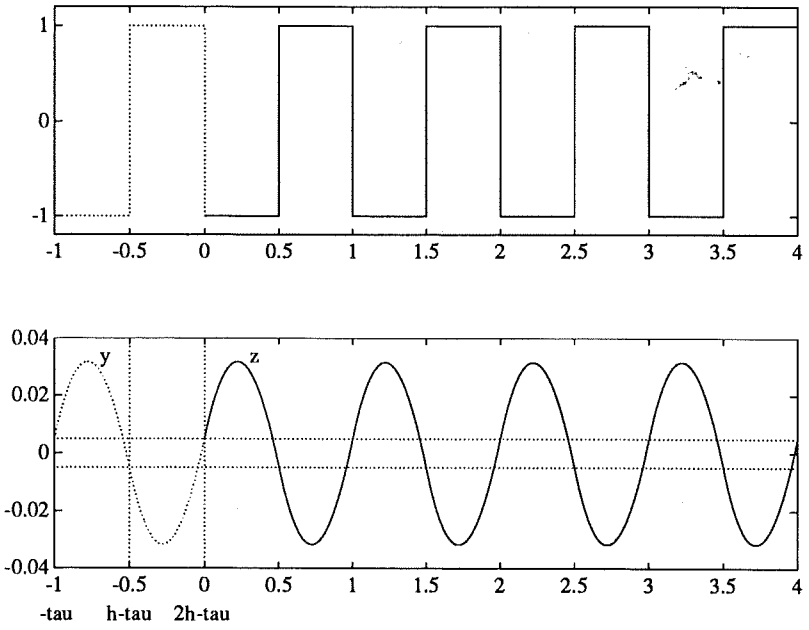

Figure 2.23 Start up of the limit cycle number (3) having $h = (T/2) = \tau/2 = 0.5$. The solution corresponds to positive relay gain and positive relay hysteresis, here chosen as $d = 1$ and $\varepsilon = 0.005$ such that $-\varepsilon/d = -0.005$.

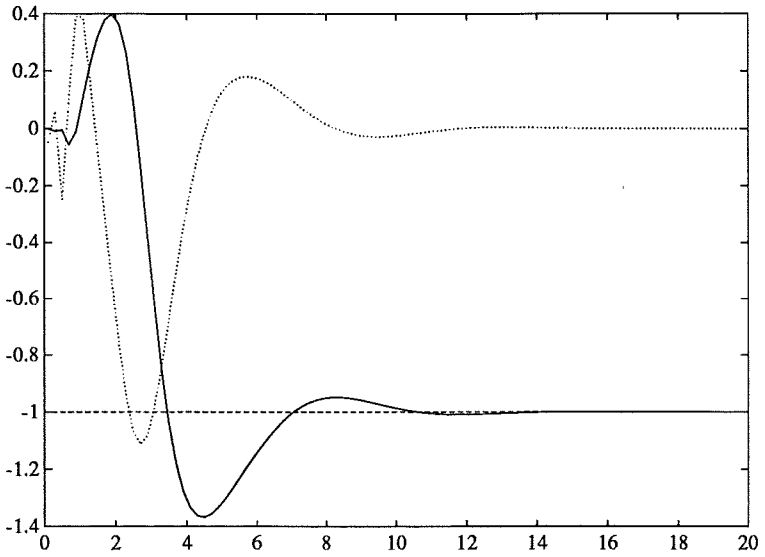

Figure 2.24 The function $H_1(-1, h)$ (solid curve), the line $-\varepsilon/d = -1$ (dashed line) and $\widehat{H}_1(-1, h)$ (dotted curve) for the system $G_0(s) = e^{-s}/(s^2 + s + 1)$. Intersections between the solid curve and the dashed line indicate limit cycle solutions according to Theorem 2.1. However, only two of them are relay feedback solutions: The one with $h = 3.5$ corresponds to $d = 1$, $\varepsilon = 1$ and the second with $h = 7$ corresponds to $d = -1$, $\varepsilon = -1$. All the other solutions are not relay feedback solutions.

that, the solutions for the first three intersections are shown. Square waves with periods corresponding to the solutions are used as inputs to the system $G_0 = e^{-s}/(s^2 + s + 1)$. By investigating the outputs and comparing with the behaviour of a relay with hysteresis we can conclude which solutions that could have been generated by a relay in a feedback loop. The one with $h = 3.5$ is shown in Figure 2.25. From the definition of the relay it is concluded that $d = 1$ and $\varepsilon = 1$. The next solution with $h = 7$ is shown in Figure 2.26. From the definition of the relay it is concluded that $d = -1$ and $\varepsilon = -1$. The third solution with $h = 10.5$ is shown in Figure 2.27. From the definition of the relay this can't be a relay feedback solution. The hysteresis is passed once before the input is switching. Thus, the input couldn't have been generated by a relay feedback. □

2.4 Conclusions

The describing function analysis (DF) is often used for relay feedback systems. The strength of it is, no doubt, its simplicity but also the intuition and

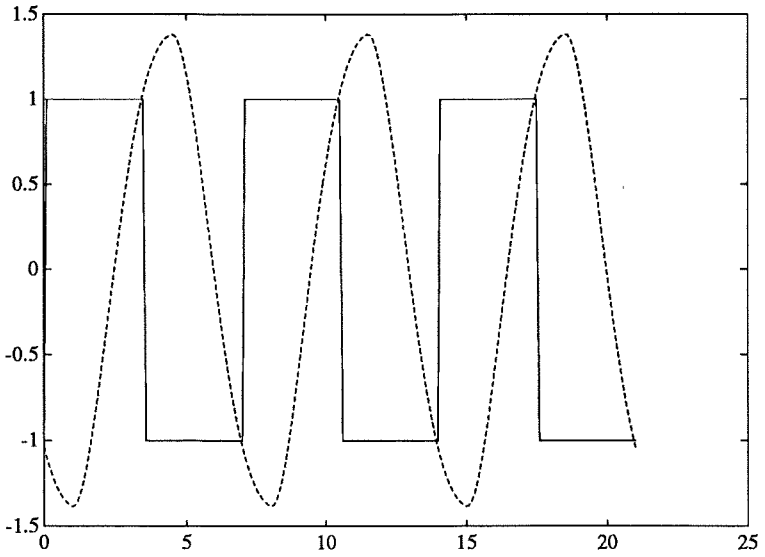

Figure 2.25 A square wave input (solid curve) to the system $G_0(s) = e^{-s}/(s^2 + s + 1)$ and the output z (dashed curve) when the period is chosen to be $T = (2h) = 7$. From the definition of a relay this could have been generated with a relay feedback with $d = 1$ and $\epsilon = 1$.

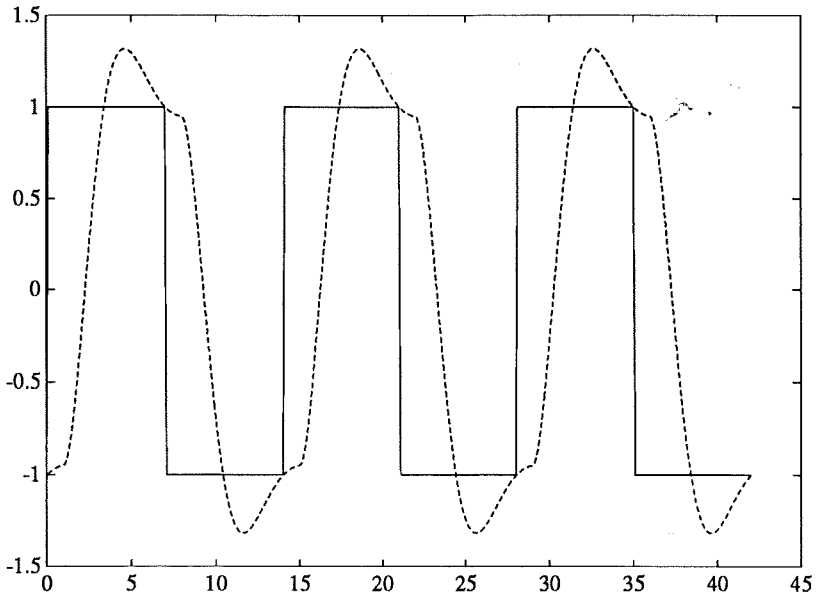

Figure 2.26 A square wave input (solid curve) to the system $G_0(s) = e^{-s}/(s^2 + s+1)$ and the output z (dashed curve) when the period is chosen to be $T = (2h) = 14$. From the definition of a relay this could have been generated with a relay feedback with $d = -1$ and $\epsilon = -1$.

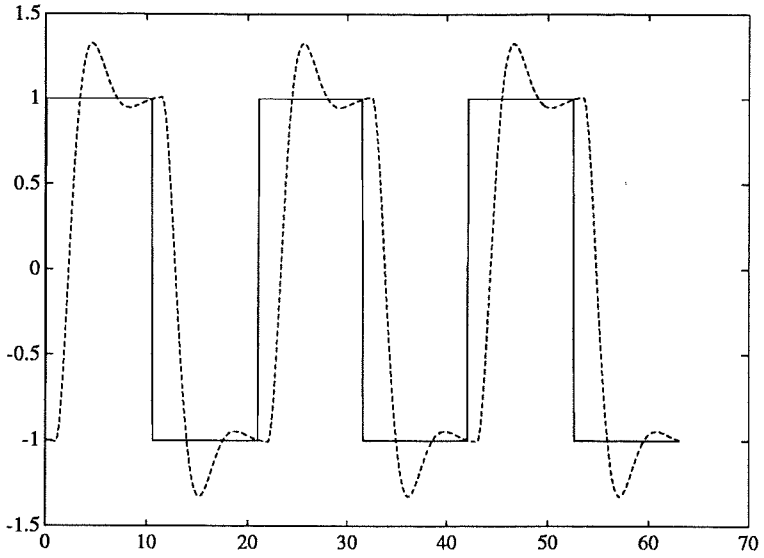

Figure 2.27 A square wave input (solid curve) to the system $G_0(s) = e^{-s}/(s^2+s+1)$ and the output z (dashed curve) when the period is chosen to be $T = (2h) = 21$. From the definition of a relay this could **not** have been generated by a relay feedback.

insight it can give. For a large number of plants the relay feedback causes oscillation into a limit cycle. The excitation at the limit cycle frequency, ω, gives information about the transfer function $G_0(i\omega)$. If G_0 is *low pass enough* above ω the DF method can be used accurately. Then the output can be approximated by a sinusoid with the frequency ω. All higher harmonics can be neglected. Distortion, $\mathcal{D}$, is a common measure of how well a function is approximated by a sinusoid. It is, however, a very crude measure and can give rise to misleading judgements, as has been demonstrated with examples.

Often, the relay hysteresis is defined to be positive. But it is also possible to generalize the definition and have a negative hysteresis. However, this is not straightforward since we then have to demand that the relay input must have been outside the hysteresis band before a switch can occur.

Actually, there is no reason why only information from the first harmonic should be used, as is the case with the DF method. Instead, all information from the relay excitation can be used in a spectral analysis. Then the low pass condition is not needed anymore.

The DF method can be used to predict the limit cycle frequency given relay characteristics, gain d and hysteresis ε. This is done by investigating the Nyquist curve. The method is simple and appealing, and is therefore often used as a first approach. Exact results are also available, but they require more elaborate calculations.

3

A relay with adaptive hysteresis

Simple tuning rules for simple controllers have always been an interesting topic for control engineers. The tuning rules use data from an experiment that reveals some basic characteristics of the system. It could be a step response experiment or a frequency domain experiment like the Ziegler-Nichols ultimate-sensitivity method. For controller design purposes it is of special interest to know the system behaviour around the phase shift -180^o. In the ultimate-sensitivity method the transfer function is identified at the phase shift of -180^o by tuning of a P-regulator to its stability boundary. The same phase shift is obtained when instead a relay feedback system is used, as described in Åström-Hägglund (1984). The system is forced into a limit cycle with the prescribed phase shift. The relay feedback system makes a self-generated experiment and is therefore suitable for autotuning purposes. It is of interest to make similar experiments for determination of points where the phase shift of the plant is specified at other values than -180^o. This chapter will describe a nonlinearity which allows this. When describing function analysis is applicable the nonlinearity can be used to perform *phase analysis* experiment. Apart from applications to autotuning the result is also useful for other problems like in expert control (Åström-Anton (1984)) when it is of interest to explore the properties of the open loop transfer function of a system.

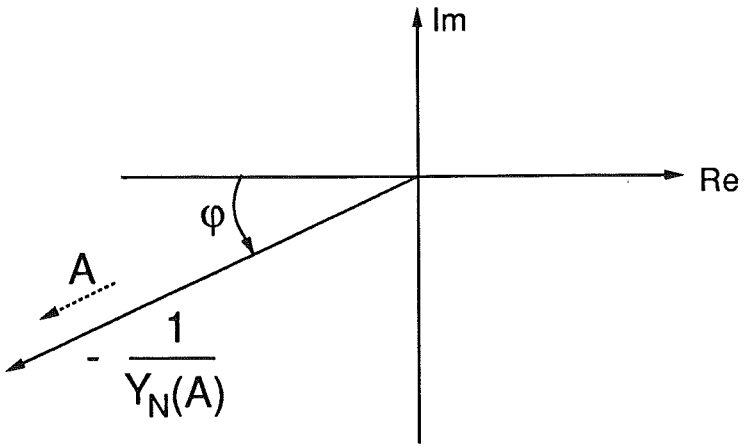

Figure 3.1 Desired negative inverse describing function

3.1 The basic idea

The key problem is to construct a nonlinear system such that the negative inverse describing function, $-1/Y_N(A)$, is a straight line segment through the origin, as shown in Figure 3.1. Consider the relay with gain, d, and hysteresis, ε. In that case we have

$$-\frac{1}{Y_N(A)} = -\frac{\pi A}{4d}[\sqrt{1-(\frac{\varepsilon}{A})^2} + i \cdot \frac{\varepsilon}{A}]$$

This is defining a horizontal line in the complex plane, with constant imaginary part. We would instead like to have a constant phase. Thus, if we let the hysteresis vary proportional to the amplitude with

$$\varepsilon = \sin(\varphi) \cdot A \tag{3.1}$$

we would get

$$-\frac{1}{Y_N(A)} = -\frac{\pi A}{4d} e^{i\varphi}$$

which gives a constant phase lag

$$\Rightarrow \quad \arg(-\frac{1}{Y_N(A)}) = \begin{cases} -\pi + \varphi & d > 0 \\ \varphi & d < 0 \end{cases}$$

By choosing the parameters φ and d properly we get a DF estimation $\widehat{G}(i\omega) = -1/Y_N(A)$ with the prescribed phase shift. To maintain the relation (3.1) it is necessary to change the hysteresis as a function of the amplitude by some feedback mechanism. Instead of scanning in frequency and measure

amplitude and phase shift like the usual frequency analysis experiment we are able to scan in phase shift and instead measure amplitude and frequency. The identification results should be the same irrespective of what method we choose; frequency analysis or phase analysis experiments. Conditioned, of course, that describing function analysis is appropriate, i.e. the system is low pass enough at the limit cycle frequency. To make frequency analysis an external sinusoidal signal has to be generated. That is not needed when using the relay excitation. The most important reason for using the phase analyzer is that we don't need to know the interesting frequency range. On the other hand, we know the interesting phase range for controller design purposes. To get a robust control design we would like to know the system around the phase $-180°$. Moreover, several points on the Nyquist curve can be identified for different phases to be used in more advanced design schemes in the frequency domain, see Lilja (1989).

3.2 Automatic tuning

The relay with phase adaptive hysteresis makes it possible to identify a system at a certain phase without knowing the corresponding frequency beforehand. This is an interesting feature especially in autotuning applications where it is of interest to find out the system Nyquist curve in the neighbourhood of -1. The implementation of the relay with phase adaptive hysteresis will be shown later. First, an example will show the use of the *phase analyzer.*

EXAMPLE 3.1—Eight order low pass system
To show the behaviour of the adaptive hysteresis relay feedback system, the low pass system $G(s) = 1/(s+1)^8$ will be investigated. Assume the DF interpretation to be valid at the resulting limit cycle frequencies. The parameter choice $\varphi = 45$, $d = 1$ would then correspond to the phase lag $\arg(G(i\widehat{\omega})) = -3\pi/4$. We would therefore expect to get the limit cycle frequency $\widehat{w} = \tan(\frac{3\pi}{4} \cdot \frac{1}{8})$, i.e $\widehat{T} \approx 21$, and an amplitude $|G(i\widehat{\omega})|4d/\pi \approx 0.89$. A simulation of the system with the phase adaptive hysteresis is shown in Figure 3.2. The experiment gives a period $T \approx 21$ and an amplitude $A \approx 0.89$. Notice, the fast convergence to the limit cycle. The parameter choice $\varphi = -45$, $d = 1$ would correspond to the phase lag $\arg(G(i\widehat{\omega})) = -5\pi/4$. We would therefore expect to get the limit cycle frequency $\widehat{w} = \tan(\frac{5\pi}{4} \cdot \frac{1}{8})$, i.e $\widehat{T} \approx 11.8$, and an amplitude $|G(i\widehat{\omega})|4d/\pi \approx 0.47$. A simulation of the system with the phase adaptive hysteresis is shown in Figure 3.3. The experiment gives a period $T \approx 11.8$ and an amplitude $A \approx 0.47$. The DF estimated $\widehat{G}(i\omega)$ for the two chosen phases $-3\pi/4$ and $-5\pi/4$ are shown in the Nyquist diagram in Figure 3.4. The gain function is calculated as $|G(i\omega)| = A\pi/(4d)$ where A is the measured amplitude.

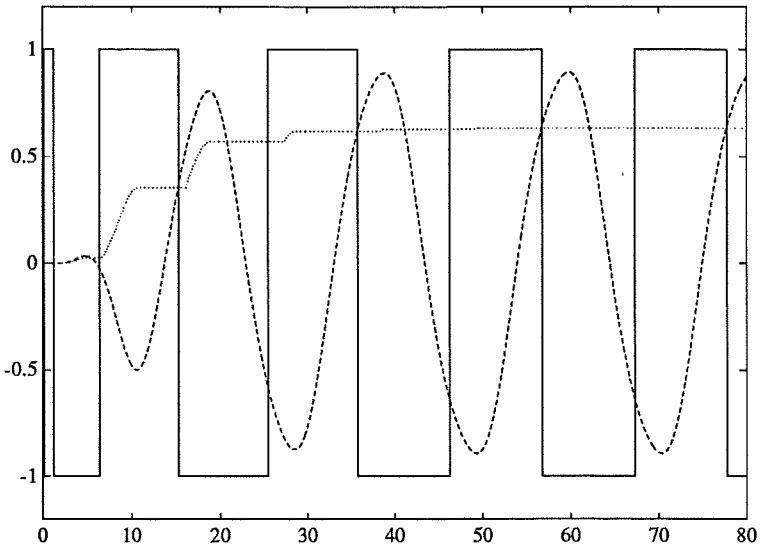

Figure 3.2 The relay output, u (solid), the output y (dashed) and the adaptive hysteresis proportional to the amplitude, i.e. $\varepsilon = \sin(\varphi)A$ (dotted). With the parameter choice $\varphi = 45$, $d = 1$ it is expected a phase lag of $\arg(G(i\widehat{\omega})) = -\frac{3\pi}{4}$, i.e. $\widehat{T} \approx 21$, and an amplitude $|G(i\widehat{\omega})| 4d/\pi \approx 0.89$. The experiment gives a period $T \approx 21$ and an amplitude $A \approx 0.89$.

3.3 Indication of nonlinearities

If a system G_0 is low pass enough for DF analysis the two identification methods: frequency response analysis and phase analysis (by the relay) should give the same result. On the other hand, if G_0 includes a nonlinearity there is no reason to expect the results to be the same since the excitations are made by different signals; sinusoidals and square waves respectively. The difference from the two experiments contains information that might be used for identification of the nonlinearity. One example is a backlash at the input. When generating a Bode diagram from a frequency analysis experiment both the gain curve and the phase curve will be changed by the backlash nonlinearity. Corresponding phase curve from a phase analysis experiment, however, will be unaffected by the backlash. The reason is that the combined effect of a relay and a backlash in series is simply another relay with different gain but with the same hysteresis. Since it is the hysteresis alone that tunes for the desired phase lag, the Bode phase curve will be the same irrespective of any backlash at the input. Figure 3.5 illustrates the combined effect of a relay and backlash in series. The relay output is either $x = d$ or $x = -d$. Then if $b < d$ the output from the backlash is $y = a(d - b)$ or $y = -a(d - b)$ respectively. Hence, the combined effect of the relay and backlash in series is the behaviour of a relay with the same hysteresis, ε, but with another relay

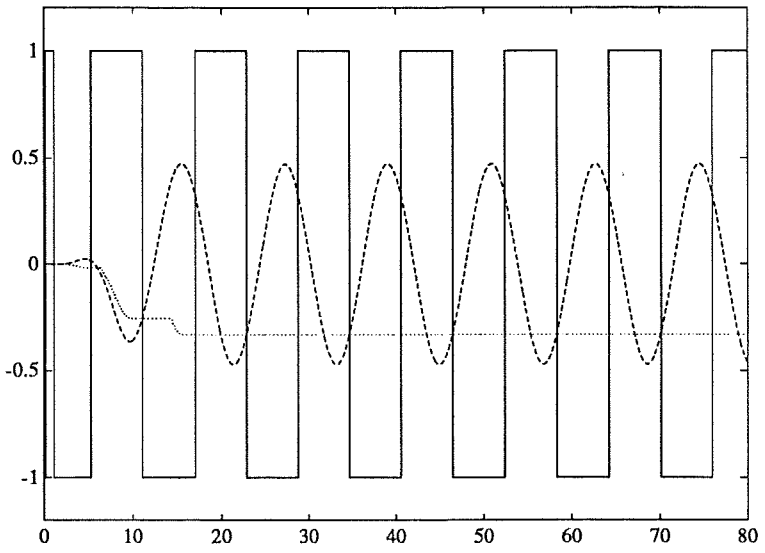

Figure 3.3 The relay output, u (solid), the output y (dashed) and the adaptive hysteresis proportional to the amplitude, i.e. $\epsilon = \sin(\varphi)A$. With the parameter choice $\varphi = -45$, $d = 1$ it is expected a phase lag of $\arg(G(i\widehat{\omega})) = -\frac{5\pi}{4}$, i.e. $\widehat{T} \approx 11.8$ and an amplitude $|G(i\widehat{\omega})|4d/\pi \approx 0.47$. The experiment gives a period $T \approx 11.8$ and an amplitude $A \approx 0.47$.

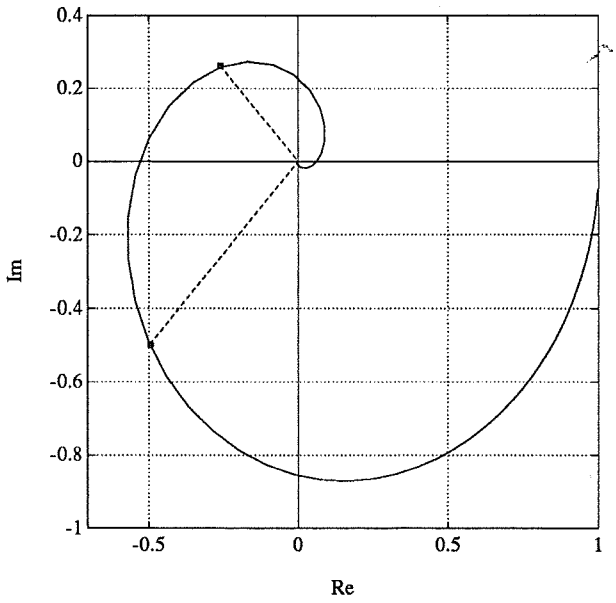

Figure 3.4 The DF estimated $\widehat{G}(i\omega)$ for the two chosen phases $-3\pi/4$ and $-5\pi/4$ for the system $G(s) = 1/(s+1)^8$. To get the prescribed phase lag the parameter choice was $\varphi = 45^o$ and $\varphi = -45^o$ respectively ($d = 1$).

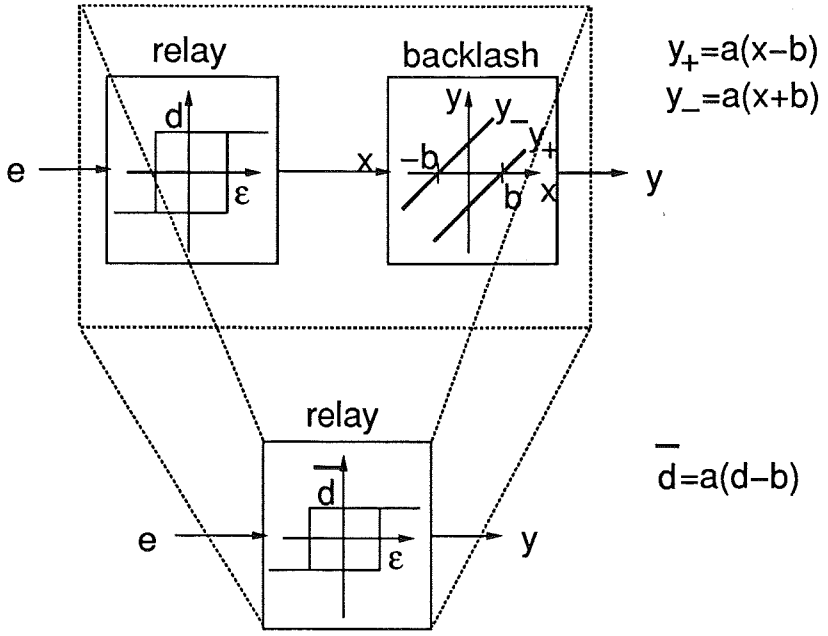

Figure 3.5 The combined effect of a relay and a backlash in series is simply another relay with different gain but with the same hysteresis.

gain, $\bar{d} = a(d - b)$. A phase analysis experiment would therefore give the right Bode phase curve, while the Bode gain curve would have a systematic error

$$|\widehat{G_0(i\omega)}| = \frac{\pi A}{4d} = |G_0(i\omega)| \cdot \frac{\bar{d}}{d}$$

The differences of the results from a phase analysis experiment compared to a frequency analysis experiment could therefore signal for presence of certain nonlinearities. The intention here is not to show how the phase analyzer should be used but rather to illustrate that it might be useful at least as an indicator for simple nonlinearities.

3.4 Implementation

A relay with hysteresis is not a memoryless static nonlinearity. Because of the hysteresis, it requires a memory—a state. When we now introduce dynamics by letting the hysteresis to be varying we can still use describing function interpretation if just the updating of ε occurs in a slower time scale than everything else. A simple way to do this is to use a peak detection as an estimate of the approximate sinusoidal amplitude A. When starting the relay with $\varepsilon = 0$ the amplitude detections will adjust ε twice a period until $\varepsilon = \sin(\varphi) \cdot A$. Peak detection for finding the amplitude A may be inappropriate if there is measurement noise. In a practical situation more

```
DISCRETE SYSTEM RELAY
INPUT  e
OUTPUT u
STATE  eold  uold  A
NEW    neold nuold nA
TIME   t
TSAMP  ts

initial
uold = d
sort

neold = e
nuold = u
WasUp = sign(uold*d)
GoUpP = e>eps  or (WasUp and e>-eps)
GoUpN = e>-eps or (e>eps and e>eold)
GoUp  = if phi>0 then GoUpP else GoUpN
u     = if GoUp then d else -d

nA    = max(A,abs(e))                  "Peak detection
eps   = sin(phi*3.1415/180)*A          "adaptive hysteresis

ts    = t + dt

phi :45  "angle from real axis (in degrees)
d   :1   "relay gain
dt  :.01 "relay sampling period
END
```

Listing 3.1 A simnon implementation of a relay with adaptive hysteresis.

elaborate schemes than a simple peak detection might be used. Ones suggestion is to use correlation techniques similar to what is used in frequency analysis experiments. The intention here, however, is to show ideas rather than practical algorithms. Therefore, for simplicity, the peak detection will be used. A simple Simnon implementation of such a relay is given in Listing 3.1.

3.5 Conclusions

A relay with hysteresis has a negative inverse describing function, $-1/Y_N(A)$, that is a segment of a horizontal line in the complex plane. The new idea here, is to let the hysteresis vary proportional to the signal amplitude A. Then, the negative inverse describing function instead becomes a segment of a straight line through the origin, with a slope that depends on the proportionality constant. This feature is useful for autotuning and for exploring of the Nyquist curve of a system. When a system is connected to the relay with adaptive

hysteresis in a feedback loop, a prespecified phase shift could be chosen to get a specific crossing with the Nyquist curve. Valuable information of the system is then received from a stable limit cycle.

The idea assumes and is dependent on the validity of describing function analysis. This restricts the use of the relay feedback system to processes having low pass behaviour around the chosen phase shift. When this is the case, the relay with adaptive hysteresis can act as a *phase analyzer* by scanning in phase rather than in frequency as is the case in usual frequency analysis experiments. If the results from the phase analyzer differs from that by the frequency analyzer this could indicate presence of nonlinearities, e.g. an input backlash.

4

First order systems with a time delay

In chapter 2, limit cycles were analyzed using describing function analysis. The approximate analysis gave an indication of stability and existence of a limit cycle. The quality of the results depend on the validity of the approximate analysis. For example, a first order system, was not suitable for describing function analysis, the reason being that higher harmonics are not sufficiently attenuated. That case will therefore be investigated thoroughly here. Conditions for convergence to different types of limit cycles will be given for relay feedback of a general first order system with a time delay. The system can be stable as well as unstable and it may include a direct term. A first order system with direct term can be thought of as being an approximation of a second order system with one fast and one slow mode. Due to the direct term and the time delay the feedback system can have different types of limit cycles with different stability properties. Also, asymmetrical limit cycles are found. Notice, that such limit cycles cannot be predicted by Theorem 2.1.

4.1 Introduction

Consider the first order system with direct term

$$G(s) = b_0 + \frac{b_1}{s+a} \tag{4.1}$$

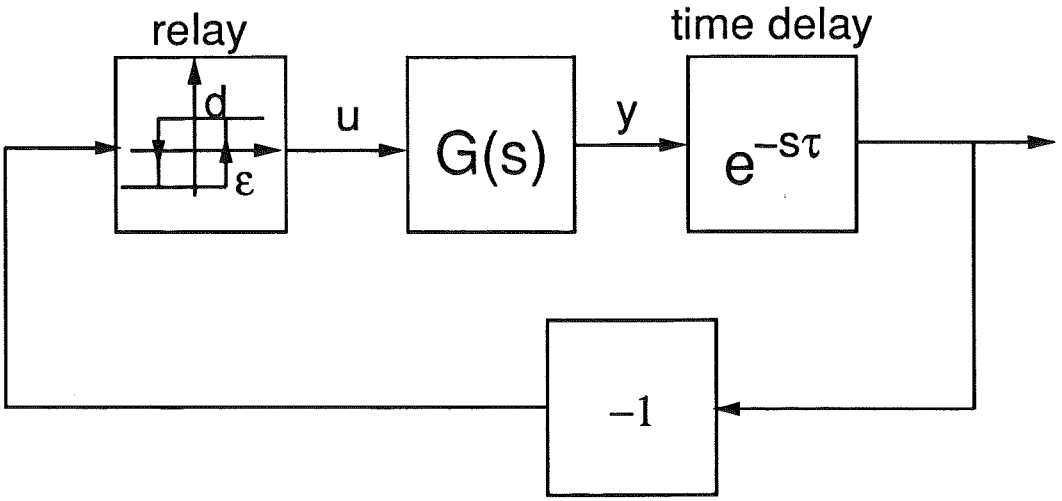

Figure 4.1 Relay feedback of a system with time delay

in series with a time delay τ in a relay feedback loop with relay amplitude d and hysteresis ε, as shown in Figure 4.1. Because of the time delay the system is infinite dimensional. This means in particular that it is possible to find infinitely many limit cycle solutions when $\varepsilon = 0$ as has been shown in Chapter 2. Most of these, however, have periods shorter than the time delay. Typically, these can be started up by letting $y(t)$ pass the hysteresis a number of times during a time equal to the time delay before the relay is connected. Relay switchings can in this way be *accumulated.* Such startups where shown in Example 2.4 in Figure 2.21 and Figure 2.22. Such solutions will not be considered in the following. Instead we will consider a more practical startup situation with no *accumulated* switchings at the time when the loop is closed. The relay is introduced at time $t = 0+$ with a switch from $-d$ to d. This first switch is deliberately made by us at the time instant when we close the loop. All following switches are then caused by the feedback system itself and not by any *accumulation* of switchings constructed before the loop was closed. The history, $y(t)$, $t \in [-\tau, 0-]$, can be regarded as the initial state of the system. The considered startup situation is the following constraints.

$$\begin{cases} y(t) < \varepsilon, & -\tau \leq t \leq 0- \\ u(0-) = -d \\ u(0+) = d \end{cases} \tag{4.2}$$

When the startup (4.2) is satisfied there are still a number of different kinds of behaviours of the feedback system to be considered. This is illustrated in Figure 4.2. Due to the direct term different types of relay switches may occur depending on how y is passing the hysteresis: One where y passes the hysteresis continuously, a C-switch, and another one where y passes the

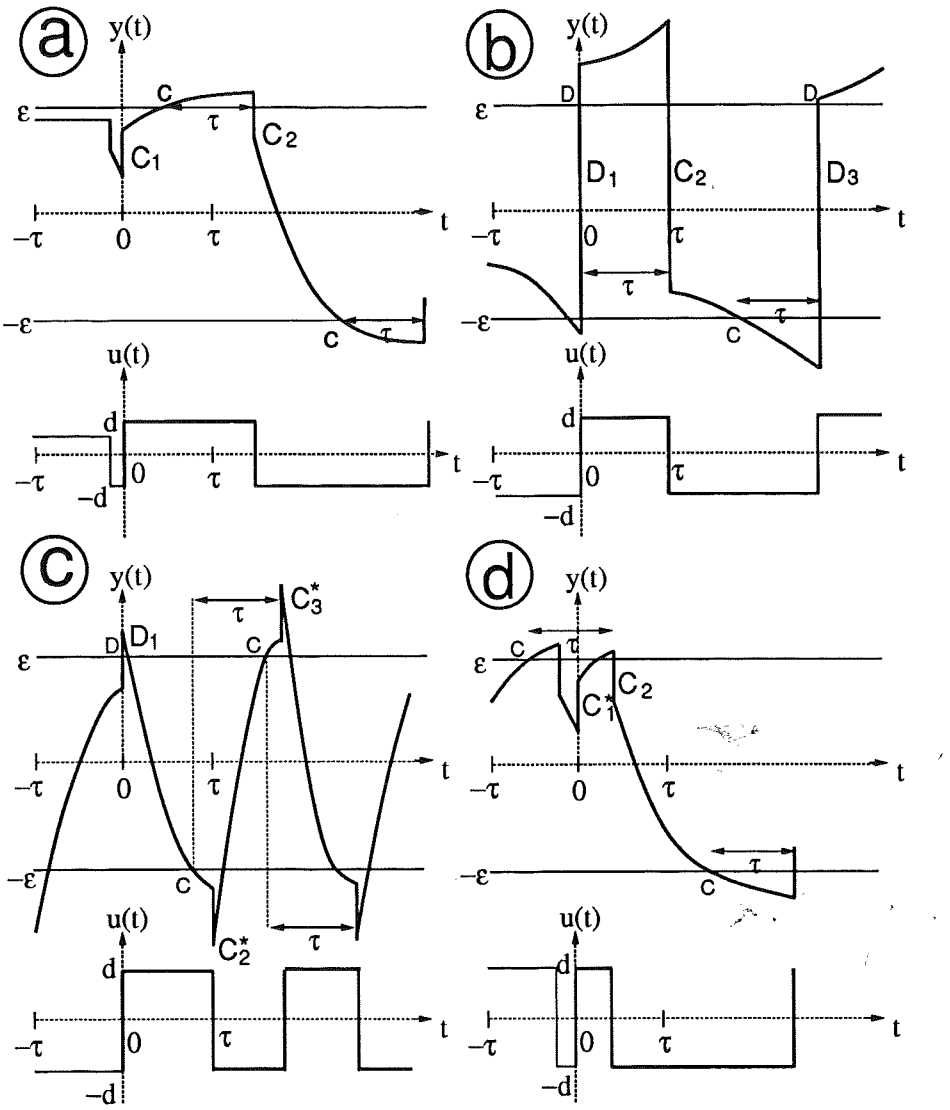

Figure 4.2 Definition of different kinds of relay switches. The Figures *a*) – *c*) show examples of the considered case where the initial condition (4.2) is satisfied while Figure *d*) does not satisfy (4.2). Suppose (4.2) is satisfied. Then a switch is a **C**-switch if y does not pass the hysteresis discontinuously and if y is passing the hysteresis continuously **after** the switch. The continuous pass is indicated by **C** and if the $i:th$ switch is a **C**-switch this is marked as $\mathbf{C}_i$. Typical **C**-switches are shown in Figure *a*) and the second switch in Figure *b*). In a **D**-switch, y instead passes the hysteresis boundary discontinuously. Note that we still assume that (4.2) is satisfied. In Figure *b*) the first and the third switch are **D**-switches. In Figure *c*) the first switch is a **D**-switch. When the second switch occurs in Figure *c*) the corresponding hysteresis boundary has already been passed, i.e. a new switch is *accumulated*. A switch that has accumulated new switches like this is a $\mathbf{C}^*$-switch. Notice that y passes the hysteresis continuously **before** a $\mathbf{C}^*$-switch while it passes the hysteresis continuously **after** a **C**-switch. Notice also that the time to the switch after passing the hysteresis is equal to τ. This means that the time between **C**-switches is $> \tau$, while it is $< \tau$ between $\mathbf{C}^*$-switches and $= \tau$ between **D**-switches.

hysteresis discontinuously, a **D**-switch. Then there are yet another continuous switch, a **C***-switch. This is shown in Figure 4.2c and can occur after starting with a **D** switch. A **C***-switch is defined by the fact that y has already passed the hysteresis and *accumulated* a switch when the **C***-switch comes. The time to the next switch after passing the hysteresis is always τ. Therefore, the time from the **C***-switch to the following switch becomes less than τ. This is contrary to a **C**-switch which has no accumulated switchings. First some time is required to reach the hysteresis and then after time τ the following switch will occur. Consequently, the following switch after a **C**-switch would occur after a time that is longer than the time delay, see Figure 4.2a. Like **C**-switchings, **D**-switchings do not have any accumulated switchings. The time to the following switch after a **D**-switch is therefore equal to τ.

If the condition $y(0+) < \varepsilon$ is added to the startup conditions (4.2) (i.e the first switch is not a **D**-switch), then **C***-switches are not possible. It will be shown that only **C**-limit cycles, **D**-limit cycles and mixtures of these, **CD**-limit cycles are possible. Also, it will be shown that in the mixed case the only possible limit cycle is when the relay switches twice each limit cycle, like **(CD)(CD)(CD)**.... For example, switches of the type **(CDD)(CDD)**... are not possible. Necessary and sufficient conditions for each of the three possible cases will be given.

However, if $y(0+) > \varepsilon$, then the first switch is a **D**-switch. From such a startup limit cycles that involve **C***-switches are also possible. The **C***-limit cycles differs from the **C**-limit cycles in that the half switch period h is less than the time delay τ. Also they differ in terms of stability. It will also be demonstrated that there are stable asymmetrical **C*D**-limit cycles. These also have different stability properties than the **CD**-limit cycles. Depending on the initial state $x(0)$ one system can reach different types of limit cycles.

Notations and definitions

Split up $u(t)$ and $y(t)$ into segments between consecutive switchings t_i and t_{i+1}. Let $h_i = t_{i+1} - t_i$ be the switch time period and define

$$\begin{cases} y_i(t) \equiv y(t + t_i) \\ u_i(t) \equiv (-1)^{i-1} d \end{cases} \qquad 0+ \leq t < h_i$$

This is illustrated in Figure 4.3. Notice that $y_i(t)$ is defined as being continuous from the right. This is emphasized by denoting $y_i(0)$ as $y_i(0+)$. The

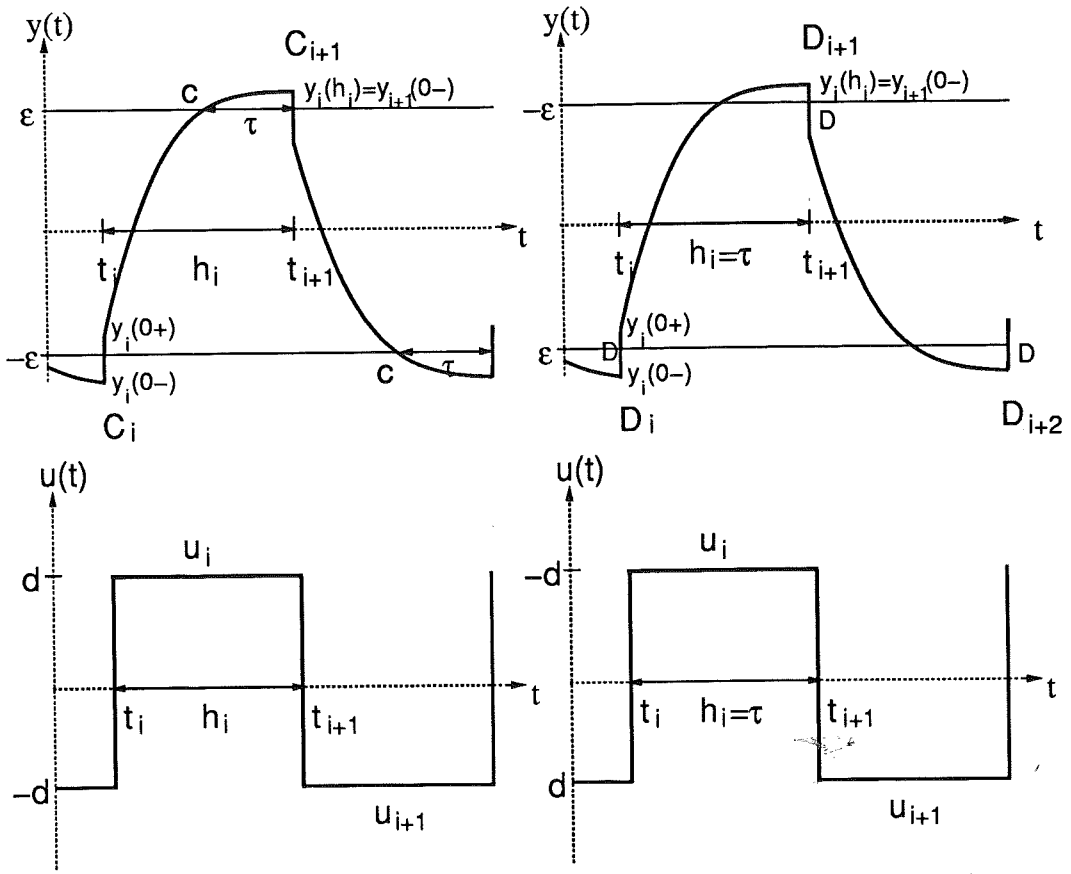

Figure 4.3 Illustrations of the notations, indexed by i. Above, y, and below, corresponding relay output, u. To the left, **C**-switches are shown when using both positive hysteresis and relay gain, $\varepsilon, d > 0$. To the right, **D**-switches are shown when using both negative hysteresis and relay gain, $\varepsilon, d < 0$.

limit of $y_i(t)$ as $t \to h_i$ is denoted $y_i(h_i) = y_{i+1}(0-)$. We have

$$y_i(t) = (-1)^{i-1} b_0 d + x_i(t) \quad ; \quad 0+ \le t < h_i$$

$$x_i(t) = \begin{cases} e^{-at} x_i(0) + \dfrac{b_1}{a}(1 - e^{-at}) u_i & a \neq 0 \\ x_i(0) + b_1 t u_i & a = 0 \end{cases} \tag{4.3}$$

where $x_i(t)$ is the state. Sometimes the shorter notation is preferred

$$x_i(t) = \Phi(t) x_i(0) + \Gamma(t) u_i$$

where

$$\Phi(t) = e^{-at} \quad \text{and} \quad \Gamma(t) = \begin{cases} (1 - e^{-at}) b_1 / a & a \neq 0 \\ b_1 t & a = 0 \end{cases}$$

Also, when $t = \tau$ the notation Φ and Γ will be used for brevity. Notice, that the direct term makes $y(t)$ discontinuous such that $y_i(h_i) = y_{i+1}(0-) \neq y_{i+1}(0+)$. In fact,

$$y_i(0+) = y_i(0-) + 2(-1)^{i-1} b_0 d \qquad i \geq 1$$

However, the state $x(t)$ is continuous, i.e. $x_i(h_i) = x_{i+1}(0)$. The conditions for the i:th switch to be a **C**- and a **D**-switch, are written for brevity $\mathbf{C}_i$ and $\mathbf{D}_i$ respectively. The definition for $\mathbf{C}_i$ is

DEFINITION 4.1—$\mathbf{C}_i$

a) y has not passed the considered hysteresis boundary during a passed time length of τ before the switch.

b) y does not pass the considered hysteresis boundary within a time length of $h_i - \tau$ after the switch, where $h_i > \tau$.

c) y passes the hysteresis boundary after the time $h_i - \tau$. □

A formal definition is given below, clarifying the meaning of *passing the hysteresis boundary.*

DEFINITION 4.1'

a) No point $t \in (t_i - \tau, t_i)$ where

$$\frac{d}{dt}(-1)^{i-1} y(t) > 0$$
$$(-1)^{i-1} y(t) = \varepsilon$$

b) No point $t \in (0, h_i - \tau), \quad h_i > \tau$ where

$$\frac{d}{dt}(-1)^{i-1} y_i(t) > 0$$
$$(-1)^{i-1} y_i(t) = \varepsilon$$

c) Passing of the hysteresis boundary

$$\frac{d}{dt}(-1)^{i-1} y_i(h_i - \tau) > 0$$
$$(-1)^{i-1} y_i(h_i - \tau) = \varepsilon, \quad h_i > \tau$$

□

The definition for $\mathbf{D}_i$ is

DEFINITION 4.2—$\mathbf{D}_i$

a) y has not passed the considered hysteresis boundary during a passed time length of τ before the switch.

b) y passes the hysteresis boundary discontinuously □

A formal definition is

DEFINITION 4.2'

a) No point $t \in (t_i - \tau, t_i)$ where

$$\frac{d}{dt}(-1)^{i-1}y(t) > 0$$
$$(-1)^{i-1}y(t) = \varepsilon$$

b) Discontinuous passing

$$(-1)^{i-1}y_i(0-) < \varepsilon \leq (-1)^{i-1}y_i(0+)$$

□

Notice, that in both cases, $\mathbf{C}_i$ and $\mathbf{D}_i$, the hysteresis is passed which guarantees a switch after the time h_i. In case of $\mathbf{C}_i$, then $h_i > \tau$, and in case of $\mathbf{D}_i$, then $h_i = \tau$ (cf. Figure 4.2b). The $\mathbf{C}^*$-switch described in Figure 4.2c is defined as

DEFINITION 4.3—$\mathbf{C}^*$

A $\mathbf{C}^*$-switch is a switch that does not satisfy the condition *a*) in the definition of a **C**- or **D**-switch. □

Violation of the condition *a*) means that the hysteresis boundary has already been passed, i.e. a switch has been *accumulated.* The following switch will therefore be within less than the time delay, $h_i < \tau$, as was shown in Figure 4.2c.

4.2 C-limit cycles

A **C**-limit cycle is defined as

DEFINITION 4.4—C-limit cycle
A C-limit cycle is a limit cycle consisting of an infinite sequence of C-switchings. □

Conditions that guarantee that a C-limit cycle is reached will be given. The conditions will be expressed in the system parameters. Also, the influence from the initial state, $x(0)$, will be investigated. It will be shown that $x(0)$ must lie in certain intervals in order to reach a C-limit cycle. To simplify the analysis the conditions in the definition of $\mathbf{C}_i$ will be reformulated, taking into account that we are dealing with a first order system. The conditions to be considered are given in the lemma below.

LEMMA 4.1
Consider the first order system (4.1) in the relay feedback loop as in Figure 4.1, and suppose the condition a) of the definition of $\mathbf{C}_i$ is satisfied. Then all conditions for $\mathbf{C}_i$ are satisfied if and only if

$$\begin{cases} (-1)^{i-1} y_i(0+) < \varepsilon \\ (-1)^{i-1} y_i(h_i - \tau) = \varepsilon, \quad h_i > \tau \end{cases} \tag{4.4}$$

Proof: After the switch at time t_i the relay output is constant when $t \in (0, h_i)$. Therefore, $y_i(t)$, $t \in (0, h_i)$ will be strictly monotone. The monotonicity of $y_i(t)$, $t \in (0, h_i)$ together with the conditions b) and c) give

$$\begin{cases} \dfrac{d}{dt}(-1)^{i-1} y_i(t) > 0 & t \in (0, h_i - \tau] \\ (-1)^{i-1} y_i(h_i - \tau) = \varepsilon & h_i > \tau \end{cases}$$

The same conditions are derived from the monotonicity together with (4.4). The equivalence is therefore established. ∎

LEMMA 4.2
The state $x_i(0)$ at time t_i is uniquely specified if the previous switch was $\mathbf{C}_{i-1}$. It is

$$\begin{aligned} x_i(0) &= \{\frac{b_1}{a} + e^{-a\tau}(\frac{\varepsilon}{d} - b_0 - \frac{b_1}{a})\} u_{i-1} && a \neq 0 \\ &= \{\frac{\varepsilon}{d} - b_0 + b_1\tau\} u_{i-1} && a = 0 \\ u_{i-1} &= (-1)^i d \end{aligned}$$

Proof: At the continuous pass after the $\mathbf{C}_{i-1}$ switch we have

$$\begin{aligned} y_{i-1}(h_{i-1} - \tau) &= (-1)^i \varepsilon \\ u_{i-1} &= (-1)^i d \end{aligned}$$

The state is then

$$x_{i-1}(h_{i-1}-\tau) = (-1)^i\varepsilon - b_0 u_{i-1} = (\varepsilon/d - b_0)u_{i-1}$$

Hence

$$\begin{aligned} x_i(0) &= \Phi x_{i-1}(h_{i-1}-\tau) + \Gamma u_{i-1} = \\ &= \{\frac{b_1}{a} + e^{-a\tau}(\frac{\varepsilon}{d} - b_0 - \frac{b_1}{a})\}u_{i-1} \qquad a \neq 0 \\ &= \{\frac{\varepsilon}{d} - b_0 + b_1\tau\}u_{i-1} \qquad a = 0 \end{aligned}$$

■

Remark. By using the notation

$$\chi \equiv -\frac{\Gamma}{1+\Phi}d = \begin{cases} -\dfrac{b_1 d}{a}\tanh(\dfrac{a\tau}{2}) & a \neq 0 \\ -\dfrac{\tau}{2}b_1 d & a = 0 \end{cases} \tag{4.5}$$

the state can be expressed as

$$(-1)^i x_i(0) = -e^{-a\tau}(\chi + b_0 d - \varepsilon) - \chi$$

This will be useful later when it is shown that the sign of $\chi + b_0 d - \varepsilon$ is important. □

Lemma 4.2 shows a fundamental property of a **C**-switch when dealing with first order systems. This has many implications, one of which is given below.

LEMMA 4.3
Suppose there are two consecutive **C**-switchings, $\mathbf{C}_j$ and $\mathbf{C}_{j+1}$. Then the system has reached a **C**-limit cycle. The limit cycle is defined by

$$(-1)^i x_i(h_{j+1}-\tau) = (-1)^j x_j(h_j - \tau) = b_0 d - \varepsilon, \quad \forall i > j$$

and the limit cycle period, T, is unique and defined by

$$T/2 = h_{j+1} = \begin{cases} \tau + \dfrac{1}{a}\ln\left\{\dfrac{2b_1/a}{b_0 + b_1/a - \varepsilon/d} - e^{-a\tau}\right\} & a \neq 0 \\ 2\tau + 2\dfrac{\varepsilon - b_0 d}{b_1 d} & a = 0 \end{cases} \tag{4.6}$$

Proof: When passing the hysteresis boundary after the **C**-switchings the corresponding states are, according to Lemma 4.1,

$$(-1)^j x_j(h_j - \tau) = (-1)^{j+1} x_{j+1}(h_{j+1} - \tau) = b_0 d - \varepsilon, \quad h_j, h_{j+1} > \tau$$

Then the next initial state, $x_{j+2}(0)$, satisfies

$$\begin{aligned}(-1)^{j+2}x_{j+2}(0) &= (-1)^{j+2}x_{j+1}(h_{j+1}) = \\ &= (-1)^{j+2}[\Phi x_{j+1}(h_{j+1}-\tau)+\Gamma u_{j+1}] = \\ &= (-1)^{j+1}[\Phi x_j(h_j-\tau)+\Gamma u_j] = (-1)^{j+1}x_j(h_j) = \\ &= (-1)^{j+1}x_{j+1}(0)\end{aligned}$$

Since $(-1)^{j+2}u_{j+2} = (-1)^{j+1}u_{j+1}$ and $(-1)^{j+2}x_{j+2}(0) = (-1)^{j+1}x_{j+1}(0)$ this implies that

$$(-1)^{j+2}x_{j+2}(h_{j+1}-\tau) = (-1)^{j+1}x_{j+1}(h_{j+1}-\tau) = b_0 d - \varepsilon$$

i.e. the $(j+2)$:th switch is also a C-switch and $h_{j+2} = h_{j+1}$. The limit cycle is reached. The half period h_{j+1} can be calculated from $(-1)^j y_{j+1}(h_{j+1}-\tau) = \varepsilon$ after rewriting (4.3) as

$$(-1)^j y_{j+1}(t) = \begin{cases} = (b_0 + b_1/a)d - [(-1)^{j+1}x_{j+1}(0) + b_1 d/a]e^{-at} & a \neq 0 \\ = b_0 d - (-1)^{j+1}x_{j+1}(0) + b_1 d \cdot t & a = 0 \end{cases}$$

This gives

$$h_{j+1} = \begin{cases} \tau + \dfrac{1}{a}\ln\left(\dfrac{(-1)^{j+1}x_{j+1}(0) + \frac{b_1 d}{a}}{(b_0 + b_1/a)d - \varepsilon}\right) & a \neq 0 \\ \tau + \dfrac{1}{b_1 d}((-1)^{j+1}x_{j+1}(0) + \varepsilon - b_0 d) & a = 0 \end{cases}$$

Then use Lemma 4.2 to express $(-1)^{j+1}x_{j+1}(0)$ into system parameters, and (4.6) follows. ∎

Remark. Notice that the lemma shows that if there are two consecutive C-switchings the C-limit cycle is reached already when passing the hysteresis boundary after the first C-switch. On the other hand, one C-switch is not enough to conclude that there will be another one. □

We will now consider conditions for two consecutive C-switchings which according to the above lemma gives a C-limit cycle. It is convenient to reformulate the conditions on $y_i(t)$ into equivalent conditions on $x_i(0)$ and system parameters. This can be done after rewriting (4.3) as

$$(-1)^{i-1}y_i(t) = \begin{cases} [b_0 + b_1/a]d - [(-1)^i x_i(0) + \dfrac{b_1 d}{a}]e^{-at} & a \neq 0 \\ b_0 d - (-1)^i x_i(0) + b_1 d \cdot t & a = 0 \end{cases}$$

Later, Lemma 4.2 can be used to express also $(-1)^i x_i(0)$ into system parameters. Assume that condition *a*) of the definition of $\mathbf{C}_i$ is satisfied. Then the conditions for the following switch to be $\mathbf{C}_i$ are, according to Lemma 4.1,

$$\begin{cases} -[(-1)^i x_i(0) + \dfrac{b_1 d}{a}] < \varepsilon - [b_0 + b_1/a]d \\ -[(-1)^i x_i(0) + \dfrac{b_1 d}{a}]e^{-a(h_i-\tau)} = \varepsilon - [b_0 + b_1/a]d, \quad h_i > \tau \end{cases} \qquad a \neq 0$$

$$\begin{cases} b_0 d - (-1)^i x_i(0) < \varepsilon \\ b_0 d - (-1)^i x_i(0) + b_1 d(h_i - \tau) = \varepsilon, \quad h_i > \tau \end{cases} \qquad a = 0$$

If $a > 0$, these conditions can hold if and only if

$$-[(-1)^i x_i(0) + \frac{b_1 d}{a}] < \varepsilon - [b_0 + b_1/a]d < 0$$

or rewritten

$$\begin{cases} [b_0 + b_1/a]d - \varepsilon > 0 \\ (-1)^i x_i(0) > b_0 d - \varepsilon \end{cases} \tag{4.7}$$

The first condition means that the stationary gain must be sufficiently large to be able to pass the hysteresis boundary, i.e. $G(0)d > \varepsilon$. The second condition rules out a **D**-switch. When $a < 0$, we get instead the conditions

$$0 < -[(-1)^i x_i(0) + \frac{b_1 d}{a}] < \varepsilon - [b_0 + b_1/a]d$$

or rewritten

$$b_0 d - \varepsilon < (-1)^i x_i(0) < -\frac{b_1 d}{a} \tag{4.8}$$

Again, the left condition is the one that rules out a **D**-switch. The right inequality guarantees that the hysteresis boundary is passed. When $a = 0$, the conditions are equivalent to

$$\begin{cases} (-1)^i x_i(0) > b_0 d - \varepsilon \\ b_1 d > 0 \end{cases} \tag{4.9}$$

Lemma 4.1 can now be reformulated into conditions on system parameters by expressing $(-1)^i x_i(0)$ according to Lemma 4.2.

LEMMA 4.4
If $\mathbf{C}_{i-1}$ then $\mathbf{C}_i$ if and only if

$$\begin{aligned} &\chi < \varepsilon - b_0 d < \frac{b_1 d}{|a|} \cdot \begin{cases} 1 & a > 0 \\ 2e^{a\tau} - 1 & a < 0 \end{cases} \\ &\chi < \varepsilon - b_0 d, \quad b_1 d > 0 \qquad a = 0 \end{aligned} \tag{4.10}$$

where χ is defined in (4.5).

Proof: Using the expression for $x_i(0)$ from Remark in Lemma 4.2, the condition $(-1)^i x_i(0) > b_0 d - \varepsilon$ in (4.7), (4.8) and (4.9) becomes

$$\begin{aligned} (-1)^i x_i(0) = -e^{-a\tau}[\chi + b_0 d - \varepsilon] - \chi > b_0 d - \varepsilon \\ \Leftrightarrow \quad \chi + b_0 d - \varepsilon < 0 \end{aligned}$$

which is the left inequality in (4.10). The conditions in (4.9) for the case $a = 0$ are now completely expressed in system parameters in (4.10). The first condition in (4.7), $b_0 d + b_1 d/a - \varepsilon > 0$, gives the right inequality of (4.10) for the case $a > 0$. When $a < 0$, Lemma 4.2 is used in the condition $(-1)^i x_i(0) < -b_1 d/a$ from (4.8). This gives

$$\begin{aligned} (-1)^i x_i(0) = \frac{b_1 d}{a} + e^{-a\tau}(\varepsilon - b_0 d - \frac{b_1 d}{a}) < -\frac{b_1 d}{a} \\ \Leftrightarrow \quad \varepsilon - b_0 d < -\frac{b_1 d}{a}(2e^{a\tau} - 1) \end{aligned}$$

which is the right inequality for the case $a < 0$. ∎

Remark. One can prove that (4.10) implies that $b_1 d > 0$. □

THEOREM 4.1
There exist initial conditions such that the relay feedback system (4.1) in Figure 4.1 enters a C-limit cycle, if and only if (4.10) is true. The period of the limit cycle, T, is unique and given by (4.6).

Proof: The fact that a C-limit cycle implies (4.10) follows directly from Lemma 4.4. The other direction, that (4.10) implies a C-limit cycle follows from Lemma 4.3 and Lemma 4.4, if initial conditions can be chosen such that the initial switch is $\mathbf{C}_1$. Thus, it remains to find $u_0(t)$, $y_0(t)$, $t \in (-\tau, 0)$ such that when the relay is connected at $t = 0$, with $u_1 = d$, there will be a C-switch. Choose $u_0(t)$ such that startup (4.2) is satisfied and such that $-x_1(0) = -\Phi[\chi + b_0 d - \varepsilon] - \chi$ as in Lemma 4.2. Then the system is started up at the limit cycle solution. Finally, the period time T follows from Lemma 4.3. ∎

second switch is a **D**-switch according to Lemma 4.6. Continuing like this gives successively that $(-1)^i x_i(0) = -\chi$, i.e. a **D**-limit cycle. The questions about the stability follow from Lemma 4.6 and the period was given in Lemma 4.5. ∎

Remark. It is not possible to have both a **C**-limit cycle and a **D**-limit cycle for the same system. □

It follows from Lemma 4.7 that the **D**-limit cycle is stable when $a \geq 0$. In order to find the initial conditions that will lead to the **D**-limit cycle a couple of lemmas will first be stated.

LEMMA 4.8
Suppose $a \geq 0$ and that there is a switch $\mathbf{C}_j$ or $\mathbf{D}_j$ followed by $\mathbf{D}_{j+1}$. Then all following switchings are **D**-switchings, $\mathbf{D}_i$ $\forall i > j+1$.

Proof: If the j:th switch is a **D**-switch the next state is

$$x_{j+1}(0) = x_j(\tau) = \Phi x_j(0) + \Gamma u_j$$

This can be written as

$$\begin{aligned}(-1)^{j+1} x_{j+1}(0) &= -\Phi(-1)^j x_j(0) + \Gamma d = \\ &= -\Phi[\chi + (-1)^j x_j(0)] - \chi\end{aligned}$$

But also the $(j+1)$:th switch is a **D**-switch. Therefore, the $(j+2)$:th switch satisfies

$$(-1)^{j+2} x_{j+2}(0) = (-\Phi)^2[\chi + (-1)^j x_j(0)] - \chi$$

It now remains to show that this switch is $\mathbf{D}_{j+2}$. If that is the case, we then have another two consecutive **D**-switchings, $\mathbf{D}_{j+1}\mathbf{D}_{j+2}$, which in the same way imply $\mathbf{D}_{j+3}$, and so on. The fact $\mathbf{D}_j\mathbf{D}_{j+1}$ implies by Lemma 4.6 that

$$\begin{matrix}\mathbf{D}_j \\ \mathbf{D}_{j+1}\end{matrix} \qquad \chi - b_0 d - \varepsilon < \left\{\begin{matrix}\chi + (-1)^j x_j(0) \\ -\Phi[\chi + (-1)x_j(0)]\end{matrix}\right\} \leq \chi + b_0 d - \varepsilon \qquad (4.13)$$

But $(-1)^{j+2} x_{j+2}(0) + \chi$ satisfies

$$\begin{aligned}(-1)^{j+2} x_{j+2}(0) + \chi &= (-\Phi)^2[\chi + (-1)^j x_j(0)] \\ &\geq \begin{cases} \chi + (-1)^j x_j(0) & \text{when} \quad \chi + (-1)^j x_j(0) < 0 \\ -\Phi[\chi + (-1)^j x_j(0)] & \text{when} \quad \chi + (-1)^j x_j(0) > 0 \end{cases} \\ &\leq \begin{cases} -\Phi[\chi + (-1)^j x_j(0)] & \text{when} \quad \chi + (-1)^j x_j(0) < 0 \\ \chi + (-1)^j x_j(0) & \text{when} \quad \chi + (-1)^j x_j(0) > 0 \end{cases}\end{aligned}$$

Remark. For every first order system with a time delay there are ε and d such that the relay feedback system will have a **C**-limit cycle. □

Remark. In the stable case when $\tau = 0$ and $\varepsilon = 0$ the conditions in the theorem implies that $G(s)$ must be nonminimum phase. □

The startup (4.2) makes all future switching conditions dependent only on $x(0)$. It now remains to investigate under what initials $x(0)$ the feedback system will enter a **C**-limit cycle. One possible startup has already been shown in the proof of Theorem 4.1. It is shown in the following theorem that there are only two ways to enter a **C**-limit cycle, either from $\mathbf{C}_1\mathbf{C}_2\ldots$ or from $\mathbf{D}_1\mathbf{C}_2\ldots$.

THEOREM 4.2
Suppose (4.10) is satisfied and that the startup is according to (4.2). Then

$$x_1(0) \in \begin{cases} I_1^C & \Leftrightarrow \quad \mathbf{C}_1\mathbf{C}_2\ldots \\ I_2^C & \Leftrightarrow \quad \mathbf{D}_1\mathbf{C}_2\mathbf{C}_3\ldots \\ I_3^C & \Leftrightarrow \quad \text{unstable stationarity} \\ I_4^C & \Leftrightarrow \quad \text{divergence} \\ I_5^C & \Leftrightarrow \quad \mathbf{D}_1\text{divergence} \end{cases}$$

When $a \geq 0$ the intervals are

$$\begin{cases} I_1^C = (-\infty, \varepsilon - b_0 d) \\ I_2^C = [\varepsilon - b_0 d, \varepsilon + b_0 d) \\ I_3^C, I_4^C, I_5^C = \emptyset \end{cases}$$

and when $a < 0$ the intervals are

$$\begin{cases} I_1^C = (\dfrac{b_1 d}{a}, \varepsilon - b_0 d) \\ I_2^C = [\varepsilon - b_0 d, \min\{\dfrac{b_1 d}{|a|}(2e^{a\tau} - 1), \quad \varepsilon + b_0 d\}) \\ I_3^C = \left\{\dfrac{b_1 d}{a}, \dfrac{b_1 d}{|a|}(2e^{a\tau} - 1)\right\} \qquad \text{when} \quad \dfrac{b_1 d}{|a|}(2e^{a\tau} - 1) < \varepsilon + b_0 d \\ I_3^C = \left\{\dfrac{b_1 d}{a}\right\} \qquad \text{when} \quad \dfrac{b_1 d}{|a|}(2e^{a\tau} - 1) > \varepsilon + b_0 d \\ I_4^C = (-\infty, \dfrac{b_1 d}{a}) \\ I_5^C = (\dfrac{b_1 d}{|a|}(2e^{a\tau} - 1), \varepsilon + b_0 d) \end{cases}$$

Proof: The startup (4.2) implies that Lemma 4.1 is applicable, which gives the conditions (4.7), (4.8) and (4.9) for the cases $a > 0$, $a < 0$ and $a = 0$ respectively. The condition (4.10) implies, by Lemma 4.3 and Lemma 4.4, that once there is a C-switch a C-limit cycle is reached. Since (4.10) is assumed, the system parameter constraints of the conditions (4.7)-(4.9) are satisfied. The remaining part is the dependence on the initial state. The conditions (4.7), (4.8) and (4.9) gives

$$\mathbf{C}_1 \quad \Leftrightarrow \quad x_1(0) \in \begin{cases} (-\infty, \varepsilon - b_0 d) & a \geq 0 \\ (b_1 d/a, \varepsilon - b_0 d) & a < 0 \end{cases}$$

But one C-switch implies by Lemma 4.3 and Lemma 4.4 that a C-limit cycle is reached, i.e.

$$I_1^C = \begin{cases} (-\infty, \varepsilon - b_0 d) & a \geq 0 \\ (b_1 d/a, \varepsilon - b_0 d) & a < 0 \end{cases}$$

On the other hand, if the first switch is $\mathbf{D}_1$, then $y(0-) < \varepsilon \leq y(0+)$, i.e.

$$\mathbf{D}_1 \quad \Leftrightarrow \quad x_1(0) \in [\varepsilon - b_0 d, \varepsilon + b_0 d)$$

and then $x_2(0) = \Phi x_1(0) + \Gamma d = -\Phi(\chi - x_1(0)) - \chi$. When $a \geq 0$, the conditions (4.7) and (4.9) give

$$\mathbf{C}_2 \quad \Leftrightarrow \quad \chi + \Phi^{-1}[\chi + b_0 d - \varepsilon] < x_1(0)$$

Thus, the conditions for $\mathbf{D}_1\mathbf{C}_2$ are

$$\left.\begin{array}{ll} D_1 & -[\chi + b_0 d - \varepsilon] \leq \\ C_2 & \Phi^{-1}[\chi + b_0 d - \varepsilon] < \end{array}\right\} x_1(0) - \chi < -[\chi - b_0 d - \varepsilon]$$

By (4.10) if follows that $\Phi^{-1}[\chi + b_0 d - \varepsilon] < 0 < -[\chi + b_0 d - \varepsilon]$. Therefore, $I_2^C = [\varepsilon - b_0 d, \varepsilon + b_0 d)$ when $a \geq 0$. The conditions (4.7) and (4.9) give no other restrictions on $x_1(0)$. Therefore, $I_3^C - I_5^C = \emptyset$ when $a \geq 0$. When $a < 0$, (4.8) gives

$$\left.\begin{array}{ll} D_1 & -[\chi + b_0 d - \varepsilon] \leq \\ C_2 & \Phi^{-1}[\chi + b_0 d - \varepsilon] < \end{array}\right\} x_1(0) - \chi < \begin{cases} -[\chi - b_0 d - \varepsilon] \\ \Phi^{-1}[\chi - b_1 d/a] \end{cases}$$

Again (4.10) implies that $\Phi^{-1}[\chi + b_0 d - \varepsilon] < 0 < -[\chi + b_0 d - \varepsilon]$. Therefore, since $\chi + \Phi^{-1}[\chi - b_1 d/a] = b_1 d/|a|(2e^{a\tau} - 1)$, the interval can be written as $I_2^C = [\varepsilon - b_0 d, \min(b_1 d/|a|(2e^{a\tau} - 1), \varepsilon + b_0 d))$ when $a < 0$. By (4.8) it follows that if $(-1)^i x_i(0) > -b_1 d/a$ then $x_i(t)$ is moving in the wrong

direction and the hysteresis will never be reached. Thus, $x_1(0) = b_1 d/a$ and $x_2(0) = -b_1 d/a$ corresponds to steady state solutions. Rewritten in $x_1(0)$ the second one becomes $x_1(0) = b_1 d/|a|(2e^{a\tau}-1)$ conditioned that the first switch is $\mathbf{D}_1$. Notice, that since $\mathbf{D}_1 \Leftrightarrow x_1(0) \in [\varepsilon - b_0 d, \varepsilon + b_0 d)$ it is only possible to reach the steady state solution $x_2(0) = -b_1 d/a$ if $b_1 d/|a|(2e^{a\tau} - 1) < \varepsilon + b_0 d$. This gives the intervals $I_3^C - I_5^C$. ∎

The two theorems will now be illustrated in an example. The system is assumed to fulfill the initial startup condition (4.2). The existence of a **C**-limit cycle is checked by Theorem 4.1 and different initials $x(0)$ are chosen according to Theorem 4.2 to show the different switching behaviours.

EXAMPLE 4.1
Consider the system (4.1) with parameters $b_0 = 0.5$, $b_1 = 1$, $a = -1$ and time delay $\tau = 1$. Let the relay characteristics be $d = 1$ and $\varepsilon = 0.1$. Then there exists a **C**-limit cycle solution, since by Theorem 4.1

$$\underbrace{\chi}_{-0.46} < \underbrace{\varepsilon - b_0 d}_{-0.40} < \underbrace{\frac{b_1 d}{|a|}(2e^{a\tau} - 1)}_{-0.26}$$

and the different startup intervals in Theorem 4.2 are

$$\begin{aligned} I_1^C &= (-1, -0.40) \\ I_2^C &= [-0.40, -0.26) \\ I_3^C &= \{-0.26, -1\} \\ I_4^C &= (-\infty, -1) \\ I_5^C &= (-0.26, 0.60) \end{aligned}$$

The following choices of $x(0)$ are illustrated in Figure 4.4.

$$x(0) = \begin{cases} -1.1 \in I_4^C & \text{divergence} \\ -1 \in I_3^C & \text{unstable stationarity} \\ -0.9 \in I_1^C & \mathbf{C}_1\mathbf{C}_2 \\ -0.45 \in I_1^C & \mathbf{C}_1\mathbf{C}_2 \\ -0.35 \in I_2^C & \mathbf{D}_1\mathbf{C}_2 \\ -0.25 \in I_5^C & \mathbf{D}_1 \text{ divergence} \end{cases}$$

The **C**-limit cycle period is $T = 3.0$. □

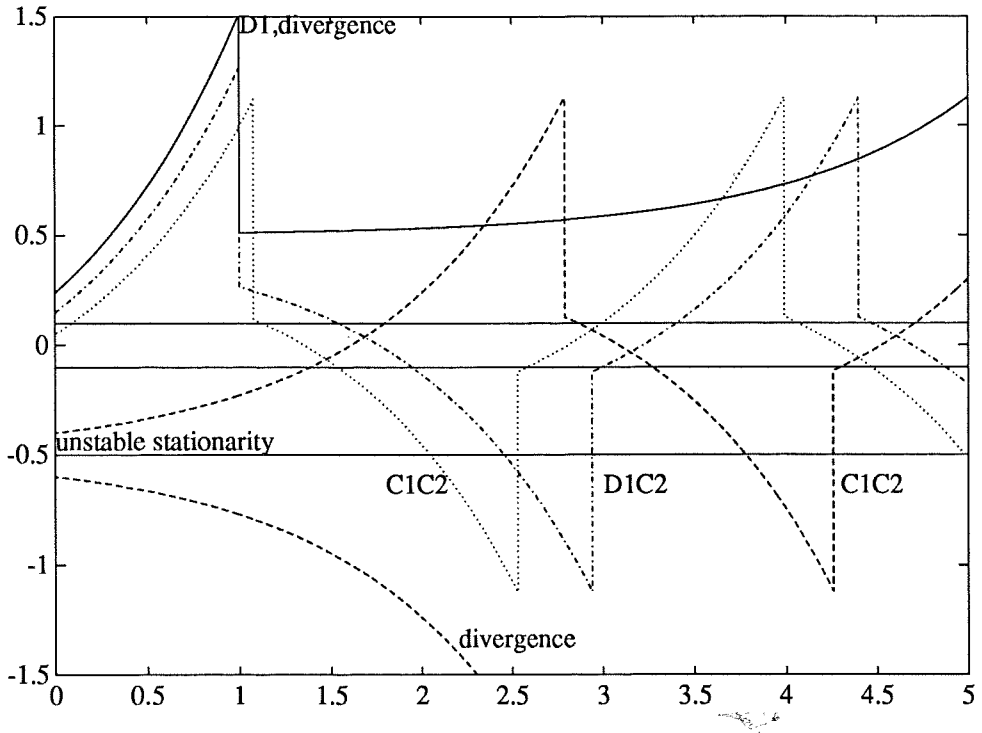

Figure 4.4 The system (4.1) with parameters $b_0 = 0.5$, $b_1 = 1$, $a = -1$ and time delay $\tau = 1$. The relay characteristics are $d = 1$ and $\varepsilon = 0.1$. Different initializations illustrate the behaviour according to Theorem 4.2. Note that $y_i(0+) = y_i(0-) + (-1)^{i-1} 2b_0 d$ and $y_i(0+) = (-1)^{i-1} b_0 d + x_i(0)$.

EXAMPLE 4.2

Modify the previous example to $a = -0.4$. Then there exists a C-limit cycle solution, since by Theorem 4.1

$$\underbrace{\chi}_{-0.49} < \underbrace{\varepsilon - b_0 d}_{-0.40} < \underbrace{\frac{b_1 d}{|a|}(2e^{a\tau} - 1)}_{0.85}$$

But

$$\underbrace{\varepsilon + b_0 d}_{0.6} < \underbrace{\frac{b_1 d}{|a|}(2e^{a\tau} - 1)}_{0.85} \quad \Rightarrow \quad \begin{cases} I_2^C = [\varepsilon - b_0 d, \varepsilon + b_0 d) \\ I_3^C = \{b_1 d/a\} \\ I_5^C = \emptyset \end{cases}$$

It is therefore not possible to get divergence after an initial D-switch. The

different startup intervals in Theorem 4.2 are

$$
\begin{aligned}
I_1^C &= (-2.5, -0.40) \\
I_2^C &= [-0.40, 0.60) \\
I_3^C &= \{-2.5\} \\
I_4^C &= (-\infty, -2.5) \\
I_5^C &= \emptyset
\end{aligned}
$$

The following choices of $x(0)$ are illustrated in Figure 4.5.

$$
x(0) = \begin{cases}
-2.51 \in I_4^C & \text{divergence} \\
-2.50 \in I_3^C & \text{unstable stationarity} \\
-2.49 \in I_1^C & \mathbf{C}_1\mathbf{C}_2 \\
\ \ 0.59 \in I_2^C & \mathbf{D}_1\mathbf{C}_2
\end{cases}
$$

The **C**-limit cycle period is $T = 2.6$.

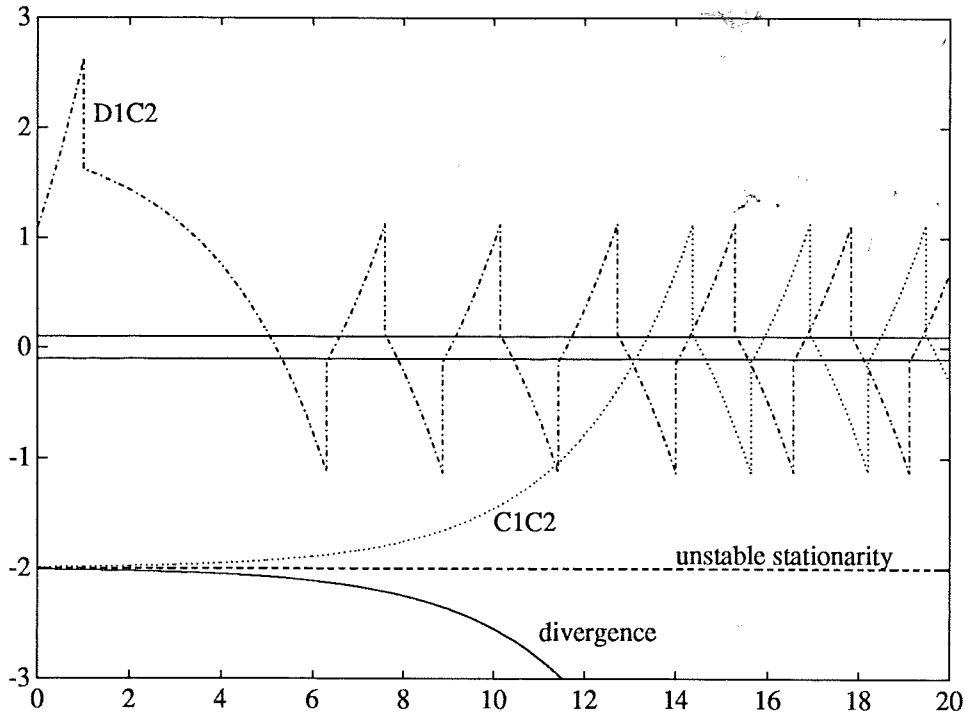

Figure 4.5 The system (4.1) with parameters $b_0 = 0.5$, $b_1 = 1$, $a = -0.4$ and time delay $\tau = 1$. The relay characteristics are $d = 1$ and $\varepsilon = 0.1$. Different initializations illustrate the behaviour according to Theorem 4.2. Note that $y_i(0+) = y_i(0-) + (-1)^{i-1} 2b_0 d$ and $y_i(0+) = (-1)^{i-1} b_0 d + x_i(0)$.

4.3 D-limit cycles

A **D**-limit cycle is defined as

DEFINITION 4.5—**D**-limit cycle
A **D**-limit cycle is a limit cycle consisting of an infinite sequence of **D**-switchings. □

The **D**-limit cycle differs form the **C**-limit cycle in many respects. First we notice that

LEMMA 4.5
All **D**-limit cycles have the period $T = 2\tau$.

Proof: Since $y(t_i)$ passes the hysteresis boundary at time t_i and, according to condition a) if the definition of $\mathbf{D}_i$, it has not passed the hysteresis boundary within a time period of τ, then the output passes the hysteresis boundary the first time at $t = t_i + \tau$. The next switch is therefore at $t_{i+1} = t_i + \tau$, i.e. the half period is $h_i = \tau$. ∎

Contrary to **C**-limit cycles, **D**-limit cycles are not reached in finite time. Nor can a stable **D**-limit cycle exist when $G(s)$ is unstable. Conditions for existence of **D**-limit cycles will be given. Also, the dependence on the initial state, $x_1(0)$, will be investigated. In order to do that the **D**-switch conditions are first reformulated into conditions on $x_i(0)$.

LEMMA 4.6
Suppose the system satisfies the condition a) in the definition of $\mathbf{D}_i$, i.e. that there has not been accumulation of switchings. Then the conditions $\mathbf{D}_i$ are satisfied, if and only if

$$-b_0 d < (-1)^i x_i(0) + \varepsilon \leq b_0 d \tag{4.11}$$

Proof: It follows from the definition of $\mathbf{D}_i$ and that $y_i(0+) = (-1)^{i-1} b_0 d + x_i(0) = y_i(0-) + (-1)^{i-1} 2 b_0 d$. ∎

Remark. In order to get **D**-switchings we have to have $b_0 d > 0$. □

Suppose there are only **D**-switchings. It is then straightforward to solve for $(-1)^{i-1} x_i(0)$ since we know that $h_i = \tau$, $\forall i$. The result is given below.

LEMMA 4.7
Suppose the system has only **D**-switchings, i.e. $\mathbf{D}_1 \mathbf{D}_2 \ldots \mathbf{D}_j$. Then

$$(-1)^i x_i(0) = (-\Phi)^{i-1} [\chi - x_1(0)] - \chi, \quad 1 \leq i \leq j+1$$

and

$$\begin{array}{lll} a>0 \quad : & & (-1)^i x_i(0) \to -\chi, \quad i \to \infty \\ a<0 \quad : & x_1(0)=\chi & (-1)^i x_i(0) = -\chi \\ a=0 \quad : & & (-1)^i x_i(0) = \begin{cases} -x_1(0) & i \text{ odd} \\ x_1(0)-2\chi & i \text{ even} \end{cases} \end{array}$$

Proof: Use that $\Gamma d = -\chi(1+\Phi)$ to eliminate Γd below

$$\begin{aligned} x_2(0) = x_1(\tau) &= \Phi x_1(0) + \Gamma d = -\Phi[\chi - x_1(0)] - \chi \\ -x_3(0) = -x_2(\tau) &= -\Phi x_2(0) + \Gamma d = (-\Phi)^2[\chi - x_1(0)] - \chi \\ &\vdots \\ (-1)^i x_i(0) &= (-\Phi)^{i-1}[\chi - x_1(0)] - \chi \end{aligned}$$

This can converge only in the stable case when $a > 0$ since then $\Phi < 1$. In the unstable case, $a < 0$, it will diverge when $x_1(0) \neq \chi$. When $a = 0$ the feedback system is at the stability boundary. Note that if $x_1(0) \neq \chi$ when $a = 0$ the limit cycle is asymmetrical. ∎

It is now possible to express the existence of **D**-limit cycles in conditions on system parameters.

THEOREM 4.3
There exist initial conditions such that the relay feedback system (4.1) in Figure 4.1 enters a **D**-limit cycle, if and only if

$$-b_0 d < -\chi + \varepsilon \leq b_0 d \tag{4.12}$$

Moreover, the limit cycle is

$$(-1)^i x_i(0) = \begin{cases} -\chi & a \neq 0 \\ \begin{cases} -x_1(0) & i \text{ odd} \\ x_1(0)-2\chi & i \text{ even} \end{cases} & a = 0 \end{cases}$$

which is stable when $a \geq 0$ and unstable when $a < 0$. The period is $T = 2\tau$.

Proof: The fact that a **D**-limit cycle implies (4.12) follows directly from Lemma 4.6 and Lemma 4.7. To realize that (4.12) implies a **D**-limit cycle we choose startup (4.2) and let $x_1(0) = \chi$. Then (4.12) implies that the first switch is a **D**-switch according to Lemma 4.6. The next state is then, according to Lemma 4.7, $x_2(0) = -\chi$. Again, then (4.12) implies that the

Now apply (4.13) which gives

$$-b_0 d < (-1)^{j+2} x_{j+2}(0) + \varepsilon \leq b_0 d$$

and Lemma 4.6 gives $\mathbf{D}_{j+2}$. The case with $\mathbf{C}_j\mathbf{D}_{j+1}$ follows in the same way with $(-1)^j x_j(0)$ replaced by $b_0 d - \varepsilon$. ∎

LEMMA 4.9
Suppose $a \geq 0$ and that (4.12) is satisfied. Also assume that $\varepsilon \geq 0$. Then after a **C**-switch, $\mathbf{C}_j$, it will follow only **D**-switchings, $\mathbf{D}_i$, $\forall i > j$. The same is true when $\varepsilon < 0$, if and only if

$$-\Phi[\chi + b_0 d - \varepsilon] > \chi - b_0 d - \varepsilon \tag{4.14}$$

otherwise no further switchings will occur.

Proof: By Lemma 4.8 it is enough to show that the $(j+1)$:th switch is a **D**-switch. The next state is

$$(-1)^{j+1} x_{j+1}(0) = -\Phi[\chi + b_0 d - \varepsilon] - \chi \leq b_0 d - \varepsilon$$

where the inequality follows from $\chi + b_0 d - \varepsilon \geq 0$ in (4.12). By Lemma 4.6 this switch therefore is $\mathbf{D}_{j+1}$ if and only if the condition (4.14) is satisfied. A **C**-switch cannot be followed by a $\mathbf{C}^*$-switch since a first order step response is monotone. Therefore, if (4.14) does not hold the hysteresis corresponding to the $(j+1)$:th switch is never passed. That can happen when $\varepsilon < 0$. However, when $\varepsilon \geq 0$, (4.14) is automatically satisfied. To see this we rewrite the state as

$$(-1)^{j+1} x_{j+1}(0) = -\Phi(b_0 d - \varepsilon) + \Gamma d = \begin{cases} -\Phi(b_0 d + b_1 d/a - \varepsilon) + b_1 d/a & a > 0 \\ -b_0 d + \varepsilon + b_1 d\tau & a = 0 \end{cases}$$

Since there was a **C**-switch we know from (4.7) and (4.9) that

$$\begin{cases} b_0 d + b_1 d/a - \varepsilon > 0 & a > 0 \\ b_1 d > 0 & a = 0 \end{cases}$$

Therefore

$$(-1)^{j+1} x_{j+1}(0) > -b_0 d + \varepsilon \geq -b_0 d - \varepsilon$$

where the assumption $\varepsilon \geq 0$ is used. Thus

$$-b_0 d < (-1)^{j+1} x_{j+1}(0) + \varepsilon \leq b_0 d$$

which imply $\mathbf{D}_{j+1}$ according to Lemma 4.6. ∎

LEMMA 4.10
After a **C**- or **D**-switch it cannot follow a **C***-switch if (4.14) holds.

Proof: If $\mathbf{C}_i^*$ then $(-1)^{i-1}y_i(0-) \geq \varepsilon$ and since $(-1)^{i-1}y(0-) = -b_0 d - (-1)^i x_i(0)$ the state must satisfy

$$(-1)^i x_i(0) \leq -b_0 d - \varepsilon$$

But after $\mathbf{C}_j$ the state satisfies

$$(-1)^{j+1}x_{j+1}(0) = -\Phi[\chi + b_0 d - \varepsilon] - \chi > -b_0 d - \varepsilon$$

where the inequality follows from (4.14). And after $\mathbf{D}_j$ the state satisfies

$$\left.\begin{aligned} &-b_0 d - \varepsilon < (-1)^j x_j(0) \leq b_0 d - \varepsilon \\ &(-1)^{j+1}x_{j+1}(0) = -\Phi[\chi + (-1)^j x_j(0)] - \chi \end{aligned}\right\} \Rightarrow$$
$$\Rightarrow \quad (-1)^{j+1}x_{j+1}(0) \geq -\Phi[\chi + b_0 d - \varepsilon] - \chi > -b_0 d - \varepsilon$$

Again, the last inequality follows from (4.14). Consequently, the $(j+1)$:th switch cannot be a **C***-switch. ∎

Remark. It is not a guarantee to get a **C***-switch when (4.14) is false. There are more conditions that must be fulfilled to get a **C***-switch. □

LEMMA 4.11
Suppose $a \geq 0$ and that (4.12) is satisfied. Also assume that startup (4.2) is used. Then the system converge to a **D**-limit cycle, by making only **D**-switchings, $\mathbf{D}_1\mathbf{D}_2\mathbf{D}_3\ldots$, if and only if

$$x(0) \in I_1^D = [\varepsilon - b_0 d, \Phi^{-1}(\chi + b_0 d - \varepsilon) + \chi] \cap (\Phi^{-1}(\chi - b_0 d - \varepsilon) + \chi, \varepsilon + b_0 d)$$

Proof: By Lemma 4.8 if is enough to show exactly the conditions for $\mathbf{D}_1\mathbf{D}_2$. According to Lemma 4.6 the conditions are

$$\begin{aligned} \mathbf{D}_1 \quad & -b_0 d < -x_1(0) + \varepsilon \leq b_0 d \\ \mathbf{D}_2 \quad & -b_0 d < x_2(0) + \varepsilon \leq b_0 d \end{aligned}$$

The second conditions can be rewritten in $x_1(0)$ by using Lemma 4.7. Then

$$\left.\begin{aligned} &\varepsilon - b_0 d \leq \\ &\Phi^{-1}(\chi - b_0 d - \varepsilon) + \chi < \end{aligned}\right\} x_1(0) \left\{\begin{aligned} &\leq \Phi^{-1}(\chi + b_0 d - \varepsilon) + \chi \\ &< \varepsilon + b_0 d \end{aligned}\right.$$

∎

LEMMA 4.12
Suppose $a \geq 0$ and that (4.12), (4.14) and

$$\begin{array}{ll} \varepsilon - b_0 d < b_1 d/a & a > 0 \\ b_1 d > 0 & a = 0 \end{array} \tag{4.15}$$

are satisfied. Also, assume that the startup (4.2) is used. Then the system converge to a **D**-limit cycle like, $\mathbf{C}_1\mathbf{D}_2\mathbf{D}_3\ldots$, if and only if

$$x(0) \in I_2^D = (-\infty, \varepsilon - b_0 d)$$

Proof: The conditions (4.15) together with $x(0) \in I_2^D$ give (4.7) and (4.9) which are exactly the conditions that give $\mathbf{C}_1$ when $a > 0$ and $a = 0$ respectively. Then the rest follows from Lemma 4.9. ∎

Remark. Notice, that when $a > 0$ it is possible to have $b_1 d < 0$ and still get $\mathbf{C}_1$, and then have convergence to a **D**-limit cycle. See Example 4.4. That is contrary to the **C**-limit cycle case.

LEMMA 4.13
Suppose $a \geq 0$ and that (4.12), (4.14) and (4.15) are satisfied. Also, assume that the startup (4.2) is used. Then the system converge to a **D**-limit cycle like, $\mathbf{D}_1\mathbf{C}_2\mathbf{D}_3\ldots$, if and only if

$$x(0) \in I_3^D = (\Phi^{-1}[\chi + b_0 d - \varepsilon] + \chi, \varepsilon + b_0 d)$$

Proof: From Lemma 4.6, an initial **D**-switch gives the constraints

$$\mathbf{D}_1 \qquad -b_0 d < -x_1(0) + \varepsilon \leq b_0 d \quad \rightarrow \quad x_1(0) \in [\varepsilon - b_0 d, \varepsilon + b_0 d) \tag{4.16}$$

Since the conditions (4.15) are satisfied a following **C**-switch will occur according to (4.7) and (4.9), if and only if

$$\mathbf{C}_2 \qquad x_2(0) + \varepsilon > b_0 d$$

where

$$x_2(0) = -\Phi[\chi - x_1(0)] - \chi$$

Expressed in $x_1(0)$ this gives the constraints

$$x_1(0) > \Phi^{-1}[\chi + b_0 d - \varepsilon] + \chi \geq \varepsilon - b_0 d \tag{4.17}$$

where the last inequality follows from $\chi + b_0 d - \varepsilon \geq 0$ in (4.12). The constraints (4.16) and (4.17) now gives I_3^D and by Lemma 4.9 all following switchings will be **D**-switchings. ∎

THEOREM 4.4
Suppose $a \geq 0$ and that (4.12) is satisfied. Also, assume that the startup is according to (4.2). Then

$$x_1(0) \in I_1^D \qquad \Leftrightarrow \qquad \mathbf{D}_1\mathbf{D}_2\ldots$$

Suppose also that (4.14) and (4.15) are satisfied. Then there can be **C**-switchings as well, but no **C***-switchings. The additional ways to reach a **D**-limit cycle are then

$$x_1(0) \in \begin{cases} I_2^D & \Leftrightarrow \quad \mathbf{C}_1\mathbf{D}_2\mathbf{D}_3\ldots \\ I_3^D & \Leftrightarrow \quad \mathbf{D}_1\mathbf{C}_2\mathbf{D}_3\ldots \end{cases}$$

The intervals are

$$\begin{cases} I_1^D = [\alpha,\beta] \cap (\mathcal{A},\mathcal{B}) \\ I_2^D = (-\infty,\alpha) \\ I_3^D = (\beta,\mathcal{B}) \end{cases}$$

where

$$\begin{cases} \alpha = \varepsilon - b_0 d \\ \beta = \Phi^{-1}[\chi + b_0 d - \varepsilon] + \chi \\ \mathcal{A} = \Phi^{-1}[\chi - b_0 d - \varepsilon] + \chi \\ \mathcal{B} = \varepsilon + b_0 d \end{cases}$$

Proof: The intervals I_1^D,I_2^D and I_3^D follows from the Lemmas 4.11-4.13 and Lemma 4.10 exclude the possibility to get a **C***-switch. ∎

Remark. The condition (4.14) is equivalent to $\alpha > \mathcal{A}$. Also, the conditions $\alpha < \mathcal{A}$ and (4.12) imply that $\mathcal{B} < \beta$. Therefore, when (4.14) fails the intervals become $I_1^D = (\mathcal{A},\mathcal{B})$ and $I_2^D = I_3^D = \emptyset$. See Example 4.3. □

Remark. Even though (4.12), (4.14) and (4.15) are satisfied it may happen that $I_3^D = \emptyset$, i.e. $\beta > \mathcal{B}$. See Example 4.4. □

Remark. The theorem does not exclude that it would be possible to get $\mathbf{D}_1\mathbf{C}_2^*$. □

EXAMPLE 4.3
Choose the parameters $b_0 = 0.1$, $b_1 = a = 1$, $\tau = 0.9$ and the relay amplitude $d = 1$ and hysteresis $\varepsilon = -0.5$. Also, assume that the startup (4.2) is used. The condition (4.12) is satisfied since

$$\underbrace{-b_0 d}_{-0.1} < \underbrace{-\chi + \varepsilon}_{-0.08} \leq \underbrace{b_0 d}_{0.1}$$

Therefore, a **D**-limit cycle exists, according to Theorem 4.3, and it is defined as $(-1)^i x_i(0) = -\chi = 0.42$. However, the convergence can not include any **C**-switchings, according to Theorem 4.4, since (4.14) is not satisfied. From the remark in Theorem 4.4 it follows that

$$I_1^D = (\mathcal{A}, \mathcal{B}) = (-0.48, -0.40)$$
$$I_2^D = I_3^D = \emptyset$$

The boundary cases $x_1(0) = -0.40$ and $x_1(0) = -0.48$ are shown as dashed and solid curves respectively in Figure 4.6.

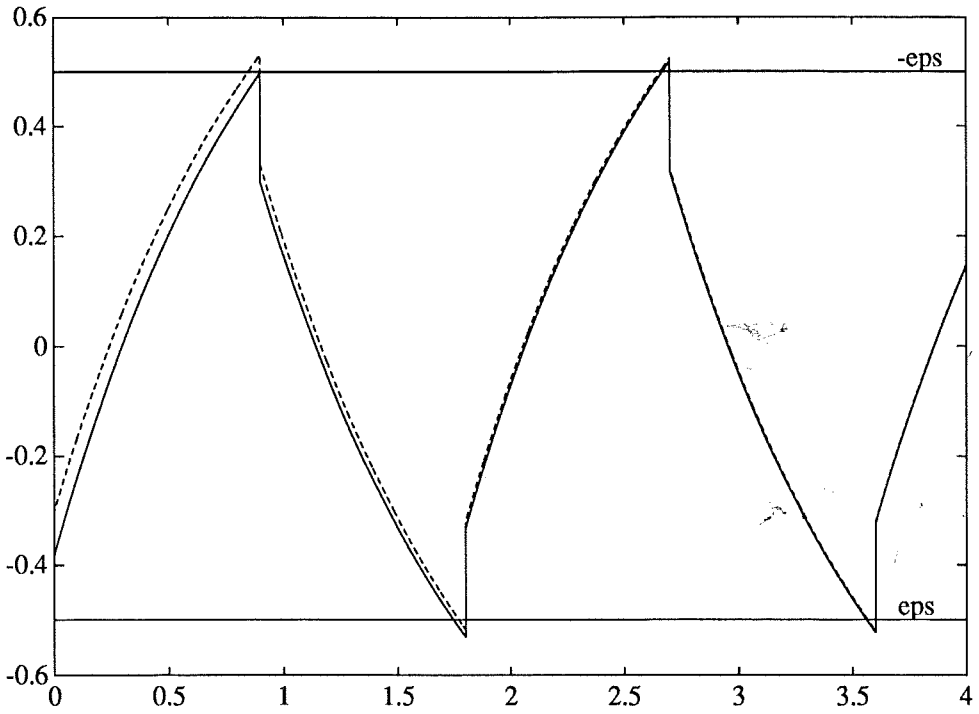

Figure 4.6 The parameters of the system (4.1) are $b_0 = 0.1$, $b_1 = a = 1$, $\tau = 0.9$ and the relay amplitude $d = 1$ and hysteresis $\varepsilon = -0.5$. The two initializations, $x_1(0) = -0.40, -0.48$, show the narrow convergence region.

□

EXAMPLE 4.4

Choose the parameters $b_0 = 0.1$, $b_1 = -0.1$, $a = 10$, $\tau = 1$ and the relay amplitude $d = 1$ and hysteresis $\varepsilon = 0.08$. Also, assume that the startup (4.2) is used. The condition (4.12) is satisfied since

$$\underbrace{-b_0 d}_{-0.1} < \underbrace{-\chi + \varepsilon}_{0.07} \leq \underbrace{b_0 d}_{0.1}$$

Therefore, a **D**-limit cycle exists, according to Theorem 4.3, and it is defined as $(-1)^i x_i(0) = -\chi = -0.01$. Also, the convergence can include a **C**-switch, according to Theorem 4.4, since (4.14) is satisfied. The interval boundaries, according to Theorem 4.4, are $\alpha = -0.02$, $\beta = 660$, $\mathcal{A} = -374$ and $\mathcal{B} = 0.18$. Since $\beta > \mathcal{B}$ then $I_3^D = \emptyset$, i.e the situation $\mathbf{D}_1\mathbf{C}_2$ is impossible. The intervals are

$$I_1^D = [\alpha, \mathcal{B}) = [-0.02, 0.18)$$
$$I_2^D = (-\infty, \alpha) = (-\infty, -0.02)$$
$$I_3^D = \emptyset$$

The following choices of $x_1(0)$ are illustrated in Figure 4.7.

$$x_1(0) = \begin{cases} -0.02 \in I_1^D & \mathbf{D}_1\mathbf{D}_2 \dots \\ 0.179 \in I_1^D & \mathbf{D}_1\mathbf{D}_2 \dots \\ -0.15 \in I_2^D & \mathbf{C}_1\mathbf{D}_2 \dots \end{cases}$$

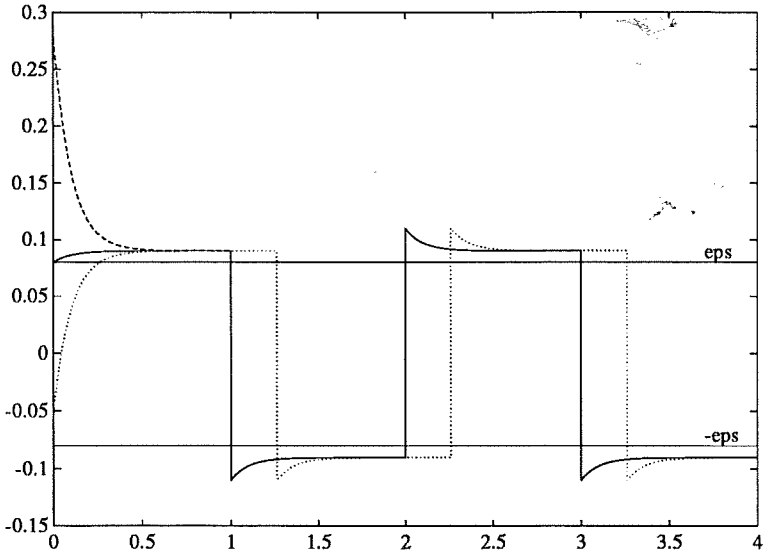

Figure 4.7 The parameters of the system (4.1) are $b_0 = 0.1$, $b_1 = -0.1$, $a = 10$, $\tau = 1$ and the relay amplitude $d = 1$ and hysteresis $\varepsilon = 0.08$. The following initializations are shown, $x_1(0) = -0.02 \in I_1^D$ (solid), $x_1(0) = 0.179 \in I_1^D$ (dashed) and $x_1(0) = -0.15 \in I_2^D$ (dotted). Notice, that it is possible to have $b_1 d < 0$, which is not possible when having a **C**-limit cycle. Notice also, that $I_3^D = \emptyset$.

□

EXAMPLE 4.5
Choose the parameters $b_0 = 0.1$, $b_1 = a = 1$, $\tau = 0.1$ and the relay amplitude $d = 1$ and hysteresis $\varepsilon = 0.04$. Also, assume that the startup (4.2) is used. The condition (4.12) is satisfied since

$$\underbrace{-b_0 d}_{-0.1} < \underbrace{-\chi + \varepsilon}_{0.09} \leq \underbrace{b_0 d}_{0.1}$$

Therefore, a **D**-limit cycle exists, according to Theorem 4.3, and it is defined as $(-1)^i x_i(0) = -\chi = 0.05$. Also, the convergence can include a **C**-switch, according to Theorem 4.4, since (4.14) is satisfied. The interval boundaries, according to Theorem 4.4, are $\alpha = -0.06$, $\beta = -0.04$, $\mathcal{A} = -0.26$ and $\mathcal{B} = 0.14$. The intervals are

$$\begin{aligned} I_1^D &= [\alpha, \beta] = [-0.06, -0.04] \\ I_2^D &= (-\infty, \alpha) = (-\infty, -0.06) \\ I_3^D &= (\beta, \mathcal{B}) = (-0.04, 0.14) \end{aligned}$$

The following choices of $x_1(0)$ are illustrated in Figure 4.8.

$$x_1(0) = \begin{cases} -0.06 \in I_1^D & \mathbf{D}_1\mathbf{D}_2\ldots \\ -0.04 \in I_1^D & \mathbf{D}_1\mathbf{D}_2\ldots \\ -0.2 \in I_2^D & \mathbf{C}_1\mathbf{D}_2\ldots \\ 0.13 \in I_3^D & \mathbf{D}_1\mathbf{C}_2\mathbf{D}_3\ldots \end{cases}$$

□

4.4 CD-limit cycles

A **CD**-limit cycle is defined as

DEFINITION 4.6—**CD**-limit cycle
A **CD**-limit cycle is a limit cycle consisting of an infinite sequence of **C**- and **D**-switchings, such that one period consists of one **C**-switch followed by one **D**-switch.
□

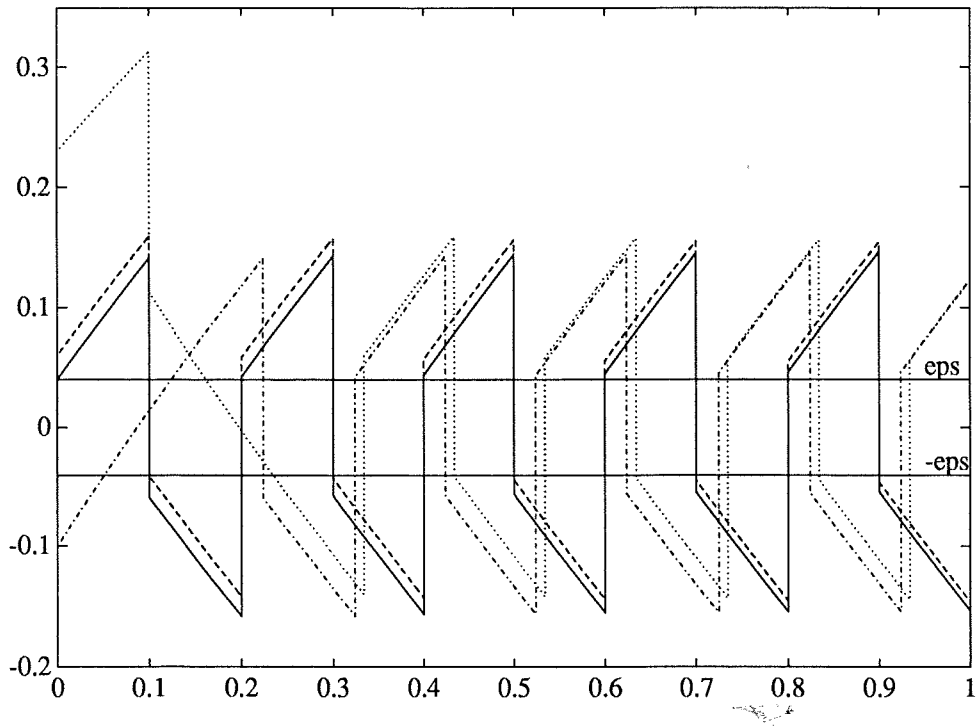

Figure 4.8 The parameters of the system (4.1) are $b_0 = 0.1$, $b_1 = a = 1$, $\tau = 0.1$ and the relay amplitude $d = 1$ and hysteresis $\varepsilon = 0.04$. The following initializations are shown, $x_1(0) = -0.06 \in I_1^D$ (solid), $x_1(0) = -0.04 \in I_1^D$ (dashed), $x_1(0) = -0.2 \in I_2^D$ (dashed-dotted) and $x_1(0) = 0.13 \in I_3^D$ (dotted).

LEMMA 4.14
Suppose $a < 0$ and there are switchings, $\mathbf{C}_j\mathbf{D}_{j+1}\mathbf{C}_{j+2}$. Then the **CD**-limit cycle is reached and the state satisfies

$$
\begin{aligned}
&(-1)^j x_j(h_j - \tau) = b_0 d - \varepsilon, \qquad h_j > \tau \\
&(-1)^{j+1} x_{j+1}(0) = (-1)^{j+1} x_j(h_j) = -\Phi[\chi + b_0 d - \varepsilon] - \chi \\
&(-1)^{j+2} x_{j+2}(0) = (-1)^{j+2} x_{j+1}(\tau) = \Phi^2[\chi + b_0 d - \varepsilon] - \chi \\
&(-1)^{j+2} x_{j+2}(h_{j+2} - \tau) = b_0 d - \varepsilon, \qquad h_{j+2} > \tau
\end{aligned}
$$

The limit cycle period, T, is unique and defined by

$$
T = 2\tau + (h_{j+2} - \tau) = 2\tau + \frac{1}{a} \ln \left\{ \frac{-\Phi^2[\chi + b_0 d - \varepsilon] + \chi - b_1 d/a}{\varepsilon - [b_0 + b_1/a]d} \right\}
$$

Proof: The remark in Lemma 4.2 gives the expression for $x_{j+1}(0)$. Then

using that $\Gamma d = -\chi(1+\Phi)$ we get

$$(-1)^{j+2}x_{j+2}(0) = (-1)^{j+2}[\Phi x_{j+1}(0) + \Gamma u_{j+1}] = -\Phi(-1)^{j+1}x_{j+1}(0) + \Gamma d =$$
$$= -\Phi[\chi + (-1)^{j+1}x_{j+1}(0)] - \chi = \Phi^2[\chi + b_0 d - \varepsilon] - \chi$$

Then use that

$$(-1)^{j+2}x_{j+2}(h_{j+2} - \tau) =$$
$$= b_0 d - \varepsilon = (-1)^{j+2}[\Phi(h_{j+2} - \tau)x_{j+2}(0) + \Gamma(h_{j+2} - \tau)u_{j+2}] =$$
$$= e^{-a(h_{j+2}-\tau)}[\Phi^2(\chi + b_0 d - \varepsilon) - \chi] - b_1 d/a(1 - e^{-a(h_{j+2}-\tau)}) =$$
$$= e^{-a(h_{j+2}-\tau)}[\Phi^2(\chi + b_0 d - \varepsilon) - \chi + b_1 d/a] - b_1 d/a$$

$$\Rightarrow \quad h_{j+2} - \tau = \frac{1}{a}\ln\left\{\frac{-\Phi^2[\chi + b_0 d - \varepsilon] + \chi - b_1 d/a}{\varepsilon - [b_0 + b_1/a]d}\right\}$$

■

THEOREM 4.5
There exist initial conditions such that the relay feedback system (4.1) in Figure 4.1 enters a **CD**-limit cycle, if and only if

$$\begin{cases} a < 0 \\ \chi - b_0 d - \varepsilon < -\Phi[\chi + b_0 d - \varepsilon] < 0 \\ \Phi^2[\chi + b_0 d - \varepsilon] - \chi < -b_1 d/a \end{cases} \tag{4.18}$$

No other limit cycles involving both **C**- and **D**-switchings are possible.

Proof: From Lemma 4.8 if follows that we must have $a < 0$. From Lemma 4.6 if follows that after $\mathbf{C}_j$ it will follow $\mathbf{D}_{j+1}$ if and only if

$$-b_0 d < (-1)^j x_j(0) + \varepsilon \leq b_0 d$$

Put in the expression for $(-1)^j x_j(0)$ from Lemma 4.14. This gives

$$\chi - b_0 d - \varepsilon < -\Phi[\chi + b_0 d - \varepsilon]$$

and

$$-\Phi[\chi + b_0 d - \varepsilon] \leq \chi + b_0 d - \varepsilon \quad \Leftrightarrow \quad \chi + b_0 d - \varepsilon \geq 0$$

respectively. But if $\chi + b_0 d - \varepsilon = 0$ a **D**-limit cycle is reached once the hysteresis is reached continuously. Because $(-1)^j x_j(h_j - \tau) = b_0 d - \varepsilon = -\chi$ gives according to Lemma 4.7, that $(-1)^i x_i(0) = -\chi$, $\forall i > j$. Therefore we

have to have $\chi + b_0 d - \varepsilon > 0$. Since $a < 0$ the following switch is $\mathbf{C}_{j+2}$ according to (4.8), if and only if

$$b_0 d - \varepsilon < (-1)^{j+2} x_{j+2}(0) < -b_1 d/a$$

Put in the expression for $(-1)^{j+2} x_{j+2}(0)$ from Lemma 4.14. This gives the constraints

$$\chi + b_0 d - \varepsilon > 0$$

and

$$\Phi^2[\chi + b_0 d - \varepsilon] - \chi < -b_1 d/a$$

respectively. Suppose instead that the switch is $\mathbf{D}_{j+2}$. Then

$$(-1)^{j+2} x_{j+2}(0) \leq b_0 d - \varepsilon$$

which after using the expression from Lemma 4.14, gives

$$\begin{cases} \chi + b_0 d - \varepsilon \geq 0 & \& \quad a \geq 0 \\ \chi + b_0 d - \varepsilon < 0 & \& \quad a < 0 \end{cases}$$

But $\chi + b_0 d - \varepsilon > 0$ and $a < 0$. Therefore $\mathbf{D}_{j+2}$ is impossible. A limit cycle involving both **C**- and **D**-switchings can therefore not have two consecutive **D**-switchings. Nor can there be two consecutive **C**-switchings, since that would imply, by Lemma 4.3, that a **C**-limit cycle is reached. ∎

THEOREM 4.6
Suppose (4.18) is satisfied and that the startup is according to (4.2). Then

$$x_1(0) \in I_j^{CD} \quad \Leftrightarrow \quad \mathbf{D}_1\mathbf{D}_2 \ldots \mathbf{D}_{j-1}\mathbf{C}_j\mathbf{D}_{j+1}\mathbf{C}_{j+2} \ldots$$

where the interval is

$$I_j^{CD} = \begin{cases} \left(\dfrac{b_1 d}{a}, \varepsilon - b_0 d\right), & j = 1 \\ \left(\chi + \Phi^{-1}[\chi + b_0 d - \varepsilon], \min\{\chi + \Phi^{-1}[\chi - \dfrac{b_1 d}{a}], \varepsilon + b_0 d\}\right), & j = 2 \\ \left[\chi - \Phi^{-(j-3)}[\chi + b_0 d - \varepsilon], \chi - \Phi^{-(j-1)}[\chi + b_0 d - \varepsilon]\right), \text{ odd} & j \geq 3 \\ \left(\chi + \Phi^{-(j-1)}[\chi + b_0 d - \varepsilon], \chi + \Phi^{-(j-3)}[\chi + b_0 d - \varepsilon]\right], \text{ even} & j \geq 4 \end{cases}$$

Proof: It follows from Lemma 4.6 and Lemma 4.7 that the conditions for $\mathbf{D}_1\mathbf{D}_2 \ldots \mathbf{D}_{j-1}$ are

$$\Phi^{-(i-1)}[\chi - b_0 d - \varepsilon] < (-1)^i (x_1(0) - \chi) \leq \Phi^{-(i-1)}[\chi + b_0 d - \varepsilon], \quad 1 \leq i \leq j-1$$

and from (4.8) that it will follow a **C**-switch if and only if

$$\Phi^{-(j-1)}[\chi + b_0 d - \varepsilon] < (-1)^i (x_1(0) - \chi) < \Phi^{-(j-1)}[\chi - b_1 d/a]$$

The function Φ^{-i} is decreasing with increasing i. Therefore, the above constraints for $\mathbf{D}_1 \ldots \mathbf{D}_{j-1}$ hold if they hold when $i = j-2$ and $i = j-1$. Thus, the conditions for $\mathbf{D}_1 \ldots \mathbf{D}_{j-1}\mathbf{C}_j$ are when $i \geq 3$

$$\begin{aligned}
\mathbf{D}_{j-2}: &\quad \Phi^{-(j-3)}[\chi - b_0 d - \varepsilon] < (-1)^j (x_1(0) - \chi) \leq \Phi^{-(j-3)}[\chi + b_0 d - \varepsilon] \\
\mathbf{D}_{j-1}: &-\Phi^{-(j-2)}[\chi + b_0 d - \varepsilon] \leq (-1)^j (x_1(0) - \chi) < -\Phi^{-(j-2)}[\chi - b_0 d - \varepsilon] \\
\mathbf{C}_j: &\quad \Phi^{-(j-1)}[\chi + b_0 d - \varepsilon] < (-1)^j (x_1(0) - \chi) < \Phi^{-(j-1)}[\chi - b_1 d/a]
\end{aligned}$$

But from (4.18) it follows that

$$\left.\begin{aligned} &\Phi^{-(j-3)}[\chi - b_0 d - \varepsilon] \\ -&\Phi^{-(j-2)}[\chi + b_0 d - \varepsilon] \end{aligned}\right\} < 0 < \Phi^{-(j-1)}[\chi + b_0 d - \varepsilon]$$

and that

$$\Phi^{-(j-3)}[\chi + b_0 d - \varepsilon] = \begin{cases} \Phi^{-(j-2)}\Phi[\chi + b_0 d - \varepsilon] < -\Phi^{-(j-2)}[\chi - b_0 d - \varepsilon] \\ \Phi^{-(j-1)}\Phi^2[\chi + b_0 d - \varepsilon] < \Phi^{-(j-1)}[\chi - b_1 d/a] \end{cases}$$

Therefore we get the constraints

$$\Phi^{-(j-1)}[\chi + b_0 d - \varepsilon] < (-1)^j (x_1(0) - \chi) \leq \Phi^{-(j-3)}[\chi + b_0 d - \varepsilon]$$

which then gives the intervals when $j \geq 3$. When $j = 1$, (4.8) gives directly I_1^{CD}. When $j = 2$, (4.8) and (4.11) give

$$\left.\begin{aligned} \mathbf{D}_1: &\quad -[\chi + b_0 d - \varepsilon] \leq \\ \mathbf{C}_2: &\quad \Phi^{-1}[\chi + b_0 d - \varepsilon] < \end{aligned}\right\} x_1(0) - \chi \begin{cases} < -[\chi - b_0 d - \varepsilon] \\ < \Phi^{-1}[\chi - b_1 d/a] \end{cases}$$

By (4.18) it follows that $-[\chi + b_0 d - \varepsilon] < \Phi^{-1}[\chi + b_0 d - \varepsilon]$. Then I_2^{CD} follows as above. ∎

EXAMPLE 4.6

Consider the system (4.1) with parameters $b_0 = b_1 = 1$, $a = -0.5$, $\tau = 0.1$ in a relay feedback loop with relay characteristics $d = 1$ and $\varepsilon = 0.1$. According to Theorem 4.5 there exists a **CD**-limit cycle, since (4.18) is satisfied.

$$\begin{cases} \underbrace{\chi - b_0 d - \varepsilon}_{-1.15} < \underbrace{-\Phi[\chi + b_0 d - \varepsilon]}_{-0.9} \\ \underbrace{\Phi^2[\chi + b_0 d - \varepsilon] - \chi}_{1} < \underbrace{-b_1 d/a}_{2} \end{cases}$$

Start with $x_1(0) = 0 \neq \chi = -0.05$. Then according to Theorem 4.6, the **CD**-limit cycle will be reached after the 58:th switch, since

$$\vdots$$
$$I_{56}^{CD} = (4 \cdot 10^{-3}, 1 \cdot 10^{-2}]$$
$$x_1(0) \in I_{58}^{CD} = (-8 \cdot 10^{-4}, 4 \cdot 10^{-3}]$$

The situation is illustrated in Figure 4.9. An oscillation starts near the unstable symmetrical **D**-limit cycle. But since, $x_1(0) \neq \chi$, the oscillations will drift over into the stable asymmetrical **CD**-limit cycle.

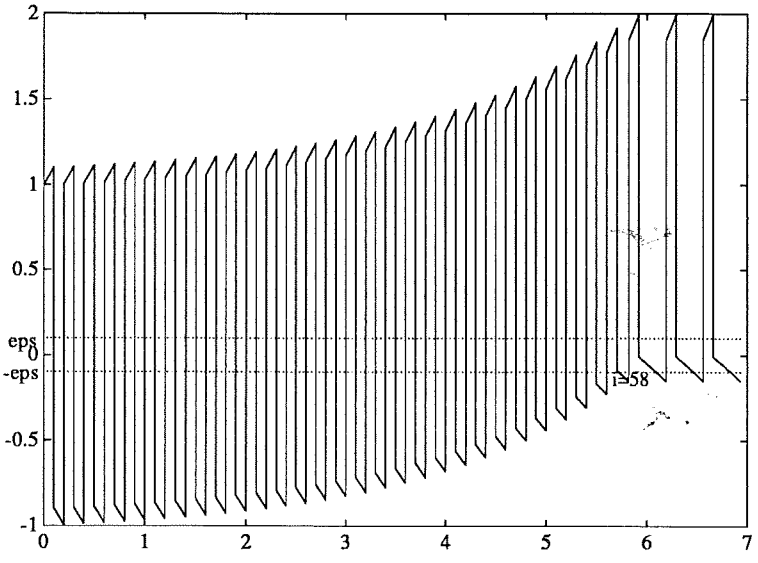

Figure 4.9 An oscillation starts near the unstable symmetrical **D**-limit cycle and drifts over to the stable asymmetrical **CD**-limit cycle. Since $x_1(0) \in I_{58}^{CD}$, the **CD**-limit cycle is reached after the 58:th switch.

The intervals giving a **CD**-limit cycle after 2 and 4 switchings respectively are

$$I_2^{CD} = (0.759, 1.100]$$
$$I_4^{CD} = (0.682, 0.759]$$

The two choices of initials

$$x_1(0) = \begin{cases} 0.76 \in I_2^{CD} \\ 0.75 \in I_4^{CD} \end{cases}$$

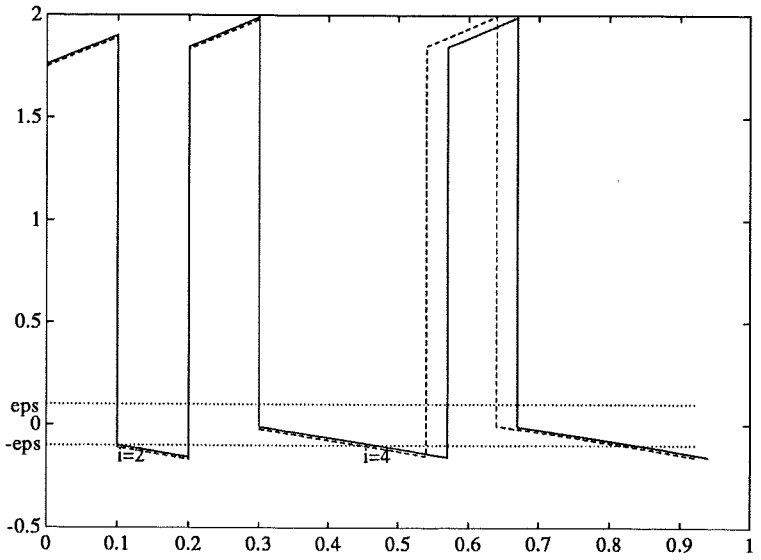

Figure 4.10 Two initials $x_1(0) \in I_2^{CD}$ (solid) and $x_1(0) \in I_4^{CD}$ (dashed), will make the relay feedback system reach a stable asymmetrical **CD**-limit cycle after the second and fourth switch respectively. The period of the **CD**-limit cycle is $T = 0.37$.

are illustrated in Figure 4.10. The period is $T = 0.37$. □

EXAMPLE 4.7—The limit cycle period in a bifurcation diagram

Consider the system (4.1) with parameters $b_0 = b_1 = 1$, $a = -0.5$ and the relay characteristics $d = 1$ and $\varepsilon = 0.1$. Depending on the time delay τ there will be one stable **C**-limit cycle solution or two solutions: one stable **CD**-limit cycle and another unstable **D**-limit cycle. This is illustrated in a bifurcation diagram in Figure 4.11, where the limit cycle period T is plotted against the time delay τ. □

4.5 C*- and C*D-limit cycles

A **C***-limit cycle is defined as

DEFINITION 4.7—**C***-limit cycle

A **C***-limit cycle is a limit cycle consisting of an infinite sequence of **C***-switchings. □

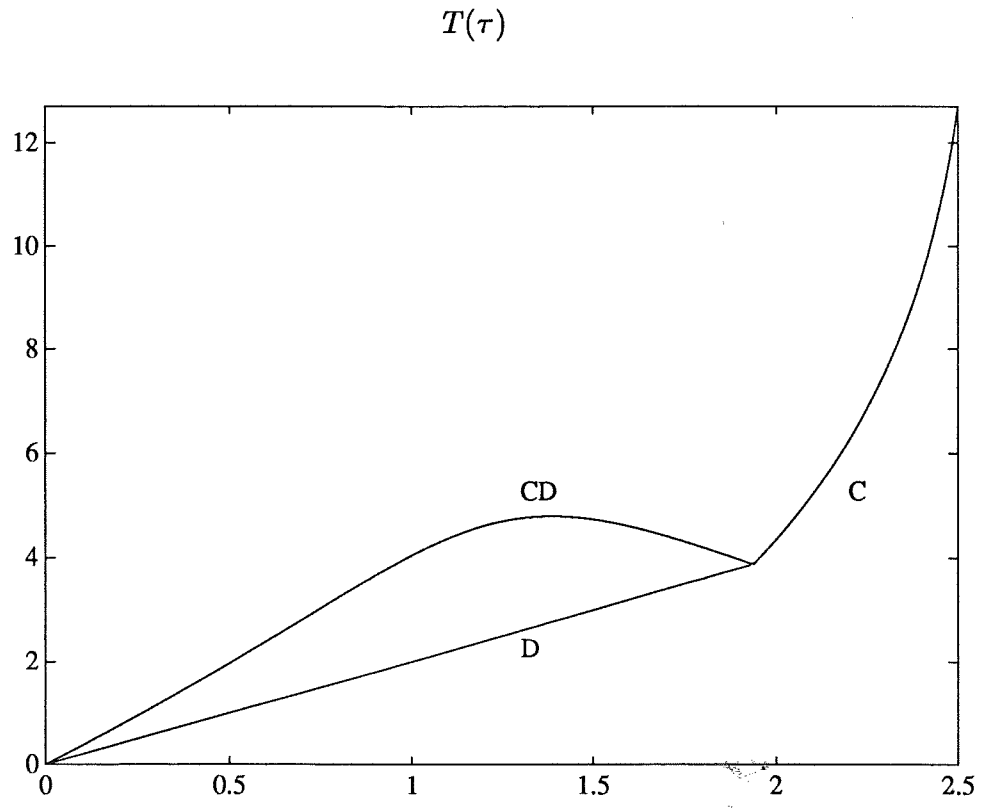

Figure 4.11 The limit cycle period T as a function of the time delay τ. The other parameters are $b_0 = b_1 = 1$, $a = -0.5$, and the relay parameters are $d = 1$ and $\varepsilon = 0.1$.

From the definition of a C*-switch it follows that

$$\mathbf{C}_i^*: \quad \begin{cases} \dfrac{d}{dt}(-1)^{i-1}y_{i-1}(t) > 0 \\ (-1)^{i-1}y_{i-1}(t) = \varepsilon \end{cases}$$

The situation is illustrated in Figure 4.12, where i is odd such that $u_i = d$. At switch i, the following hysteresis has been passed already at θ_{i-1} time units earlier. Since (4.3) gives that

$$(-1)^{i-1}y_{i-1}(t) = b_0 d + (-1)^{i-1}x_{i-1}(t) = \\ = \begin{cases} -[b_0 + b_1/a]d + [(-1)^{i-1}x_{i-1}(0) + b_1 d/a]e^{-at} & a \neq 0 \\ (-1)^{i-1}x_{i-1}(0) - b_0 d - b_1 d \cdot t & a = 0 \end{cases}$$

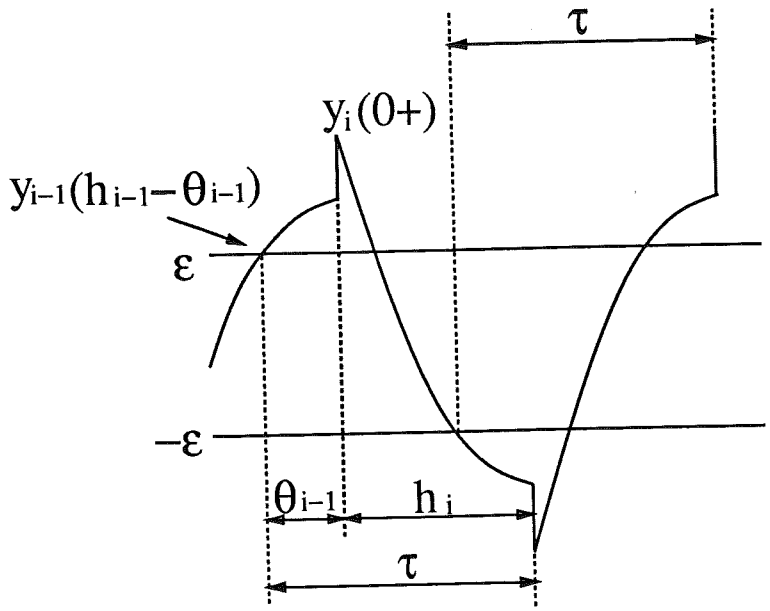

Figure 4.12 Illustration of $\mathbf{C}^*$-switches where the time between the switches are less then the time delay, $h_i < \tau$.

the conditions for $\mathbf{C}_i^*$ becomes

$$\begin{cases} (-1)^{i-1}x_{i-1}(0) + b_1 d/a < \varepsilon + [b_0 + b_1/a]d < 0 & a > 0 \\ 0 < (-1)^{i-1}x_{i-1}(0) + b_1 d/a < \varepsilon + [b_0 + b_1/a]d & a < 0 \\ (-1)^{i-1}x_{i-1}(0) < \varepsilon + b_0 d, \quad b_1 d < 0 & a = 0 \end{cases} \tag{4.19}$$

The following boundaries of a $\mathbf{C}^*$-limit cycle can be estimated.

LEMMA 4.15
If a $\mathbf{C}^*$-limit cycles, $(-1)^i x^*$, exists, it must satisfy

$$\begin{aligned} b_1 d/a < (-1)^i x^* < 0 \qquad & a > 0 \\ -b_1 d/a < (-1)^i x^* < 0 \qquad & a < 0 \\ b_1 d < 0, \quad (-1)^i x^* < 0 \qquad & a > 0 \end{aligned} \tag{4.20}$$

Proof: From the definition of $\mathbf{C}_i^*$ it follows that

$$\begin{aligned} (-1)^{i-1}x_{i-1}(0) &< \varepsilon + b_0 d \\ (-1)^{i-1}x_{i-1}(h_{i-1} - \theta_{i-1}) &= \varepsilon + b_0 d \\ (-1)^{i-1}x_{i-1}(h_{i-1}) &\geq \varepsilon + b_0 d \end{aligned}$$

The last inequality gives

$$(-1)^i x_i(0) = (-1)^i x_{i-1}(h_{i-1}) \leq -(\varepsilon + b_0 d)$$

i.e. a C*-limit cycle satisfies both $(-1)^i x^* < \varepsilon + b_0 d$ and $(-1)^i x^* \leq -(\varepsilon + b_0 d)$. Therefore

$$(-1)^i x^* < 0$$

Then (4.20) follows from (4.19) when $a \leq 0$. It remains the boundary $b_1 d/a < (-1)^i x^*$ when $a > 0$. But a C*-switch gives when $a > 0$ that

$$\begin{aligned}(-1)^i x_i(0) &= (-1)^i[\Phi(\theta_{i-1})x_{i-1}(h_{i-1} - \theta_{i-1}) + \Gamma(\theta_{i-1})u_{i-1}] = \\ &= -e^{-a\theta_{i-1}}(\varepsilon + b_0 d) + \frac{b_1 d}{a}(1 - e^{-a\theta_{i-1}}) = \\ &= -e^{-a\theta_{i-1}}[\varepsilon + (b_0 + b_1/a)d] + \frac{b_1 d}{a} > \frac{b_1 d}{a}\end{aligned}$$

where the inequality follows from (4.19). ∎

Remark. It follows from the lemma that $b_1 d < 0$. Notice, that such a constraint can not give a C-limit cycle. □

The map $(-1)^i x_i(0) \to (-1)^{i+1} x_{i+1}(0)$, caused by a C*-switch, will now be derived and its stability properties will be investigated. First, we notice that

$$\begin{aligned}(-1)^i x_i(0) &= (-1)^i x_{i-1}(h_{i-1}) = \\ &= (-1)^i[\Phi(\theta_{i-1})x_{i-1}(h_{i-1} - \theta_{i-1}) + \Gamma(\theta_{i-1})u_{i-1}] = \\ &= \begin{cases} -e^{-a\theta_{i-1}}[\varepsilon + (b_0 + b_1/a)d] + \dfrac{b_1 d}{a} & a \neq 0 \\ -(\varepsilon + b_0 d) + b_1 d \cdot \theta_{i-1} & a = 0 \end{cases}\end{aligned} \tag{4.21}$$

At the next switch we get

$$\begin{aligned}(-1)^{i+1} x_{i+1} x(0) &= (-1)^{i+1} x_i(h_i) = -\Phi(h_i)(-1)^i x_i(0) + \Gamma(h_i)d = \\ &= \begin{cases} -e^{-ah_i}[(-1)^i x_i(0) + \dfrac{b_1 d}{a}] + \dfrac{b_1 d}{a} & a \neq 0 \\ -(-1)^i x_i(0) + b_1 d \cdot h_i & a = 0 \end{cases}\end{aligned}$$

Use that $h_i = \tau - \theta_{i-1}$ and from (4.21) that

$$\begin{aligned} e^{a\theta_{i-1}} &= -\frac{(b_0 + b_1/a)d + \varepsilon}{(-1)^i x_i(0) - b_1 d/a} && a \neq 0 \\ -b_1 d\theta_{i-1} &= -(\varepsilon + b_0 d) - (-1)^i x_i(0) && a = 0 \end{aligned}$$

Then we get

$$(-1)^{i+1} x_{i+1}(0) = \begin{cases} e^{-a\tau}[(b_0 + \dfrac{b_1}{a})d + \varepsilon]\dfrac{(-1)^i x_i(0) + b_1 d/a}{(-1)^i x_i(0) - b_1 d/a} + \dfrac{b_1 d}{a}, & a \neq 0 \\ b_1 d\tau - (\varepsilon + b_0) - 2(-1)^i x_i(0) & a = 0 \end{cases}$$

Introduce for brevity

$$\begin{cases} x_i := (-1)^i x_i(0) \\ A := e^{-a\tau}[(b_0 + b_1/a)d + \varepsilon] \\ B := \dfrac{b_1 d}{a} \end{cases}$$

then the map can be written

$$x_{i+1} = f(x_i) = \begin{cases} A\dfrac{x_i + B}{x_i - B} + B & a \neq 0 \\ b_1 d\tau - (\varepsilon + b_0 d) - 2x_i & a = 0 \end{cases}$$

THEOREM 4.7
All $\mathbf{C}^*$-limit cycles are unstable.

Proof: The case $a = 0$ is clear since $f'(x) = -2$, $\forall x$. When $a \neq 0$ the derivative is

$$f'(x) = -\frac{2AB}{(x - B)^2}$$

At the limit cycle solution, x^*, we have

$$x^* = f(x^*) \quad \Rightarrow \quad (x^* - B)^2 = A(x^* + B)$$

Thus,

$$f'(x^*) = -\frac{2B}{x^* + B} < -1$$

where the inequality follows from Lemma 4.15. ∎

A $\mathbf{C}^*\mathbf{D}$-limit cycle is defined as

DEFINITION 4.8—$\mathbf{C}^*\mathbf{D}$-limit cycle
A $\mathbf{C}^*\mathbf{D}$-limit cycle is a limit cycle consisting of an infinite sequence of $\mathbf{C}^*$- and $\mathbf{D}$-switchings, such that one period consists of one $\mathbf{C}^*$-switch followed by one $\mathbf{D}$-switch. □

LEMMA 4.16
Suppose there exists a $\mathbf{C}^*$-limit cycle and that $a \neq 0$. Then after $\mathbf{C}_j^*$ it will follow

$$\begin{aligned} \mathbf{C}_{j+1}^* \quad &\Leftrightarrow \quad -\chi \leq x_j \leq -(b_0 d + \varepsilon) \\ \mathbf{D}_{j+1} \quad &\Leftrightarrow \quad f^{-1}(b_0 d - \varepsilon) \leq x_j < -\chi \end{aligned}$$

Proof: Since the j :th switch is a C*-switch, then $(-1)^{i-1}y_i(0-) \geq \varepsilon$. This gives

$$x_i \leq -(b_0 d + \varepsilon)$$

The next switch is a C*-switch, if and only if

$$x_{i+1} = f(x_i) \leq -(b_0 d + \varepsilon) \tag{4.22}$$

But

$$f'(x) = \frac{-2AB}{(x-B)^2} < 0$$

since $A < 0$ and $A > 0$ when $a > 0$ and $a < 0$ respectively by (4.19), and $B < 0$ and $B > 0$ when $a > 0$ and $a < 0$ respectively by Lemma 4.15. Therefore the constraint (4.22) can be written

$$f^{-1}(-(b_0 d + \varepsilon)) < x_i$$

According to (4.11) the next switch is instead a D-switch, if and only if

$$-b_0 d - \varepsilon < f(x_i) \leq b_0 d - \varepsilon$$

Again, since $f' < 0$ this gives the constraints

$$f^{-1}(b_0 d - \varepsilon) \leq x_i < f^{-1}(-b_0 d - \varepsilon)$$

Then since

$$f^{-1}(x) = B\frac{A + x - B}{-A + x - B}$$

it follows that $f^{-1}(-b_0 d - \varepsilon) = -\chi$. ∎

The map $x_i \rightarrow x_{i+1}$, caused by a D-switch, is

$$x_{i+1} = (-1)^{i+1}x_{i+1}(0) = -(-1)^i x_i(\tau) = -\Phi(-1)^i x_i(0) + \Gamma d =$$
$$= g(x_i) = \begin{cases} -\Phi[x_i + B] + B & a \neq 0 \\ -x_i + b_1 d\tau & a = 0 \end{cases}$$

Define the map $x_{i+2} = F(x_i)$, where $F(x_i) = f(f(x_i))$ if there are two consecutive C*-switches and $F(x_i) = g(f(x_i))$ if the i:th switch is a C*-switch and the following switch is a D-switch, i.e.

$$F: \begin{cases} f \circ f: & x_i \longrightarrow x_{i+2} & -\chi \leq x_i \leq -(b_0 d + \varepsilon) \\ g \circ f: & x_i \xrightarrow{f} x_{i+1} \xrightarrow{g} x_{i+2} & f^{-1}(b_0 d - \varepsilon) \leq x_i < -\chi \end{cases}$$

LEMMA 4.17
There exists no **C*D**-limit cycle when $a < 0$.

Proof: When $a < 0$ the conditions for $\mathbf{C}_i^*$ gives

$$\begin{aligned} x_i &= (-1)^i[\Phi(\theta_{i-1})x_{i-1}(h_{i-1} - \theta_{i-1}) + \Gamma(\theta_{i-1})u_{i-1}] = \\ &= -e^{-a\theta_{i-1}}[\varepsilon + (b_0 + b_1/a)d] + b_1 d/a \\ &\begin{cases} \leq -\varepsilon - b_0 d < B \\ > -e^{-a\tau}[\varepsilon + (b_0 + b_1/a)d] + b_1 d/a = -A + B \end{cases} \end{aligned}$$

Hence, $0 < B - x_i < A$ which gives that $A/(B - x_i) > 1$. Now, suppose x is a **C*D**-limit cycle solution. Then

$$x = g(f(x)) = -\Phi[(A\frac{x+B}{x-B} + B) + B] + B$$

i.e.

$$x - B = \Phi[\frac{A}{B-x}(x+B) - 2B]$$

But the right hand side gives that

$$\underbrace{\Phi}_{>1}[\underbrace{\frac{A}{B-x}}_{>1}(x+B) - 2B] \begin{cases} > x - B & \text{when } x + B > 0 \\ < x - B & \text{when } x + B < 0 \end{cases}$$

Consequently, there is no such solution x. ∎

THEOREM 4.8
Suppose there exist both a **C***- and a **C*D**-limit cycle. Then the **C*D**-limit cycle is stable.

Proof: The derivative of the map that is defining a **C***-switch followed by a **D**-switch is

$$F'(x) = \frac{d}{dt}g(f(x)) = \frac{2AB\Phi}{(x-B)^2} > 0$$

The inequality follows from that, when $a > 0$, then $A < 0$ by (4.19) and $B < 0$ by Lemma 4.15. By the assumptions there exist both a **C***- and a **C*D**-limit cycle and the **C***-limit cycle is unstable, by Theorem 4.7. But $F(x)$ is continuous. Therefore, there can only exist a **C*D**-limit cycle solution, x, if $0 < F'(x) < 1$, i.e. a stable solution. ∎

Remark. This doesn't mean that a **C*D**-limit cycle always is stable. When $\chi - b_0 d - \varepsilon < 0$ there exists no **C***-limit cycle. In spite of that a **C*D**-limit

cycle can exist. Also, a stable **D**-limit cycle can exist under such a constraint. It seems, thought, that the **C*D**-limit cycle then always becomes unstable. □

EXAMPLE 4.8—**C***- and **C*D**-limit cycles
Consider the system (4.1) with $b_0 = 0.1$, $b_1 = -1$, $a = 1$, the time delay $\tau = 1$ and the relay characteristics $d = 1$ and $\varepsilon = 0.3$. Suppose the startup situation is $y(t) < \varepsilon$ then $t \in [-\tau, 0-]$ and $u(0+) = d$. Then $y(0+) > \varepsilon$ if $x(0) > \varepsilon - b_0 d = 0.2$ which will cause a **D**-switch. Choose $x(0) = 0.55$ which will make a startup close to the unstable **C***-limit cycle. The map F is defined as

$$F : \begin{cases} f \circ f & \text{when } -0.462 < x_i < -0.4 \\ g \circ f & \text{when } -0.56 < x_i < -0.462 \end{cases}$$

The map $x_{i+2} = F(x_i)$ is shown in Figure 4.13. The convergence is shown starting with x_2 near the unstable **C***-limit cycle and successively drifting down to the left towards the stable asymmetrical **C*D**-limit cycle.

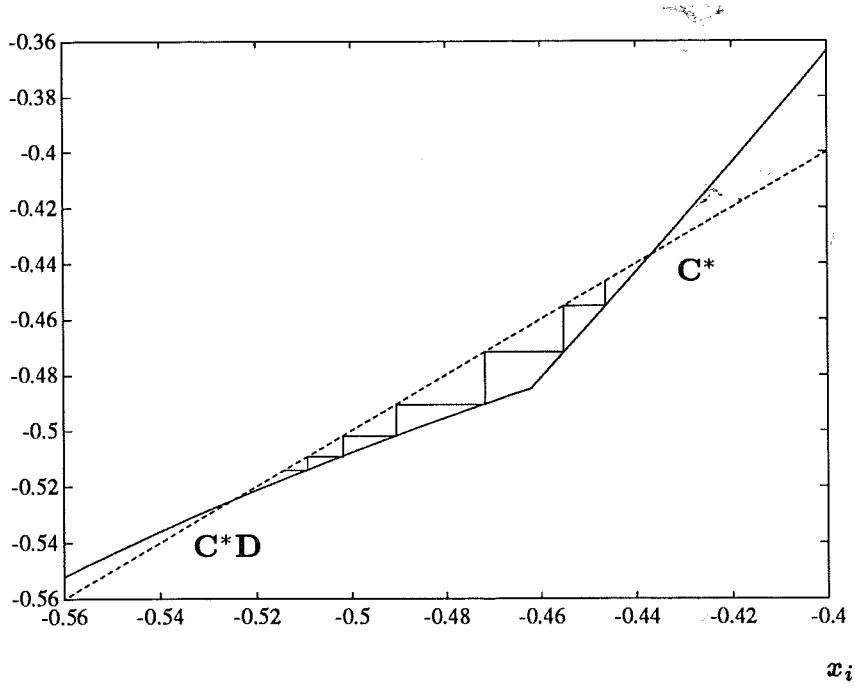

Figure 4.13 The map $x_{i+2} = F(x_i)$ (solid curve) and the unity map $x_{i+2} = x_i$ (dashed line). Starting with x_2 near the unstable **C***-limit cycle successive maps, shown as the staircase, will converge to the asymmetrical **C*D**-limit cycle.

The corresponding curve $y(t)$ is shown in Figure 4.14. □

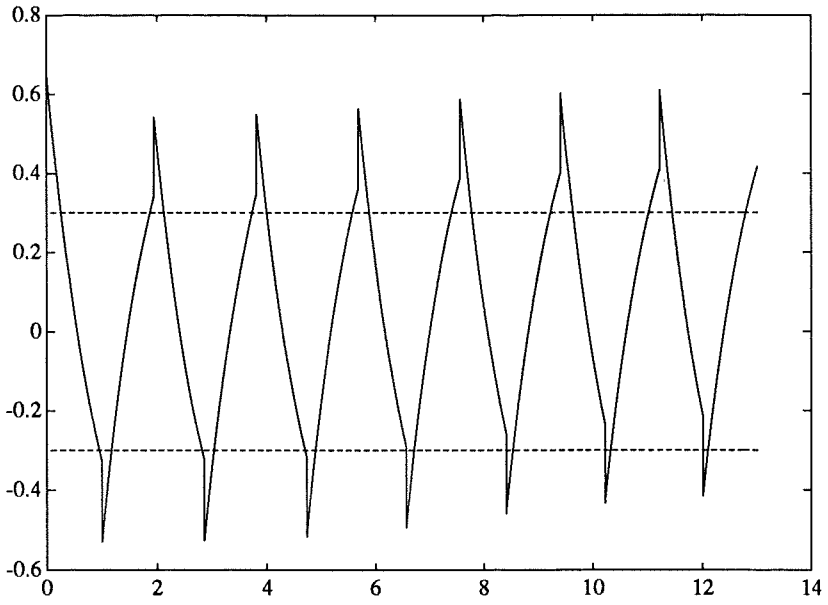

Figure 4.14 Convergence to a $\mathbf{C^*D}$-limit cycle when starting near the unstable $\mathbf{C^*}$-limit cycle. Compare with Figure 4.13.

4.6 Summary

It has been shown that relay feedback of first order systems with direct term and a time delay can exhibit different types of limit cycles. It is interesting to notice that a few expressions repeatedly show up in the analysis as conditions associated with the different types of limit cycles. To give a quick overview these expressions are listed below.

$$\begin{cases} \mathbf{C} - \text{limit cycle} & \Rightarrow \quad \chi + b_0 d - \varepsilon < 0 \\ \mathbf{D} - \text{limit cycle} & \Rightarrow \quad \chi + b_0 d - \varepsilon \geq 0 \end{cases}$$

$$\begin{cases} \mathbf{D} - \text{limit cycle} & \Rightarrow \quad \chi - b_0 d - \varepsilon < 0 \\ \mathbf{C^*} - \text{limit cycle} & \Rightarrow \quad \chi - b_0 d - \varepsilon \geq 0 \end{cases}$$

$$\begin{cases} \mathbf{C} - \text{limit cycle} & \Rightarrow \quad b_1 d > 0 \\ \mathbf{C^*} - \text{limit cycle} & \Rightarrow \quad b_1 d < 0 \end{cases}$$

$$\begin{cases} \mathbf{CD} - \text{limit cycle} & \Rightarrow \quad \chi - b_0 d - \varepsilon < -\Phi(\chi + b_0 d - \varepsilon) \\ \mathbf{C^*D} - \text{limit cycle} & \Rightarrow \quad \chi - b_0 d - \varepsilon \geq -\Phi(\chi + b_0 d - \varepsilon) \end{cases}$$

Where χ is given by (4.5) and $\Phi = e^{-a\tau}$. Notice that a system can sometimes reach different types of limit cycles depending on initial conditions. There

are systems that can reach

$$\begin{cases} \text{unstable} & \mathbf{D} - \text{limit cycle} \\ \text{stable} & \mathbf{CD} - \text{limit cycle} \end{cases}$$

Another possibility is

$$\begin{cases} \text{unstable} & \mathbf{C}^* - \text{limit cycle} \\ \text{stable} & \mathbf{C}^*\mathbf{D} - \text{limit cycle} \end{cases}$$

However, a system can have a $\mathbf{C}^*\mathbf{D}$-limit cycle without having a $\mathbf{C}^*$-limit cycle. Such a system might instead have a **D**-limit cycle. It is not clear whether the $\mathbf{C}^*\mathbf{D}$-limit cycle in such a case must be unstable. No example have been found where a system can have more than one type of stable limit cycle. It has, however, not been shown and is left as a conjecture, i.e.

$$\begin{cases} \text{unstable?} & \mathbf{C}^*\mathbf{D} - \text{limit cycle} \\ \text{stable} & \mathbf{D} - \text{limit cycle} \end{cases}$$

The particular studied startup (4.2) assumes that no prior passing of the hysteresis has been made before the relay is connected. If there is no passing at the moment of connection, i.e. if the first switch is not a **D**-switch, then a first switch can only be a **C**-switch. This particular startup, without an initial **D**-switch, can only give rise to three different types of limit cycles. Thus, if the first switch is a **C**-switch one system can only reach one of the following types of limit cycles.

$$\begin{cases} \mathbf{C} - \text{limit cycle} \\ \mathbf{D} - \text{limit cycle} \\ \mathbf{CD} - \text{limit cycle} \end{cases}$$

Which one of these that can be reached is depending only on the system parameters. How the limit cycle is reached is depending on initial conditions.

5

Second order systems

Consider the second order system

$$\ddot{y} + a_1\dot{y} + a_2 y = b_1\dot{u} + b_2 u \qquad (5.1)$$

in a feedback loop with a relay having amplitude, d, and the hysteresis, ε. The behaviour of the system is quite complex. For the purpose of analysis a number of different cases are considered separately.

- Transfer function with real poles and no zero
- Transfer function with complex poles and no zero
- Transfer function with real poles and a zero

First a theorem of general nature will be given. This guarantees convergence to a limit cycle for any stable second order system during relay feedback provided, however, that a unique limit cycle exists. The existence and uniqueness questions are then answered in separate subsections for the different cases above. Conditions for the existence and the uniqueness are shown for the case with no zero in the transfer function. Before the study of the different special cases another theorem of general nature is also given. The theorem is relating results for stable systems to corresponding results for unstable systems. This is useful when investigating all possible situations of stable and unstable systems in the special cases above. There are, however, some borderline cases where one or two of the eigenvalues are zero that are not considered. Also, the case with a zero in the transfer function is not fully explored. Examples are given to show that in this case there is not always a unique limit cycle solution.

We will address the question of convergence to a limit cycle. It is convenient to introduce the Poincaré map, $\mathcal{P}$.

DEFINITION 5.1—The Poincaré map, $\mathcal{P}$
The above relay feedback system (5.1) has two switch lines in the phase plane, see Figure 5.1. One where the relay output changes from $u = d$ to $u = -d$, defined as $\mathcal{S}_{+-} = \{y = \varepsilon, \dot{y} > 0\}$ and another for the opposite switch, $\mathcal{S}_{-+} = \{y = -\varepsilon, \dot{y} < 0\}$. From the symmetry $\mathcal{S}_{+-} = -\mathcal{S}_{-+}$. The Poincaré map is the map from $\mathcal{S}_{+-}$ to itself, i.e. $\mathcal{P}((\varepsilon, \dot{y}(0))) = -(\varepsilon, \dot{y}(t))$. For brevity we use $\mathcal{P}(\dot{y}(0)) = -y(t)$ where it is assumed that $y(0) = \varepsilon$ and $y(t) = -\varepsilon$. When there is a zero in the transfer function, $b_1 \neq 0$, then $\dot{y}(0)$ is discontinuous. In such a case the map is defined from $t = 0-$, i.e. $\mathcal{P}(\dot{y}(0-))$. □

The Poincaré map is useful since a fixpoint of the map, $\mathcal{P}(\dot{y}^*) = \dot{y}^*$, corresponds to a limit cycle solution in the phase plane, $(y, \dot{y})$. The limit cycle is stable if $|\mathcal{P}'| < 1$.

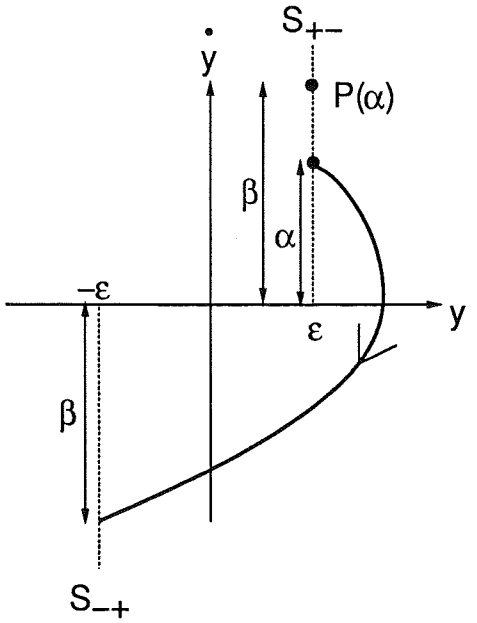

Figure 5.1 Definition of the Poincaré map, $\mathcal{P} : \mathcal{S}_{+-} \to \mathcal{S}_{+-}$, i.e. $\mathcal{P}(\dot{y}(0)) = -\dot{y}(t)$, where $y(0) = \varepsilon$ and $-y(t) = \varepsilon$. In the Figure we have $\mathcal{P}(\alpha) = \beta > \alpha$.

When $b_1 \neq 0$ there is a discontinuity at $\mathcal{S}_{+-}$ when the relay switches from $u = d$ to $u = -d$. Introduce the notation $G(s) = B(s)/A(s)$ and let $t = 0$ at the switch line $\mathcal{S}_{+-}$. Then the Laplace transformed system is

$$Y = G(s)U + \frac{s + a_1}{A(s)} y(0-) + \frac{1}{A(s)} \dot{y}(0-) - \frac{b_1}{A(s)} u(0-)$$

where $Y = \mathcal{L}[y]$, $U = \mathcal{L}[u] = -d/s$, $y(0-) = \varepsilon$, $\dot{y}(0-) > 0$, $u(0-) = d$. From the initial value theorem it follows that $y(0+) = y(0-) = \varepsilon$ and that the discontinuity is

$$\dot{y}(0+) = \dot{y}(0-) - 2b_1 d$$

The following theorem uses the fact that phase plane trajectories cannot cross each other. This means that the $\mathcal{P}$-map will be monotone and growing, i.e. $\mathcal{P}'(\dot{y}(0-)) > 0$, as long as $\dot{y}(0+) > 0$. However, if $b_1 d > 0$, then $\dot{y}(0+) < 0$ when $\dot{y}(0-) < 2b_1 d$. This will make the $\mathcal{P}$-map nonmonotone, i.e. $\mathcal{P}'(\dot{y}(0-)) < 0$ when $\dot{y}(0-) < 2b_1 d$ and $\mathcal{P}'(\dot{y}(0-)) > 0$ when $\dot{y}(0-) > 2b_1 d$. In the theorem, only the monotone part of $\mathcal{S}_{+-}$ is considered, i.e. where $\mathcal{P}' > 0$.

THEOREM 5.1—Global stability for stable systems during relay feedback
Assume that the second order system (5.1) is asymptotically stable and connected in a relay feedback loop with the relay gain, d, and hysteresis, ε. Also, assume there exists a unique limit cycle $\mathcal{P}(\dot{y}^*) = \dot{y}^* > \max(2b_1 d, 0)$ on $\mathcal{S}_{+-}$. Then for all initials $\dot{y}(0) > \max(2b_1 d, 0)$ on $\mathcal{S}_{+-}$, the system will converge monotonously to the limit cycle, i.e.

$$\mathcal{P}(\dot{y}_i) = \dot{y}_{i+1} \to \dot{y}^*, \quad i \to \infty$$

where $\dot{y}_0 = \dot{y}(0)$ and $0 < \mathcal{P}'(\dot{y}^*) < 1$.

Proof: The solution must be finite since an asymptotically stable system is always bounded-input-bounded-output stable. Thus, if the Poincaré map, $\mathcal{P}$, is monotone, consecutive mappings $\mathcal{P}(\dot{y}_0) = \dot{y}_1, \mathcal{P}(\dot{y}_1) = \dot{y}_2, \ldots$ must in the limit reach a finite fixpoint, $\mathcal{P}(\dot{y}^*) = \dot{y}^*$, i.e. a limit cycle in the phase plane $(y, \dot{y})$. The monotonicity is realized from the fact that trajectories in the phase plane cannot cross each other for an autonomous, linear, time invariant, second order system. When $b_1 = 0$ the transformation, $z = y + b_2 d/a_2$, makes the system autonomous between the switch lines $\mathcal{S}_{+-}$ and $\mathcal{S}_{-+}$, i.e. $\ddot{z} + a_1 \dot{z} + a_2 z = 0$. Once the uniqueness is established, we know that the solution is stable and that the convergence is global, $\mathcal{P}^k(\dot{y}(0)) \to \dot{y}^*$, $k \to \infty$, for all $(y(0), \dot{y}(0)) \in \mathcal{S}_{+-}$.

Now let $b_1 \neq 0$. Then there is a discontinuity $\dot{y}(0+) - \dot{y}(0-) = -2b_1 d$ on $\mathcal{S}_{+-}$. But this doesn't change the monotonicity of $\mathcal{P}$ as long as $\dot{y}(0+) > 0$. If $\dot{y}(0+) < 0$ when $\varepsilon > 0$, then the $\mathcal{P}$-map is nonmonotone, $\mathcal{P}'(\dot{y}(0-)) < 0$. The relay function will be undefined if $\dot{y}(0+) < 0$ when $\varepsilon < 0$ since the trajectory will reach $\mathcal{S}_{+-}$ once again instead of reaching $\mathcal{S}_{-+}$ as we want. The demand $\dot{y}(0+) > 0$ is guaranteed if $\dot{y}(0-) > \max(2b_1 d, 0)$, which is a restriction of $\mathcal{S}_{+-}$. ∎

The theorem gives information about the behaviour of a stable second order system during relay feedback only when an assumed unique limit cycle

exists. It does not say anything about conditions for existence or uniqueness of a limit cycle. These conditions will be given for the special case where there is no zero in the transfer function.

The results for stable systems can be transferred to results for unstable systems by use of duality. The duality will be defined in a theorem. The idea is to recognize a symmetry between different trajectories in the phase plane $(y, \dot{y})$. The state vector $x = (y, \dot{y})^T$ gives the realization

$$\dot{x} = Ax + Bu = \begin{pmatrix} 0 & 1 \\ -\lambda_1\lambda_2 & \lambda_1 + \lambda_2 \end{pmatrix} x + \begin{pmatrix} 0 \\ b \end{pmatrix} u$$

Assume $u = -d$. Then the stationary point is

$$\hat{x} = -A^{-1}B(-d) = \begin{pmatrix} -bd/(\lambda_1\lambda_2) \\ 0 \end{pmatrix}$$

In all expressions, the factors b and d always appear as the product bd. It is therefore no restriction to reparameterize such that $\bar{b}\bar{d} = bd$, where $\bar{b} = |\lambda_1\lambda_2|$ and $\bar{d} = bd/\bar{b}$. In the interest of brevity we skip the bar and assume in the following that $b = |\lambda_1\lambda_2|$. The stationary point is then $\hat{y} = -d$ for the cases $\lambda_1, \lambda_2 > 0$ and $\lambda_1, \lambda_2 < 0$ while it is $\hat{y} = d$ in the saddle point case, $\lambda_1 > 0 > \lambda_2$. The eigenvectors corresponding to λ_1 and λ_2 are

$$v_1 = \begin{pmatrix} 1 \\ \lambda_1 \end{pmatrix}, \qquad v_2 = \begin{pmatrix} 1 \\ \lambda_2 \end{pmatrix}$$

These will be useful in the following study of the behaviour of the phase plane trajectories. When the eigenvalues are real, v_1 and v_2 define line segments in the phase plane that cannot be crossed by the trajectories. This will be illustrated when studying transfer functions with real poles. But first another general result is presented below that will hold also for complex eigenvalues.

THEOREM 5.2—Dual limit cycle solutions
Suppose one stable limit cycle, $\mathcal{P}(\dot{y}^*) = \dot{y}^* > \max(2b_1d, 0)$, with period T, exists for the second order system

$$G_1(s) = \frac{b_1 s + b_2}{s^2 + a_1 s + a_2}$$

connected in a relay feedback loop with relay gain d and hysteresis ε. Then, relay feedback of the system

$$G_2(s) = \frac{-b_1 s + b_2}{s^2 - a_1 s + a_2}$$

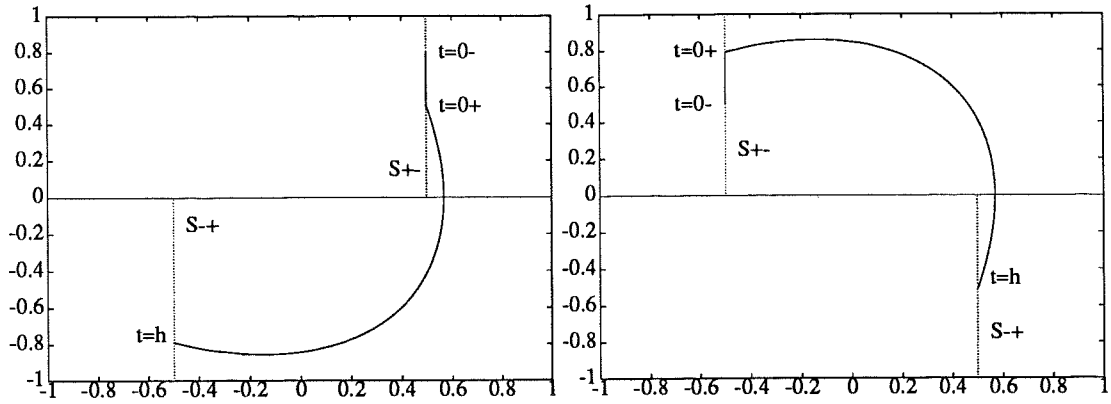

Figure 5.2 Trajectories illustrating the limit cycles for the dual feedback systems in Theorem 5.2. The discontinuity at $\mathcal{S}_{+-}$ is caused by the zero, i.e if $b_1 \neq 0$.

with relay gain d and hysteresis $-\varepsilon$ has an unstable limit cycle solution with period T.

Proof: The situation is visualized in Figure 5.2. Consider the phase plane trajectories, $(y, \dot{y})$, between $\mathcal{S}_{+-}$ and $\mathcal{S}_{-+}$ when $u = -d$, for system G_1. The stationary point is $\hat{y} = -G_1(0)d = -b_2 d/a_2$. Let the eigenvalues to the system $G_1(s)$ be λ_1 and λ_2. First assume that $b_1 = 0$. Then the general solution in the phase plane $(y - \hat{y}, \dot{y})$ is formed by a linear combination of the eigenvectors v_1 and v_2. Hence

$$\begin{pmatrix} y(t) - \hat{y} \\ \dot{y}(t) \end{pmatrix} = c_1 e^{\lambda_1 t} v_1 + c_2 e^{\lambda_2 t} v_2 \quad ; \quad v_1 = \begin{pmatrix} 1 \\ \lambda_1 \end{pmatrix} \quad ; \quad v_2 = \begin{pmatrix} 1 \\ \lambda_2 \end{pmatrix}$$

Now, consider the other system, $G_2(s)$, with eigenvalues $-\lambda_1$ and $-\lambda_2$. Denote the corresponding output $z(t)$. The stationary point will be the same, i.e. $\hat{z} = \hat{y}$, and the general solution is

$$\begin{pmatrix} z(t) - \hat{z} \\ \dot{z}(t) \end{pmatrix} = d_1 e^{-\lambda_1 t} \begin{pmatrix} 1 \\ -\lambda_1 \end{pmatrix} + d_2 e^{-\lambda_2 t} \begin{pmatrix} 1 \\ -\lambda_2 \end{pmatrix}$$

Choose the initial condition as $(z(0), \dot{z}(0)) = (y(h), -\dot{y}(h))$. Then

$$\begin{pmatrix} z(0) - \hat{z} \\ \dot{z}(0) \end{pmatrix} = d_1 \begin{pmatrix} 1 \\ -\lambda_1 \end{pmatrix} + d_2 \begin{pmatrix} 1 \\ -\lambda_2 \end{pmatrix} =$$

$$= \begin{pmatrix} y(h) - \hat{y} \\ -\dot{y}(h) \end{pmatrix} = c_1 e^{\lambda_1 h} \begin{pmatrix} 1 \\ -\lambda_1 \end{pmatrix} + c_2 e^{\lambda_2 h} \begin{pmatrix} 1 \\ -\lambda_2 \end{pmatrix}$$

$$\Rightarrow \quad \begin{cases} d_1 = c_1 e^{\lambda_1 h} \\ d_2 = c_2 e^{\lambda_2 h} \end{cases}$$

$$\Rightarrow \quad \begin{pmatrix} z(t) - \hat{z} \\ \dot{z}(t) \end{pmatrix} = \begin{pmatrix} y(h-t) - \hat{y} \\ -\dot{y}(h-t) \end{pmatrix}$$

Hence, if the first system has a limit cycle, $\dot{y}(0) = -\dot{y}(h)$, so has the second system, $\dot{z}(0) = -\dot{y}(h) = \dot{y}(0) = -\dot{z}(h)$. Thus, the phase plane trajectories for the system with eigenvalues $-\lambda_1$ and $-\lambda_2$ will be the same as those for the system with eigenvalues λ_1 and λ_2 after reflection along the y-axis and change of time direction. The rotation along the y-axis also gives a new interpretation of the hysteresis, now being $-\varepsilon$, i.e. after the rotation the old $\mathcal{S}_{+-}$ has become our new $\mathcal{S}_{-+}$ and vise versa because of the change of time direction. The change of time direction gives the systems opposite stability properties. Now, suppose $b_1 \neq 0$. Then we choose $\dot{z}(0+) = -\dot{y}(h)$ which gives $\dot{y}(0+) = -\dot{z}(h)$. The discontinuities at the respective switch lines $\mathcal{S}_{+-}$ are

$$\dot{y}(0+) = \dot{y}(0-) - 2b_1 d$$
$$\dot{z}(0+) = \dot{z}(0-) + 2b_1 d$$

If the first system has a limit cycle then $\dot{y}(0-) = -\dot{y}(h)$. But then the second system also must have a limit cycle solution with the same half period h since

$$\dot{z}(0-) = \dot{z}(0+) - 2b_1 d = -\dot{y}(h) - 2b_1 d = \dot{y}(0-) - 2b_1 d = \dot{y}(0+) = -\dot{z}(h)$$

■

Remark. If the process transfer function does not have zeroes the theorem implies that $H(-1, h)$ changes sign if the corresponding continuous time system eigenvalues changes signs. □

To get some intuition about the phase plane trajectories and convergence rates we start to investigate the case with real poles.

5.1 Transfer function with real poles and no zero

Restrict the consideration to the system

$$G(s) = \frac{b}{(s-\lambda_1)(s-\lambda_2)} = \frac{b}{\lambda_1-\lambda_2}\left(\frac{1}{s-\lambda_1} - \frac{1}{s-\lambda_2}\right) \tag{5.2}$$

with λ_1 and λ_2 real. The following three situations will be investigated: the stable case, $\lambda_1, \lambda_2 < 0$, the unstable case, $\lambda_1, \lambda_2 > 0$, and the unstable saddle point case, $\lambda_1 > 0 > \lambda_2$.

Uniqueness of limit cycle solution

A necessary condition for a limit cycle with period $T = 2h$ is according to Theorem 2.1 that $H(-1,h) = -\varepsilon/d$. It will be shown in the following that this equation can have only one solution when $\lambda_1 + \lambda_2 \neq 0$. Zero order hold sampling of the transfer function (5.2) gives

$$H(-1,h) = \frac{b}{\lambda_1-\lambda_2}\left(\frac{1}{\lambda_2}\tanh(\frac{h}{2}\lambda_2) - \frac{1}{\lambda_1}\tanh(\frac{h}{2}\lambda_1)\right) \tag{5.3}$$

The derivative with respect to h is

$$\frac{dH}{dh} = \frac{b/2}{\lambda_1-\lambda_2}\left(\frac{1}{\cosh^2(\frac{h}{2}\lambda_2)} - \frac{1}{\cosh^2(\frac{h}{2}\lambda_1)}\right) =$$
$$= \frac{[\cosh(h\lambda_1) - \cosh(h\lambda_2)]b/4}{(\lambda_1-\lambda_2)(\cosh(\frac{h\lambda_1}{2})\cosh(\frac{h\lambda_2}{2}))^2}$$

Choose $\lambda_1 > \lambda_2$ and assume $b > 0$. Then since $\cosh(\lambda_1) - \cosh(\lambda_2) > 0$ when $|\lambda_1| > |\lambda_2|$ we get $\frac{dH}{dh} > 0$ if and only if $\lambda_1 > -\lambda_2$. The other cases follow correspondingly. Summarized we get

$$\frac{dH}{dh} = \begin{cases} > 0 & \lambda_1 + \lambda_2 > 0 \\ = 0 & \lambda_1 + \lambda_2 = 0 \\ < 0 & \lambda_1 + \lambda_2 < 0 \end{cases}$$

The case, $\lambda_1 + \lambda_2 = 0$, has infinitely many solutions when $\varepsilon = 0$, since $H(-1,h) = 0$ for all h. In all other cases $H(-1,h)$ is monotone, either increasing or decreasing. Hence, generically there is only one solution, h, to the equation $H(-1,h) = -\varepsilon/d$. The other part of Theorem 2.1 can be used to specify the signs of d and ε. This will not be done here. Instead, we will use phase plane analysis. This will give the correspondence between the constraints of solutions to $H(-1,h) = -\varepsilon/d$ and the behaviour in the phase plane $(y,\dot{y})$. Examples with trajectories in the phase plane will then also illustrate the convergence rate to the limit cycle.

Existence of limit cycle solution

Since $H(-1,h)$ is monotonically increasing ($\lambda_1+\lambda_2>0$) or decreasing ($\lambda_1+\lambda_2<0$) there are the following constraints for existence of solution to the equation $H(-1,h)=-\varepsilon/d$.

$$\begin{aligned} H(-1,\infty) > -\frac{\varepsilon}{d} > H(-1,0)=0 \qquad & \lambda_1+\lambda_2>0 \\ H(-1,\infty) < -\frac{\varepsilon}{d} < H(-1,0)=0 \qquad & \lambda_1+\lambda_2<0 \end{aligned} \tag{5.4}$$

Since $\tanh(\lambda h)\to \operatorname{sign}(\lambda)$, when $h\to+\infty$ we get

$$H(-1,\infty)=\begin{cases} \dfrac{b}{\lambda_1\lambda_2}=1 & 0<\lambda_2<\lambda_1 \\ -\dfrac{(\lambda_1+\lambda_2)b}{(\lambda_1-\lambda_2)\lambda_1\lambda_2}=\dfrac{\lambda_1+\lambda_2}{\lambda_1-\lambda_2} & \lambda_2<0<\lambda_1 \\ -\dfrac{b}{\lambda_1\lambda_2}=-1 & \lambda_2<\lambda_1<0 \end{cases}$$

where the factorization $b=|\lambda_1\lambda_2|$ has been used. Thus, the constraints for the stable case, $0>\lambda_1>\lambda_2$, and unstable case, $\lambda_1>\lambda_2>0$, have always the same form respectively, while for the saddle point case they take one of two forms whether $\lambda_1+\lambda_2>0$ or $\lambda_1+\lambda_2<0$. By Theorem 5.2, it follows that one of these cases has a stable limit cycle. It will be shown later that the stable solution occurs when $\lambda_1+\lambda_2<0$.

The different cases

- The stable case: $\lambda_2<\lambda_1<0$
- The unstable case: $0<\lambda_2<\lambda_1$
- The saddle point case: $\lambda_2<0<\lambda_1$

will now be explored in the phase plane. This will give the signs of d and ε. Also, it will illustrate both the existence and the stability/instability of the limit cycle solution.

The stable case , $\lambda_2<\lambda_1<0$: If the point $\hat{y}=-d$ is to the left of the switch line $\mathcal{S}_{-+}$, i.e. $-d<-\varepsilon$, then there will always be relay switches and therefore convergence to the stable limit cycle. On the other hand, if $\hat{y}$ is to the right of $\mathcal{S}_{-+}$ there will be no oscillations. Compare with the constraints earlier, $H(-1,\infty)=-1<-\varepsilon/d<H(-1,0)=0$. Together with the phase plane constraint, $d>\varepsilon$, this yields $0<\varepsilon<d$.

EXAMPLE 5.1—The stable case, $\lambda_2 < \lambda_1 < 0$
The phase plane is illustrated in Figure 5.3. The eigenvalues are $\lambda_1 = -1$ and $\lambda_2 = -2$ and the relay characteristics are $d = 1$ and $\varepsilon = 0.5$. Two phase plane trajectories emerging from $\mathcal{S}_{+-}$ have been plotted. One with the initial condition $\dot{y}(0) = 0$ and the other with $\dot{y}(0) = 1$. Note that these curves cannot cross each other. Nor can they cross the *slow* eigenvector, v_1, i.e. $\mathcal{P}(\dot{y}) < -\lambda_1(d-\varepsilon) = 0.5$, when $(y, \dot{y}) \in \mathcal{S}_{+-}$. The fast contraction of the Poincaré map gives fast convergence rate to the limit cycle solution. In this example $\mathcal{P}(1) - \mathcal{P}(0) = 0.004$. In fact, all $\dot{y} > 0$ are mapped into the narrow interval $\mathcal{P}(0) = 0.4494 < \mathcal{P}(\dot{y}) < \mathcal{P}(\infty) = 0.5$. □

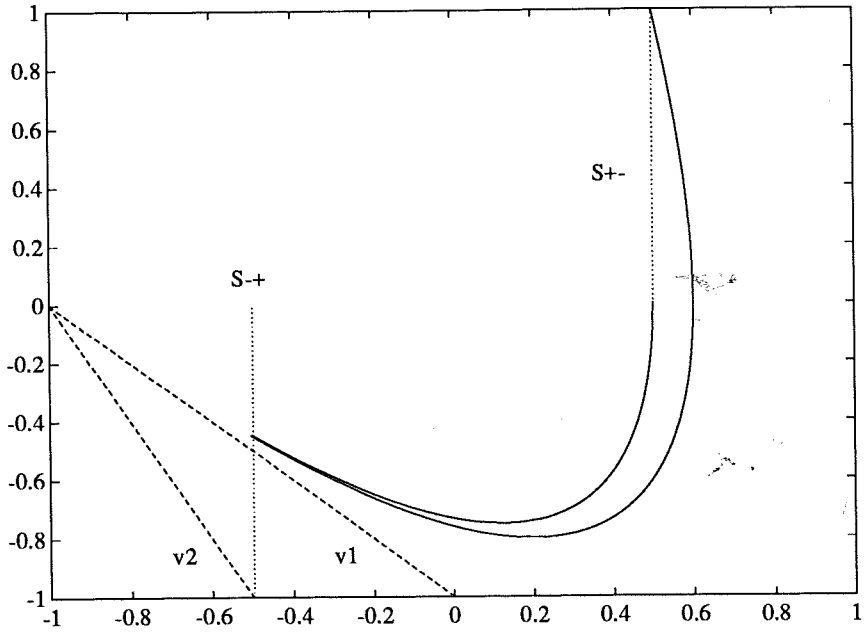

Figure 5.3 The stable case in Example 5.1, with eigenvalues $\lambda_1 = -1$ and $\lambda_2 = -2$ with corresponding eigenvectors v_1 and v_2. The relay characteristics are $d = 1$ and $\varepsilon = 0.5$.Two phase plane trajectories with $\dot{y}(0) = 0$ and $\dot{y}(0) = 1$ are plotted between the switch lines, from $\mathcal{S}_{+-}$ to $\mathcal{S}_{-+}$, illustrating the fast contraction of the Poincaré map in this case, $\mathcal{P}(1) - \mathcal{P}(0) = 0.004$.

The rate of convergence depends on the ratio λ_2/λ_1. When λ_2/λ_1 goes to infinity the second order system will become a first order system. We know already that a first order system reaches the limit cycle directly after the first switch. In the phase plane this is realized in that all trajectories from $\mathcal{S}_{+-}$ will move infinitely fast towards v_1. Then for all initial conditions $(y, \dot{y}) \in \mathcal{S}_{+-}$, the trajectories pass the hysteresis infinitely close along v_1. The limit cycle is therefore reached after the first switch with the Poincaré

fixpoint $-\dot{y}^* \in v_1$. The limit cycle is defined as $\mathcal{P}(\dot{y}^*) = \dot{y}^*$ where $\dot{y}^* = -\lambda_1(d-\varepsilon)$. The same follows from the conditions in Chapter 4 used on the system $G(s) = -\lambda_1/(s-\lambda_1)$.

The unstable case , $\lambda_1 > \lambda_2 > 0$: This case is a direct application of Theorem 5.2 used on the stable case previously. After changing the signs on the eigenvalues and ε there will be an unstable limit cycle. The phase plane picture looks like the previous stable case reflected along the y-axis, see Figure 5.4. But now the trajectories are emerging out from the unstable node. The switch line $\mathcal{S}_{+-}$ corresponds to a negative hysteresis. Together with the constraints $H(-1,0) = 0 < -\varepsilon/d < H(-1,\infty) = 1$, this yields the condition $0 < -\varepsilon < d$ for existence of a limit cycle solution.

EXAMPLE 5.2—The unstable case, $\lambda_1 > \lambda_2 > 0$
In the example in Figure 5.4, the eigenvalues are $\lambda_1 = 2$ and $\lambda_2 = 1$ and the relay characteristics are $d = 1$ and $\varepsilon = -0.5$. Just as the $\mathcal{P}$-map was contracting in the stable case, in Figure 5.3, the map is diverging in the unstable case, $\mathcal{P}(0.4494) = 0 < \mathcal{P}(\dot{y}) < \mathcal{P}(0.5) = \infty$, $(y,\dot{y}) \in \mathcal{S}_{+-}$. The limit cycle is unstable. □

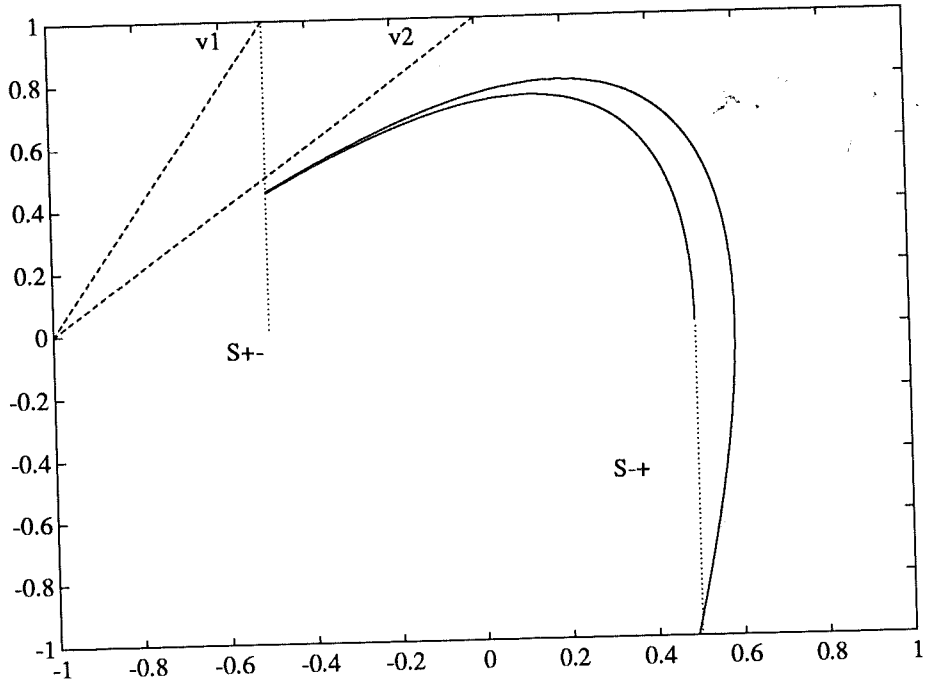

Figure 5.4 Phase plane trajectories for the unstable case in Example 5.2, dual to the stable case in Figure 5.3. Thus, the eigenvalues are $\lambda_1 = 2$, $\lambda_2 = 1$ and the relay characteristics are $d = 1$, $\varepsilon = -0.5$. The limit cycle is unstable.

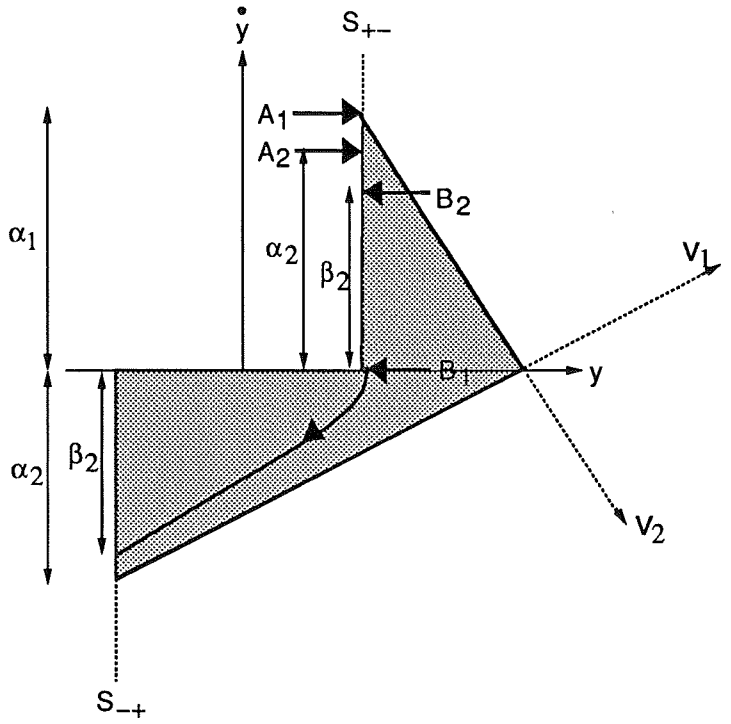

Figure 5.5 Illustration of convergence to a stable limit cycle for the case when $\lambda_1 + \lambda_2 < 0$ and $\varepsilon > 0$. The point A_1 is mapped down to A_2 ($\mathcal{P}(A_1) = A_2 < A_1$), while the point B_1 is mapped up to B_2 ($\mathcal{P}(B_1) = B_2 > B_1$). Hence, there is a stable limit cycle, $\mathcal{P}(\dot{y}^*) = \dot{y}^*$, in the interval $B_2 < \dot{y}^* < A_2$. The region of contraction is the shadowed area, provided that $\alpha_1 > \alpha_2$.

The saddle point case , $\lambda_1 > 0 > \lambda_2$: Consider the phase plane shown in Figure 5.5. A curve starting on $\mathcal{S}_{+-}$ under the eigenvector v_2 must always reach $\mathcal{S}_{-+}$ since it cannot pass v_1 or v_2 and it passes the y-axis vertically. This of course, provided that the stationary point, $\hat{y} = d$, is in the right half plane, i.e. $d > 0$. If $\alpha_1 > \alpha_2$ then the point A_1 on $\mathcal{S}_{+-}$ is mapped to A_2 on $\mathcal{S}_{+-}$ (after the reflection $\mathcal{S}_{+-} = -\mathcal{S}_{-+}$), which is below A_1. However, another point B_1 is mapped upwards to B_2. Clearly we have in this case contraction to a limit cycle positioned somewhere between A_2 and B_2 on $\mathcal{S}_{+-}$. Straight forward trigonometric calculations give

$$\begin{cases} \lambda_1 = \dfrac{\alpha_2}{\varepsilon + d} \\ -\lambda_2 = \dfrac{\alpha_1}{-(\varepsilon - d)} \end{cases} \quad \Rightarrow \quad \begin{cases} \alpha_1 = \lambda_2(\varepsilon - d) \\ \alpha_2 = \lambda_1(\varepsilon + d) \end{cases}$$

and the condition $\alpha_1 - \alpha_2 > 0$ can be written

$$\begin{aligned} \alpha_1 - \alpha_2 &= d(\lambda_1 + \lambda_2) - \varepsilon(\lambda_1 - \lambda_2) > 0 \\ \Rightarrow \quad -\frac{\varepsilon}{d} &> \frac{\lambda_1 + \lambda_2}{\lambda_1 - \lambda_2} = H(-1, \infty) \end{aligned}$$

According to (5.4) this corresponds to a limit cycle solution if and only if $\lambda_1 + \lambda_2 < 0$. Since $d > 0$ the conditions (5.4) can be written

$$(\lambda_1 + \lambda_2)d/(\lambda_1 - \lambda_2) < -\varepsilon < 0$$

The other case, $\lambda_1 + \lambda_2 > 0$, follows now from Theorem 5.2 by duality, i.e. the limit cycle is unstable and corresponds to $\varepsilon < 0$ and $d > 0$. Together with the existence constraints (5.4) this yields

$$0 < -\varepsilon < (\lambda_1 + \lambda_2)d/(\lambda_1 - \lambda_2)$$

Figure 5.6 illustrate the situation. Note that the existence of a limit cycle now governs by the condition $\alpha_1 < \alpha_2$.

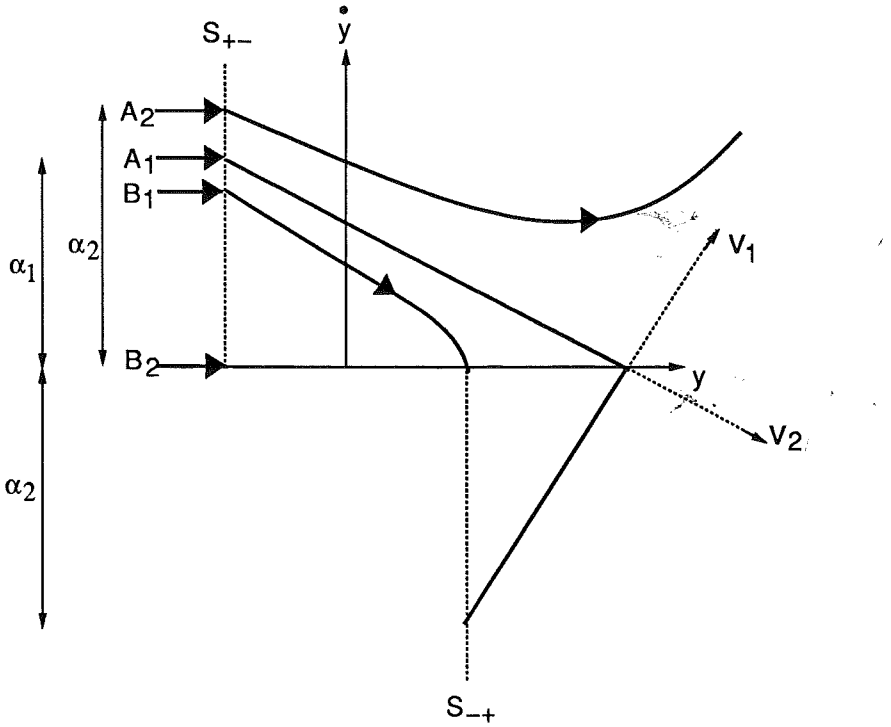

Figure 5.6 Illustration of divergence from an unstable limit cycle for the case $\lambda_1 + \lambda_2 > 0$ and $\varepsilon < 0$. The point A_1 is mapped up to A_2 ($\mathcal{P}(A_1) = A_2 > A_1$), while the point B_1 is mapped down to B_2 ($\mathcal{P}(B_1) = B_2 < B_1$). Hence, there is an unstable limit cycle, $\mathcal{P}(\dot{y}^*) = \dot{y}^*$, in the interval $B_1 < \dot{y}^* < A_1$.

The case $\lambda_1 + \lambda_2 = 0$ when $\varepsilon = 0$ was shown to have infinitely many solutions. The phase plane interpretation is shown in Figure 5.7. From the figure it is clear that $d > 0$ since the fixpoint, $\hat{y} = d$, must be in the right half plane. The case, real poles without zero, is summarized in the following theorem.

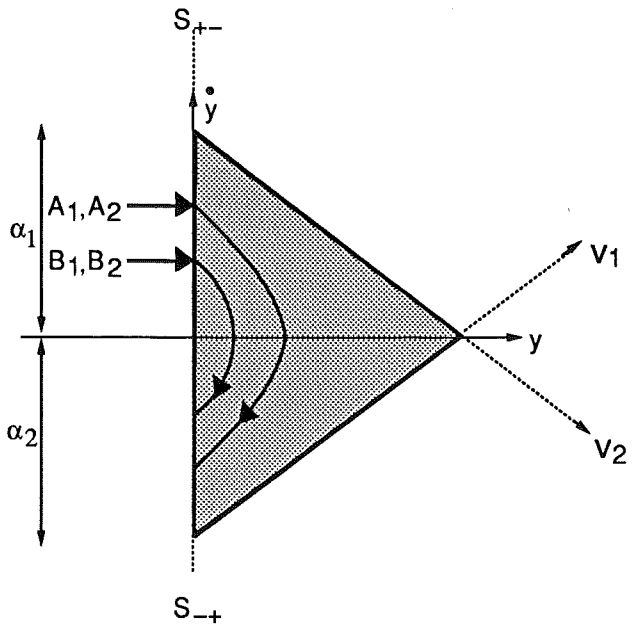

Figure 5.7 Illustration of existence of infinitely many limit cycles in the shadowed area, for the case $\lambda_1 + \lambda_2 = 0$ and $\varepsilon = 0$. The fixpoint $\hat{y} = d$ is positive, i.e. $d > 0$. All of solutions are at the stability boundary. The existence condition is now $\alpha_1 = \alpha_2$.

THEOREM 5.3—Transfer function with real poles and no zero
Consider the second order system, $G(s) = b/(s - \lambda_1)(s - \lambda_2)$, with real, nonzero, eigenvalues, $\lambda_1 > \lambda_2$, in a relay feedback loop with the relay gain d and hysteresis ε. Factorize bd such that $b = |\lambda_1\lambda_2|$. Then the following is true.

The stable case, $0 > \lambda_1 > \lambda_2$: There is a unique globally stable limit cycle, $\mathcal{P}(\dot{y}^*) = \dot{y}^*$, if and only if $0 < \varepsilon < d$. The limit cycle satisfies $0 < \dot{y}^* < -\lambda_1(d - \varepsilon)$.

The unstable case, $\lambda_1 > \lambda_2 > 0$: There is a unique unstable limit cycle, $\mathcal{P}(\dot{y}^*) = \dot{y}^*$, if and only if $0 < -\varepsilon < d$. The limit cycle satisfies $0 < \dot{y}^* < \lambda_1(d + \varepsilon)$.

The saddle point case, $\lambda_1 > 0 > \lambda_2$: Here three different situations can occur depending on whether $\lambda_1 + \lambda_2 <, >$, or $= 0$. When $\lambda_1 + \lambda_2 < 0$ there is a unique stable limit cycle if and only if $(\lambda_1 + \lambda_2)d/(\lambda_1 - \lambda_2) < -\varepsilon < 0$. The region of convergence is $0 < \dot{y} < \lambda_2(\varepsilon - d)$ on $\mathcal{S}_{+-}$. When $\lambda_1 + \lambda_2 > 0$ there is a unique unstable limit cycle if and only if $0 < -\varepsilon < (\lambda_1 + \lambda_2)d/(\lambda_1 - \lambda_2)$. When $\lambda_1 + \lambda_2 = 0$ there are infinitely many limit cycles if and only if $\varepsilon = 0$ and $d > 0$. They are all on the stability boundary and are in the region $0 < \dot{y} < -\lambda_2 d$ on $\mathcal{S}_{+-}$.

Proof: See above! ∎

5.2 Transfer function with complex poles and no zero

Now, restrict the consideration to a relay feedback of a second order system with complex poles

$$G(s) = \frac{\omega^2}{s^2 + 2\zeta\omega s + \omega^2} \qquad 0 < \zeta < 1 \tag{5.5}$$

We already know by Theorem 5.1 that there is global convergence to a stable limit cycle, conditioned that the limit cycle solution is unique. Thus, what remains in order to use Theorem 5.1, is to show that there is just one limit cycle solution to the relay feedback of (5.5), given the relay characteristics d and ε.

Uniqueness of limit cycle solution

Again, we will show that for a chosen relay gain, d, and hysteresis, ε, there is only one limit cycle solution to $H(-1,h) = -\varepsilon/d$ that corresponds to the chosen relay feedback. However, contrary to the real poles case, the equation $H(-1,h) = -\varepsilon/d$ can have many solutions. The equation reflects the behaviour of the open system driven by a square wave input. It does not, however, take into account the behaviour of a relay feedback. This need to be done in order to show uniqueness of the limit cycle solution. Some calculations give

$$H(-1,h) = -\frac{e^{\zeta\omega h} - 2\frac{\zeta\omega}{\omega_1}\sin(\omega_1 h) - e^{-\zeta\omega h}}{e^{\zeta\omega h} + 2\cos(\omega_1 h) + e^{-\zeta\omega h}} \qquad ; \quad \omega_1 = \omega\sqrt{1-\zeta^2}$$

Written in this form it is easy to see that $H(-1,h)$ is an odd function of ζ, in agreement with Theorem 5.2. The derivative with respect to h can be shown to be

$$\frac{dH(-1,h)}{dh} = -\left[\frac{4(\frac{(\zeta\omega)^2}{\omega_1} + \omega_1)\sinh(\zeta\omega h)}{(e^{\zeta\omega h} + 2\cos(\omega_1 h) + e^{-\zeta\omega})^2}\right] \cdot \sin(\omega_1 h)$$

The factor within the brackets has constant sign. Thus,

$$\frac{dH(-1,h)}{dh} = 0 \qquad \text{when} \qquad \omega_1 h = 0, \pi, 2\pi, \ldots$$

Denote $\gamma = \frac{\zeta\omega\pi}{2\omega_1}$. Then

$$H(-1,\pi/\omega_1) = -\frac{e^{2\gamma} - e^{-2\gamma}}{e^{2\gamma} - 2 + e^{-2\gamma}} = -\frac{(e^{\gamma} + e^{-\gamma})(e^{\gamma} - e^{-\gamma})}{(e^{\gamma} - e^{-\gamma})^2} =$$

$$= -\frac{e^{\gamma} + e^{-\gamma}}{e^{\gamma} - e^{-\gamma}} = -\coth(\gamma)$$

Correspondingly

$$H(-1, 2\pi/\omega_1) = \ldots = -\tanh(2\gamma)$$

The function $H(-1, h)$ is shown in Figure 5.8.

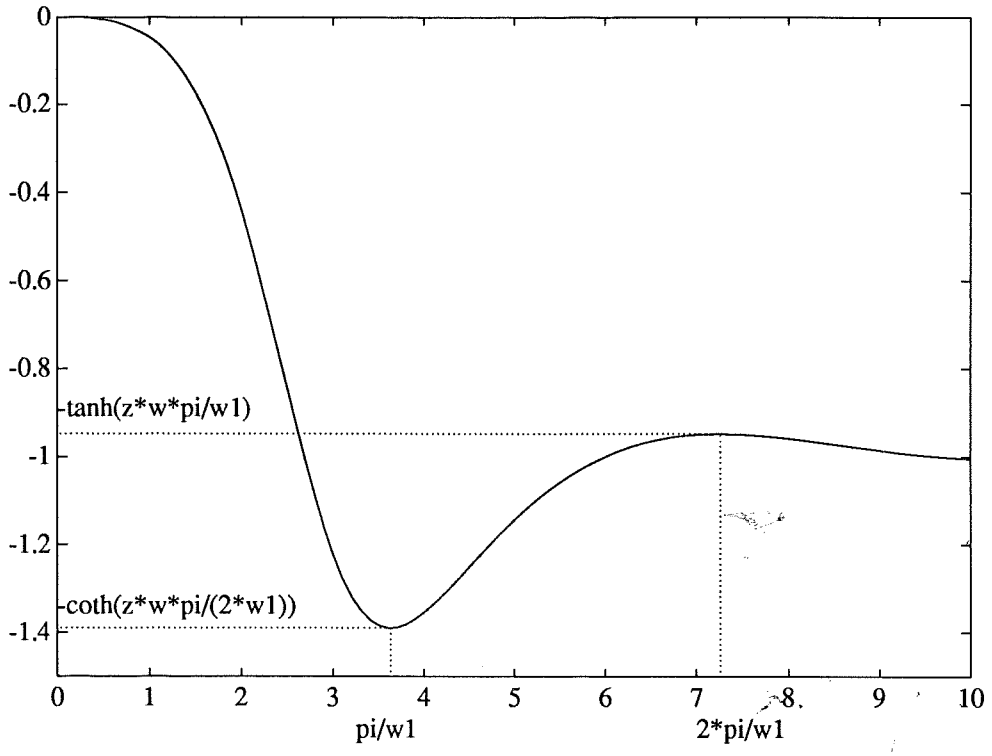

Figure 5.8 The function $H(-1, h)$ for the system (5.5) where $\zeta = 0.5$ and $\omega = 1$. A solution to the equation $H(-1, h) = -\varepsilon/d$ in the interval $0 < \omega_1 h \leq \pi$ corresponds to $d, \varepsilon > 0$. A solution in the interval $\pi \leq \omega_1 h \leq 2\pi$ corresponds to $d, \varepsilon < 0$. No other solutions correspond to a relay feedback limit cycle.

It will be shown in the following that all solutions in the interval $0 < h \leq \pi/\omega_1$ correspond to $d > 0$ and $\varepsilon > 0$. The solutions in the interval $\pi/\omega_1 \leq h \leq 2\pi/\omega_1$ correspond to $d < 0$ and $\varepsilon < 0$. No other relay feedback limit cycle solutions exist.

Between the switch line $\mathcal{S}_{+-}$ and $\mathcal{S}_{-+}$, the phase plane solution $(y, \dot{y})$ is

$$\begin{cases} y(t) = -d + e^{-\zeta\omega t} A \sin(\omega_1 t + \varphi) \\ \dot{y}(t) = -\omega e^{-\zeta\omega t} A \sin(\omega_1 t + \varphi - \theta) \end{cases} \quad ; \quad \theta = \arccos(\zeta)$$

where A and φ are chosen such that $(y(0), \dot{y}(0)) \in \mathcal{S}_{+-}$. The limit cycle

solution corresponding to $\omega_1 h = \pi$ must satisfy

$$\begin{aligned}\dot{y}(0) &= -\omega A \sin(\varphi - \theta) = -\dot{y}(h) = \omega e^{-\zeta\omega h} A \sin(\omega_1 h + \varphi - \theta) = \\ &= -\omega A \sin(\varphi - \theta) \cdot e^{-\zeta\omega h} \\ &\Rightarrow \dot{y}(0) = -\dot{y}(h) = 0\end{aligned}$$

This corresponds to a relay that is switching at the maximal overshoot. This is the boundary case that can occur both with $d > 0$, $\varepsilon > 0$ and $d < 0$, $\varepsilon < 0$, see Figure 5.9.

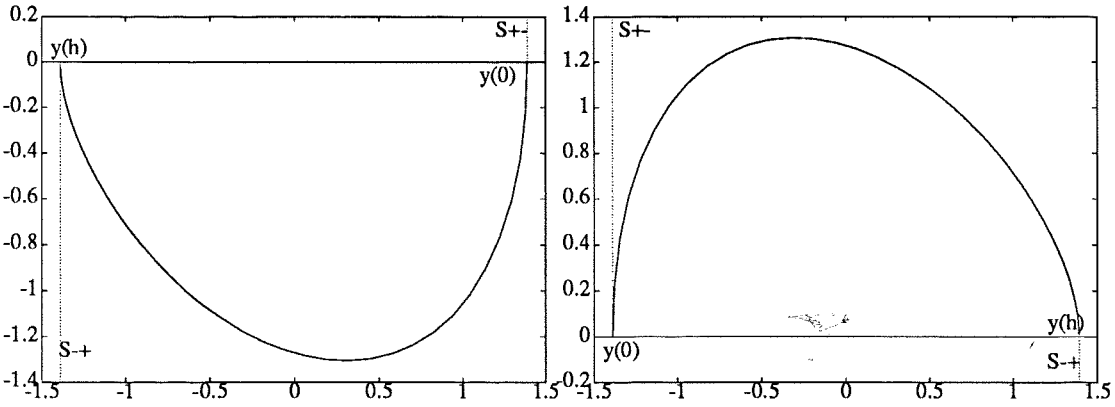

Figure 5.9 The boundary case, $\varepsilon/d = \coth(\zeta\omega\pi/(2\omega_1))$, can occur both with $d > 0$, $\varepsilon > 0$ (left) and $d < 0$, $\varepsilon < 0$ (right). Both correspond to relay switches at the maximal overshoot.

Similarly, it is shown that $h = 2\pi/\omega_1$ corresponds to switches at the maximal undershoot. This is caused by $d < 0$ and $\varepsilon < 0$ as is illustrated in Figure 5.10. Solutions where $\omega_1 h > 2\pi$ do not correspond to relay feedback solutions since the hysteresis boundary is then passed more than once by over- and undershoots before a switch occurs. The function of a relay doesn't allow that.

It is now plausible that all solutions in the interval $0 < \omega_1 h \leq \pi$ are caused by $d > 0$, $\varepsilon > 0$ and the solutions in the interval $\pi \leq \omega_1 h \leq 2\pi$ are caused by $d < 0$, $\varepsilon < 0$. In fact, this is true and is shown in the following theorem.

THEOREM 5.4—Transfer function with complex poles and with no zero
Suppose the system (5.5) is stable and connected in a relay feedback loop with relay gain d and hysteresis ε. Let $\omega_1 = \omega\sqrt{1-\zeta^2}$. Then there is a

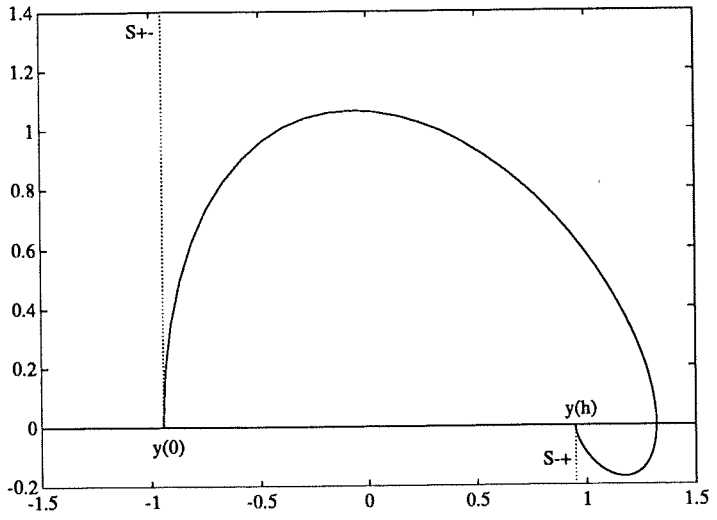

Figure 5.10 The boundary case, $\varepsilon/d = \tanh(\zeta\omega\pi/\omega_1)$, when $d < 0$, $\varepsilon < 0$, corresponds to relay switches at the maximal undershoot.

unique stable limit cycle solution with period $T = 2h$ satisfying

$$H(-1,h) = -\varepsilon/d \quad \Rightarrow \quad \begin{cases} 0 < \omega_1 h \leq \pi & \text{when} \quad d,\varepsilon > 0 \\ \pi \leq \omega_1 h \leq 2\pi & \text{when} \quad d,\varepsilon < 0 \end{cases}$$

The convergence is global, $\mathcal{P}^k(\dot{y}(0)) \to \dot{y}^*$, $k \to \infty$, for all $(y(0),\dot{y}(0)) \in \mathcal{S}_{+-}$.

Proof: A solution h in the interval, $0 < h \leq \pi/\omega_1$, must satisfy

$$0 > -\frac{\varepsilon}{d} = H(-1,h) \geq H(-1,\frac{\pi}{\omega_1}) = -\coth(\gamma) = -\frac{1+e^{-2\gamma}}{1-e^{-2\gamma}}$$

where $\gamma = \zeta\omega\pi/(2\omega_1)$. Depending on the signs of d and ε we get the following inequalities.

$$-d(1+e^{-2\gamma}) \begin{cases} \leq -\varepsilon(1-e^{-2\gamma}) & d,\varepsilon > 0 \\ \geq -\varepsilon(1-e^{-2\gamma}) & d,\varepsilon < 0 \end{cases} \tag{5.6}$$

Regard the map from $\dot{y}(0) = \dot{y}^* \in \mathcal{S}_{+-}$ to $-\dot{y}(t)$ where $t = \pi/\omega_1$. We will now show that $t \geq h$ when $d,\varepsilon > 0$ and that $t \leq h$ when $d,\varepsilon < 0$. Another way to put it is to show that $y(t) < -\varepsilon$ ($\mathcal{S}_{-+}$ already passed, i.e. $h \leq t$) when $d,\varepsilon > 0$ and that $y(t) > -\varepsilon$ ($\mathcal{S}_{-+}$ not yet passed, i.e. $h \geq t$) when $d,\varepsilon < 0$.

$$\begin{aligned} y(0) = \varepsilon = -d + A\sin(\varphi) \quad &\Rightarrow \quad A\sin(\varphi) = d + \varepsilon \\ y(t) = -d + Ae^{-\zeta\omega t}\sin(\omega_1 t + \varphi) &= -d - e^{-2\gamma}A\sin(\varphi) = \\ = -d - e^{-2\gamma}(d+\varepsilon) &= -\varepsilon e^{-2\gamma} - d(1+e^{-2\gamma}) \end{aligned}$$

Use (5.6) to get

$$y(t)\begin{cases} \leq -\varepsilon & d,\varepsilon > 0 \quad \Rightarrow \quad h \leq t = \pi/\omega_1 \\ \geq -\varepsilon & d,\varepsilon < 0 \quad \Rightarrow \quad h \geq t = \pi/\omega_1 \end{cases}$$

For the global convergence, see Theorem 5.1. There are no limit cycles such that $h > 2\pi/\omega_1$ since the hysteresis can just be passed once. ∎

Remark. Notice, that Theorem 5.2 can be used only to partly cover the unstable case. It is not covered completely since more solutions are found in the unstable case. These correspond to spiraling phase plane trajectories that make several revolutions before reaching the hysteresis boundary. Such solutions can also give chaos. See Cook (1985) and Amrani-Atherton (1989). □

5.3 Transfer function with real poles and a zero

When $b_1 \neq 0$ there is a zero in the transfer function. The influence from the zero on the switching behaviour will be considerable more complicated since

- the $\mathcal{P}$-map will not always be monotone
- $H(-1,h)$ will not always be monotone

In the case with no zero in the transfer function there could be no more than one limit cycle solution, stable or unstable. Even when $H(-1;h)$ was nonmonotone the different solutions to $H(-1,h) = -\varepsilon/d$ was shown to correspond to different signs of d and ε. When a zero is introduced in the transfer function this is no longer always true. The different solutions may or may not correspond to different relay characteristics d and ε. As an illustration of the phenomena we restrict our consideration to the real poles case

$$G(s) = \frac{b_1 s + b_2}{(s-\lambda_1)(s-\lambda_2)} = \frac{1}{\lambda_1 - \lambda_2}\left[\frac{b_2 + \lambda_1 b_1}{s-\lambda_1} - \frac{b_2 + \lambda_2 b_1}{s-\lambda_2}\right]$$

The function $H(-1,h)$ (compare (5.3)) is then modified to

$$H(-1,h) = \frac{1}{\lambda_1 - \lambda_2}\left[\frac{b_2 + \lambda_2 b_1}{\lambda_2}\tanh(\frac{h}{2}\lambda_2) - \frac{b_2 + \lambda_1 b_1}{\lambda_1}\tanh(\frac{h}{2}\lambda_1)\right]$$

In some situations $H(-1,h)$ will no longer be monotone. This is seen by investigating the sign of

$$\frac{dH(-1,h)}{dh} = \frac{1/2}{\lambda_1 - \lambda_2}\frac{(b_2 + \lambda_2 b_1)\cosh^2(\frac{h}{2}\lambda_1) - (b_2 + \lambda_1 b_1)\cosh^2(\frac{h}{2}\lambda_2)}{(\cosh(\frac{h}{2}\lambda_1)\cosh(\frac{h}{2}\lambda_2))^2}$$

Since one of the $\cosh^2(\cdot)$-terms in the numerator always will grow faster than the other, $H'(-1,h)$ must be monotone. So is $H(-1,h)$ if $\text{sign}[H'(-1,0)] = \text{sign}[H'(-1,\infty)]$. For all cases we have

$$\text{sign}[H'(-1,0)] = -\text{sign}[b_1]$$

On the other hand

$$\text{sign}[H'(-1,\infty)] = \begin{cases} \text{sign}[b_2 + \lambda_2 b_1] & \lambda_1 + \lambda_2 > 0 \\ -\text{sign}[b_2 + \lambda_1 b_1] & \lambda_1 + \lambda_2 < 0 \end{cases}$$

This is realized from the following. Let $\lambda_1 + \lambda_2 < 0$. Then $|\lambda_2| > |\lambda_1|$, since $\lambda_1 > \lambda_2$ by definition. The term with $\cosh^2(h\lambda_2/2)$ will then dominate over that with $\cosh^2(h\lambda_1/2)$. The sign of the coefficient in front of $\cosh^2(h\lambda_2/2)$ is then determining the sign of $H'(-1,h)$ when $h \to \infty$. The case $\lambda_1 + \lambda_2 > 0$ follows correspondingly. In the following, the case $\lambda_1 + \lambda_2 < 0$ will be investigated. Many results are then automatically transferred to the other case by using the duality in Theorem 5.2.

Monotone $H(-1,h)$***:*** Assume that

$$\begin{cases} \text{sign}[b_1] = \text{sign}[b_2 + \lambda_1 b_1] > 0 \\ \lambda_1 + \lambda_2 < 0 \end{cases}$$

Then $H(-1,h)$ is monotonously decreasing and there will be a unique solution if

$$H(-1,\infty) < -\frac{\varepsilon}{d} < H(-1,0)$$

The interpretation of the signs of d and ε will be the same as for the case with no zero in the transfer function. This is realized from the following. Suppose $b_1 = 0$ and there is a limit cycle $\mathcal{P}(\dot{y}^*) = \dot{y}^*$ for a particular choice of d and ε. Choose a $\dot{y}_0 \neq \dot{y}^*$ and let $\dot{y}_1 = \mathcal{P}(\dot{y}_0)$. Now, choose b_1 such that $\dot{y}_1 - \dot{y}_0 = 2b_1 d$, which corresponds to the discontinuity at $\mathcal{S}_{+-}$ where $\dot{y}(0-) = \dot{y}_1$ and $\dot{y}(0+) = \dot{y}_0$. Then the new system will have a limit cycle defined as $\mathcal{P}(\dot{y}_1) = \dot{y}_1$ and the relay characteristics d and ε are still the same. Note that when $\varepsilon > 0$ it is possible to choose $\dot{y}_0 < 0$ (but with $\dot{y}_1 > 0$) if we extend $\mathcal{S}_{+-}$ to include $\dot{y}_0$. The resulting limit cycle, $\dot{y}_1$, is then nonmonotone in the sense that $\mathcal{P}'(\dot{y}_1) < 0$. However, in such a case Theorem 5.1 cannot be used since $\dot{y}_1 < 2b_1 d$.

In the stable case we can choose $b_2 = \lambda_1\lambda_2$ as before. Then the only possibility for $H(-1,h)$ to be monotone when $b_1 > 0$ is that

$$b_1 < -\lambda_2$$

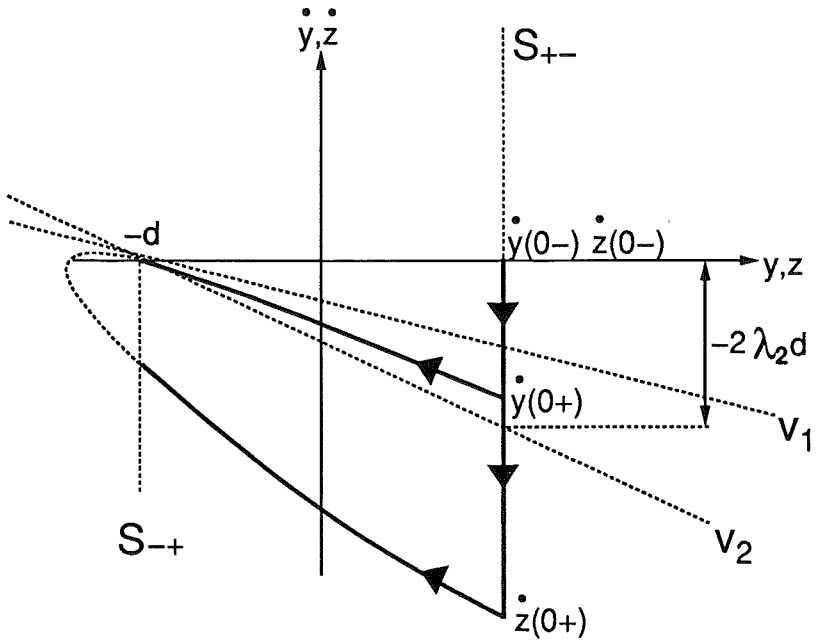

Figure 5.11 When $H(-1,h)$ is monotone for a stable system, then the condition $b_1 < -\lambda_2$ holds. The condition guarantees that it is possible to choose ε such that $\mathcal{P}(0) = 0$. Here, two curves y and z, satisfying and not satisfying the inequality respectively, illustrate the phase plane behaviour. The boundary case $-\varepsilon/d = H(-1,\infty)$ is only possible with the y-curve. The z-curve case must have a nonmonotone $H(-1,h)$.

The inequality can be interpreted as follows. If $H(-1,h)$ is monotone it should be possible to choose ε such that $h \to \infty$, i.e. $-\varepsilon/d \to H(-1,\infty) = -1$. This is only possible if $\hat{y} \in \mathcal{S}_{-+}$, i.e. $\dot{y}^* = 0$. Then $t \to \infty$ when the trajectory reaches $\mathcal{S}_{-+}$. In Figure 5.11, it is shown that the map $\mathcal{P}(0) = 0$ is only possible when the discontinuous part of the map doesn't pass the eigenvector v_2, i.e. when $b_1 < -\lambda_2$. Two curves are shown, one that satisfies $\dot{y}(0-) - \dot{y}(0+) = 2b_1 d < -\lambda_2(2d)$, and another that does not.

The boundaries, $H(-1,0)$ and $H(-1,\infty)$, are the same as for the case with no zero in the transfer function except for the saddle point case where there is a dependence on b_1, as

$$H(-1,\infty) = \frac{1}{\lambda_1 - \lambda_2}\left[\frac{-b_2}{\lambda_1\lambda_2}(\lambda_1 + \lambda_2) - 2b_1\right] \qquad \lambda_2 < 0 < \lambda_1$$

The dependence on b_1 in the saddle point case is illustrated in Figure 5.12. (Note that $b_2 = -\lambda_1\lambda_2$ such that the stationary point is $\hat{y} = d$.) The discontinuity at $\mathcal{S}_{+-}$ is $\dot{y}(0-) - \dot{y}(0+) = 2b_1 d$. According to the Figure 5.12, the condition for existence (and stability) of a limit cycle is

$$2b_1 d + \alpha_1 > \alpha_2$$

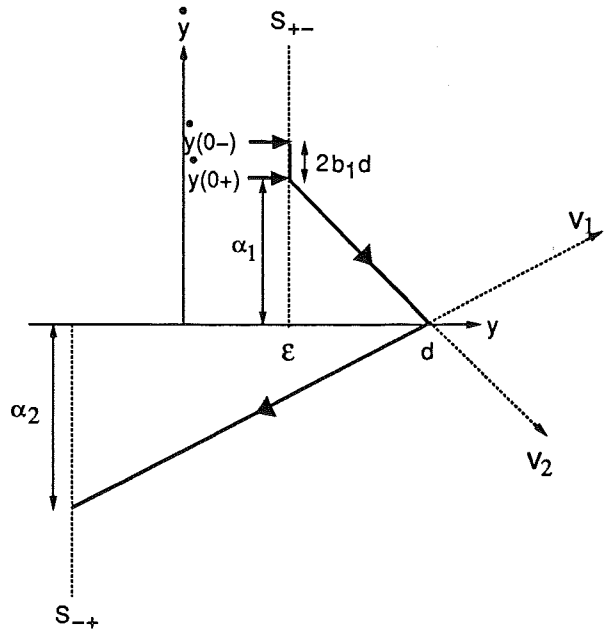

Figure 5.12 Illustration of the boundary case $-\varepsilon/d \to H(-1,\infty)$ when $b_1 \neq 0$. Then $P(\dot{y}^*) = \dot{y}^* \to \alpha_2$.

Since $v_1 = \begin{pmatrix} 1 & \lambda_1 \end{pmatrix}^T$ and $v_2 = \begin{pmatrix} 1 & \lambda_2 \end{pmatrix}^T$ we get

$$\begin{cases} \alpha_1 = -\lambda_2(d-\varepsilon) \\ \alpha_2 = \lambda_1(d+\varepsilon) \end{cases}$$

Thus,

$$2b_1 d - \lambda_2(d-\varepsilon) > \lambda_1(d+\varepsilon)$$

$$\Rightarrow \quad -\frac{\varepsilon}{d} > \frac{1}{\lambda_1 - \lambda_2}[\lambda_1 + \lambda_2 - 2b_1] = H(-1,\infty)$$

Nonmonotone $H(-1,h)$**:** It is more interesting to notice what happens when

$$\operatorname{sign}[b_1] = -\operatorname{sign}[b_2 + \lambda_1 b_1]$$

Then $H(-1,h)$ is nonmonotone and $H(-1,h) = -\varepsilon/d$ can have two solutions, h_1 and h_2 $(> h_1)$. In the case $\lambda_1 + \lambda_2 < 0$, the solution h_2 can be constructed as before in the monotone case, i.e we conclude that $d > 0$. It will be shown that the other solution h_1 is associated with either $d < 0$ or $d > 0$. Thus, for some relay characteristics there could be two limit cycle solutions. However, just one of them (h_2) is stable.

In the stable case when $b_2 = \lambda_1\lambda_2$, we get

$$-\operatorname{sign}[b_2 + \lambda_1 b_1] = \operatorname{sign}[\lambda_2 + b_1]$$

Thus, a stable system that is nonminimum phase has always a nonmonotone $H(-1,h)$, while if it is minimum phase there is the additional condition, $b_1 > -\lambda_2$, for nonmonotonicity.

EXAMPLE 5.3—A stable nonminimum phase system
Consider the stable nonminimum phase system

$$G(s) = \frac{-s+2}{(s+1)(s+2)}$$

The nonmonotone function $H(-1,h)$ is shown in Figure 5.13.

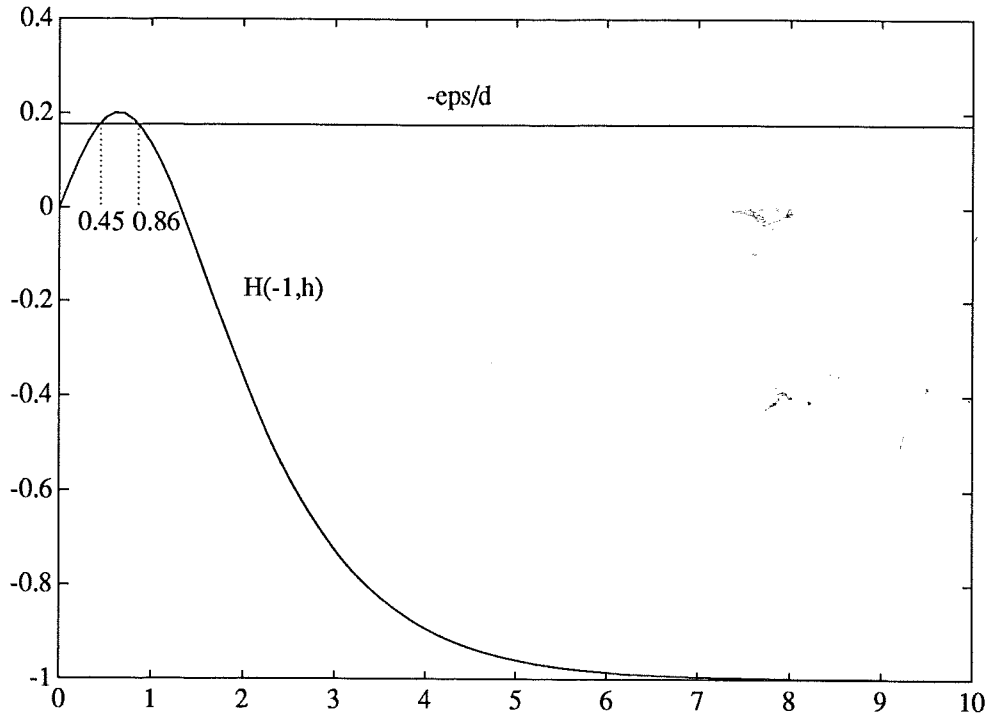

Figure 5.13 Example 5.3, where the function $H(-1,h)$ intersects the boundary case $-\varepsilon/d = 0.177$, A limit cycle solution in the interval $0 < h \leq 0.45$ corresponds to $d < 0$. In the interval $0.45 \leq h \leq 0.86$, there are two solutions both corresponding to $d > 0$. A solution where $h > 0.86$ corresponds to $d > 0$.

One might expect, that one type of solution (signs of d and ε) is associated with solutions to the left of $\max[H(-1,h)]$ and another one to the right. That was the case when the transfer function had no zero. That is, however, *not* the case now. Instead, two solutions $h = 0.45$ and $h = 0.86$ have been

indicated at the intersection of $-\varepsilon/d = 0.177$. These are the *boundary* solutions for this example. The following signs of the relay gain d, corresponding to different relay feedback limit cycle solutions, can occur

$$\begin{cases} 0 < h \leq 0.45 & \text{one solution with } d < 0 \\ 0.45 \leq h \leq 0.86 & \text{two solutions with } d > 0 \\ 0.86 < h & \text{one solution with } d > 0 \end{cases}$$

First consider the case when $d = 1$ and let $\varepsilon = -0.177$. Then there are two solutions $h_1 = 0.45$ and $h_2 = 0.86$. When ε is reduced to -0.2 the two solutions coincide, $h_1 = h_2 = 0.6$. The Poincaré map, $\mathcal{P}(\dot{y})$, where $(y, \dot{y}) \in \mathcal{S}_{+-}$, is given in Figure 5.14 for the two situations, $\varepsilon = -0.177$ and $\varepsilon = -0.2$.

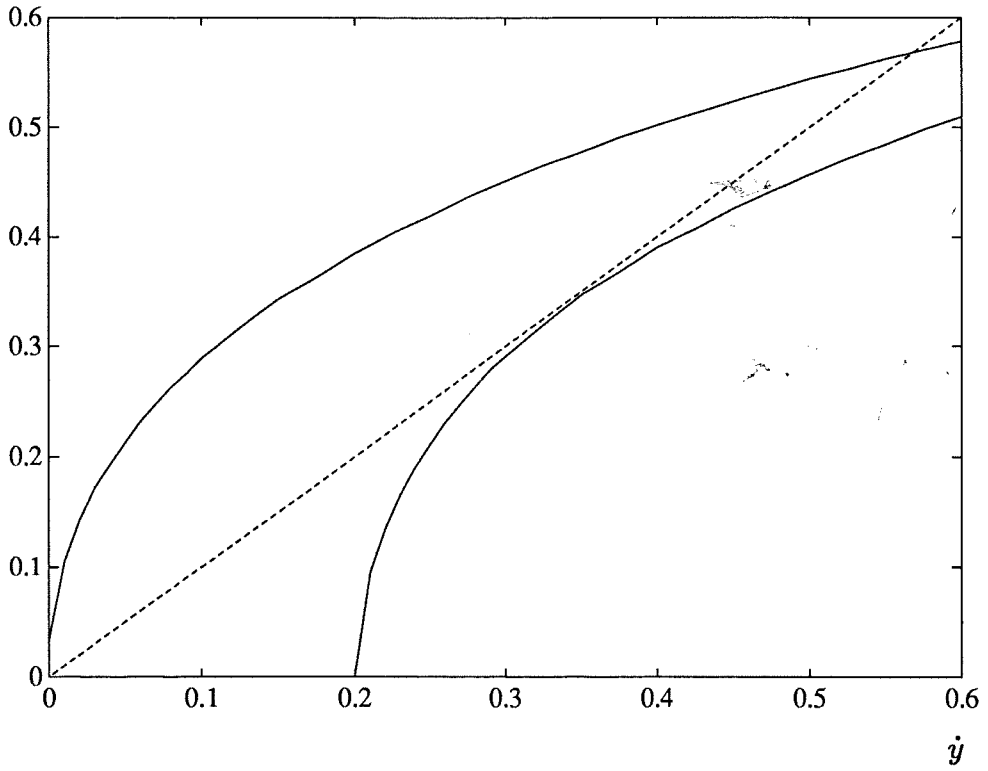

Figure 5.14 The Poincaré map, $\mathcal{P}(\dot{y})$ (solid curve), for the two cases $\varepsilon = -0.177$ and $\varepsilon = -0.2$, in Example 5.3. The limit cycle solutions, $\mathcal{P}(\dot{y}^*) = \dot{y}^*$, are the intersection by the dashed line. When $\varepsilon = -0.177$, this gives two solutions $\dot{y}^* = 0$ and $\dot{y}^* = 0.56$, corresponding to $h = 0.45$ and $h = 0.86$ respectively, while when $\varepsilon = -0.2$, the two solutions coincide. The left solution is always unstable and the right one is stable.

Since the $\mathcal{P}$-map is continuous and monotone in this case it can be concluded that the largest of the two limit cycles, $\dot{y}^*$, must be stable, $0 <$

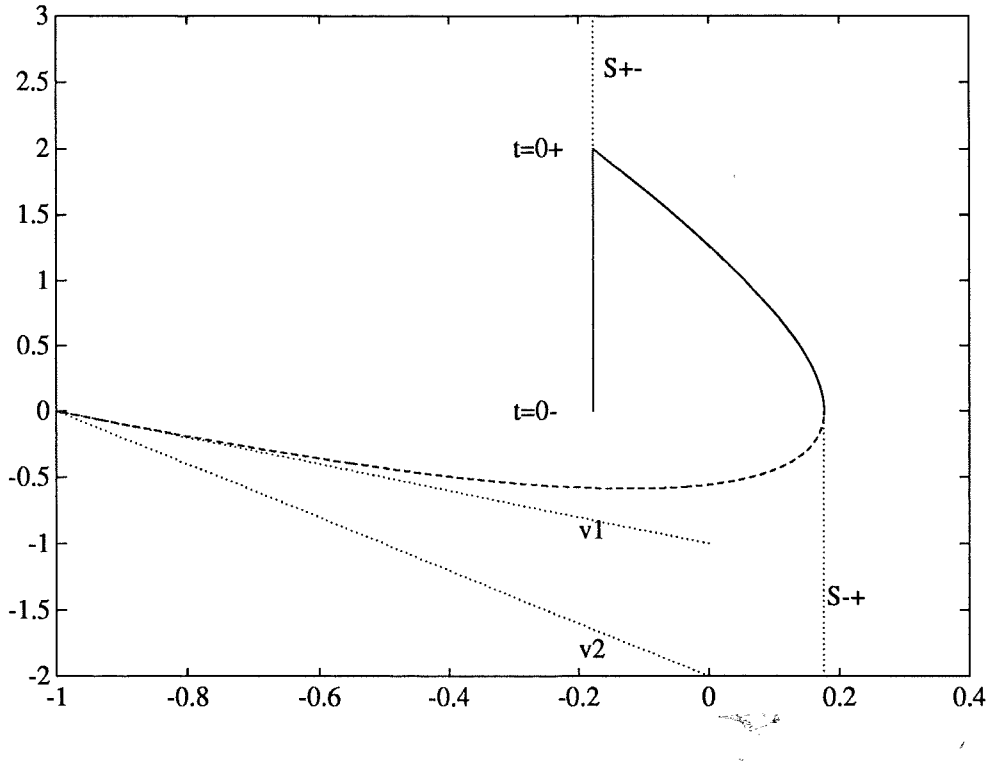

Figure 5.15 The unstable limit cycle, $\dot{y}^* = 0$, corresponding to $h = 0.45$ in Example 5.3. The relay is $d = 1$ and $\varepsilon = -0.177$.

$\mathcal{P}'(\dot{y}^*) < 1$, and the smallest unstable, $\mathcal{P}'(\dot{y}^*) > 1$, as is shown in Figure 5.14. Otherwise there would be solutions growing to infinity which is impossible since the system $G(s)$ is asymptotically stable driven by a bounded input. The phase plane trajectory for the limit cycle solution associated with $h = 0.45$ are shown in Figure 5.15, where $\dot{y}^* = 0$. In Figure 5.16, the limit cycle associated with $h = 0.86$, where $\dot{y}^* = 0.56$, is shown.

When $d = -1$ and $\varepsilon = 0.177$ there is another limit cycle with the half period $h = 0.45$. This solution, where $\dot{y}^* = 0$, is shown is Figure 5.17, and corresponds to a nonmonotone $\mathcal{P}$-map, i.e. $\mathcal{P}'(0) < 0$. □

EXAMPLE 5.4—A stable minimum phase system
Consider the stable minimum phase system

$$G(s) = \frac{3s + 2}{(s + 1)(s + 2)}$$

which is satisfying the condition $b_1 > -\lambda_2$, giving a nonmonotone $H(-1, h)$. The function $H(-1, h)$ is shown in Figure 5.18. The function $H(-1, h)$ intersects the boundary case $-\varepsilon/d = -1.177$ at $h = 1.55$ and $h = 1.80$. Like the

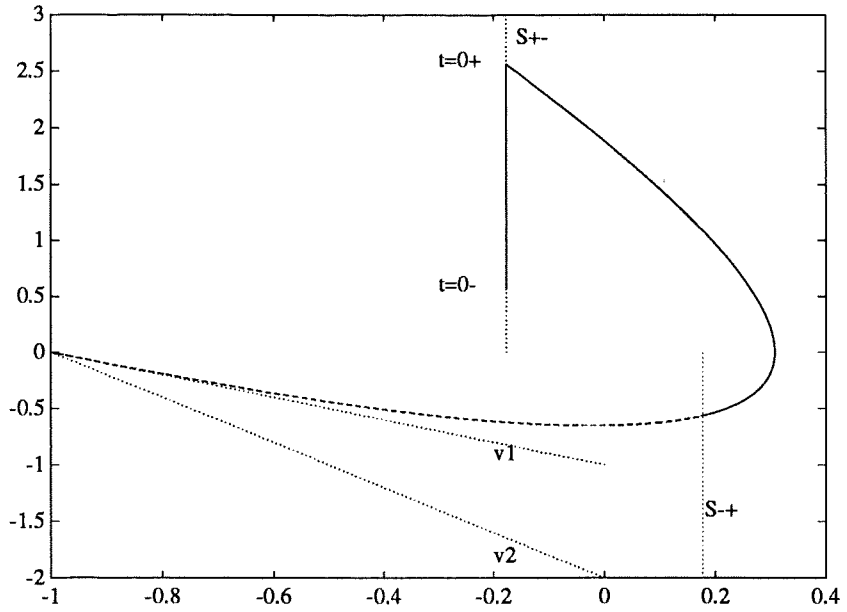

Figure 5.16 The stable limit cycle, $\dot{y}^* = 0.56$, corresponding to $h = 0.86$ in Example 5.3. The relay is $d = 1$ and $\epsilon = -0.177$.

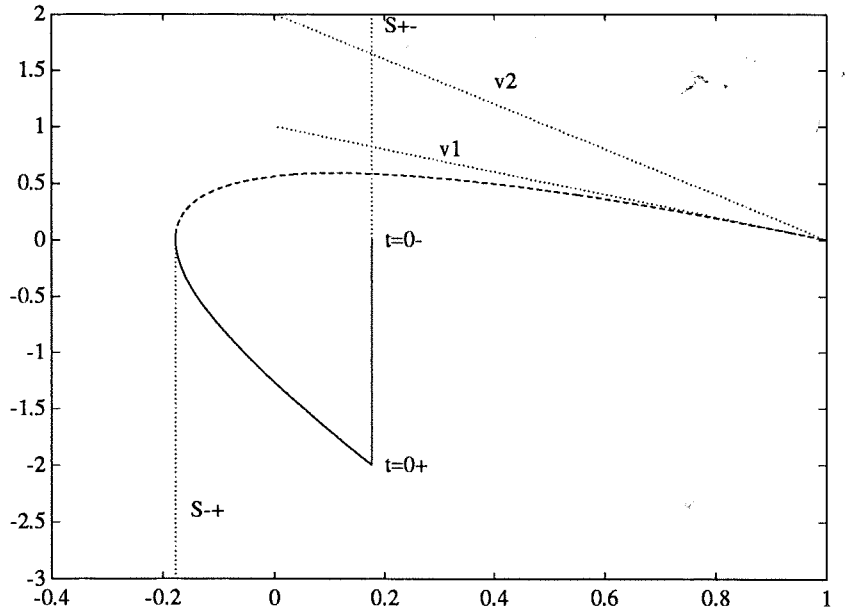

Figure 5.17 A limit cycle, $\dot{y}^* = 0$, corresponding to $h = 0.45$ in Example 5.3. The relay is $d = -1$ and $\epsilon = 0.177$.

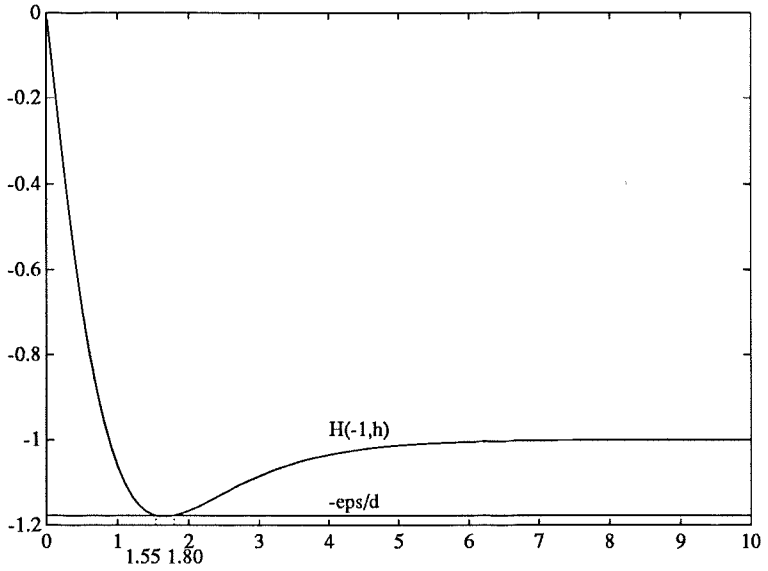

Figure 5.18 Example 5.4, where the function $H(-1,h)$ intersects the boundary case $-\varepsilon/d = -1.177$ at $h = 1.55$ and $h = 1.80$. A limit cycle solution in the interval $0 < h \leq 1.55$ corresponds to $d > 0$. In the interval $1.55 \leq h \leq 1.80$, there are two solutions both corresponding to $d < 0$. The solution for $h > 1.80$ corresponds to $d < 0$.

previous nonminimum phase example these are defining an interval where two limit cycle solutions exist, associated with the same relay feedback. The following signs of the relay gain d, corresponding to different relay feedback limit cycle solutions, can occur

$$\begin{cases} 0 < h \leq 1.55 & \text{one solution with } d > 0 \\ 1.55 \leq h \leq 1.80 & \text{two solutions with } d < 0 \\ 1.80 < h & \text{one solution with } d < 0 \end{cases}$$

First consider the case when $d = -1$ and $\varepsilon = -1.177$. Then there are two solutions $h_1 = 1.55$ and $h_2 = 1.80$. When ε is reduced to $\varepsilon = -1.180$ the two solutions coincide, $h_1 = h_2 = 1.67$. The Poincaré map, $\mathcal{P}(\dot{y})$, $(y, \dot{y}) \in \mathcal{S}_{+-}$, is given in Figure 5.19 for the two situations, $\varepsilon = -1.177$ and $\varepsilon = -1.180$. As in the previous example, the largest of the two limit cycles, $\dot{y}^*$, must be stable, $0 < \mathcal{P}'(\dot{y}^*) < 1$, and the smallest unstable, $\mathcal{P}'(\dot{y}^*) > 1$,

The unstable limit cycle solution, where $\dot{y}^* = 0$, is shown in Figure 5.20. Note that the condition $b_1 > -\lambda_2$, guarantees that the trajectory always passes the eigenvector v_2 at the discontinuity on $\mathcal{S}_{+-}$. This in turn, means that the trajectory, which must tend toward $\hat{y}$ along v_1, is making a turn and enters $\mathcal{S}_{-+}$ from the right, as it should. □

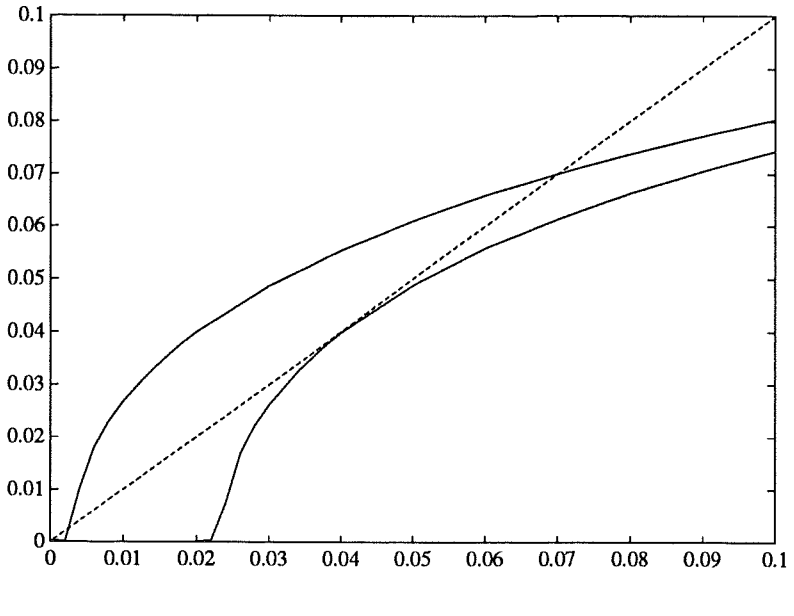

Figure 5.19 The Poincaré map, $\mathcal{P}(\dot{y})$,for the two cases $\epsilon = -1.177$ and $\epsilon = -1.180$, in Example 5.4. When $\epsilon = -1.177$, there are two solutions $\dot{y}^* = 0$ and $\dot{y}^* = 0.07$, corresponding to $h_1 = 1.55$ and $h_2 = 1.80$ respectively, while when $\epsilon = -1.180$, the two solutions coincide. The left solution is always unstable and the right one is stable.

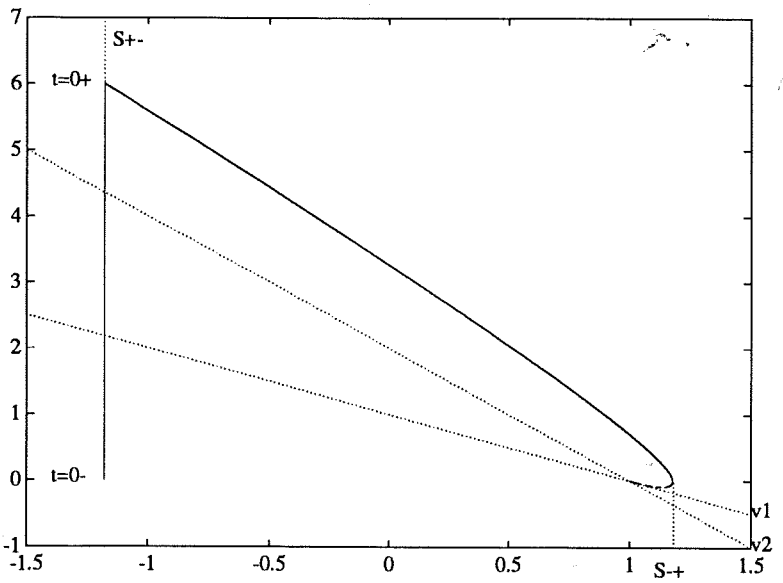

Figure 5.20 One of the limit cycle solution, $\dot{y}^* = 0$, for the boundary case in Example 5.4, where $h = 1.55$. The relay is $d = -1$ and $\epsilon = -1.177$.

5.4 Summary

Second order systems with relay feedback can have a complex behaviour. In order to simplify the analysis the strategy was to look for conditions that guarantee

- a unique limit cycle solution
- a monotone $\mathcal{P}$-map

Such conditions were found for the case with no zero in the transfer function. Conclusions about stability and convergence regions were drawn. In particular, stable second order systems with relay feedback have global convergence to the unique limit cycle. Stable limit cycles for unstable systems were also found.

Complete results were not given for transfer functions having a zero. Instead it was illustrated by analysis of a special case that there is

- not always a unique limit cycle solution
- not always a monotone $\mathcal{P}$-map

Both items make the analysis more complicated. The convergence has only been shown for the case when the $\mathcal{P}$-map is monotone. The nonuniqueness of limit cycle solution has nothing to do with the $\mathcal{P}$-map being nonmonotone or not. Nor has it to do with nonminimum phaseness that may be introduced by the zero. In fact, two examples; one minimum phase and another nonminimum phase, both with monotone $\mathcal{P}$-maps were shown to have two limit cycle solutions for some relay feedback.

6

Chaos in relay feedback systems

Quite peculiar behaviour was discovered in Chapter 4, where feedback of an unstable first order system with direct term and a time delay showed both symmetrical and unsymmetrical limit cycles solutions. The system can be thought of as an approximation of a second order system where the direct term is a faster mode. If the poles are complex, however, it is possible to get even more complex behaviour. In Cook (1985) an example was given of a second order system, containing a relay with hysteresis, which can display chaotic motion. The idea is there to let the second order system have unstable complex poles. This makes a phase plane trajectory to spiral away from the equilibrium point until it reaches the appropriate switching line defined by the relay. Depending on initial conditions different numbers of revolutions may be needed before the switching line is reached. This makes the Poincaré map from one switching line to the other discontinuous. The same example was further investigated in Amrani-Atherton (1989). In this chapter a similar approach is used to construct chaotic systems. The similarity is the expanding spiral. But here, the influence of a time delay is also considered. For some time delays, there is a bounded region in the state space which no trajectory can leave. Inside that region, the behaviour depends on the highly irregular Poincaré map. The system will exhibit strange behaviour like, multi switch limit cycles and chaos. Unlike the Cook example, some of the limit cycles are found to be stable. Also, in order to get chaos in the Cook example it is crucial to have positive feedback. When having a time delay, chaos is

possible also during negative feedback.

6.1 Second order system with a time delay

Second order systems with time delay are infinite dimensional. It turns out, however, that much insight can be derived from analysis in a two dimensional phase space. To analyse the system we will consider a phase space representation for the linear second order system in Figure 6.1.

The solutions to a second order system step response for different initial values will give rise to curves in the phase plane that cannot cross each other. This noncrossing fact implies that the Poincaré map, $\mathcal{P}$, is monotone. This was used in Chapter 5 to prove that a stable second order system during relay feedback had global convergence to a limit cycle. However, if a time delay is introduced in the loop, as in Figure 6.1, the Poincaré map will not always be monotone.

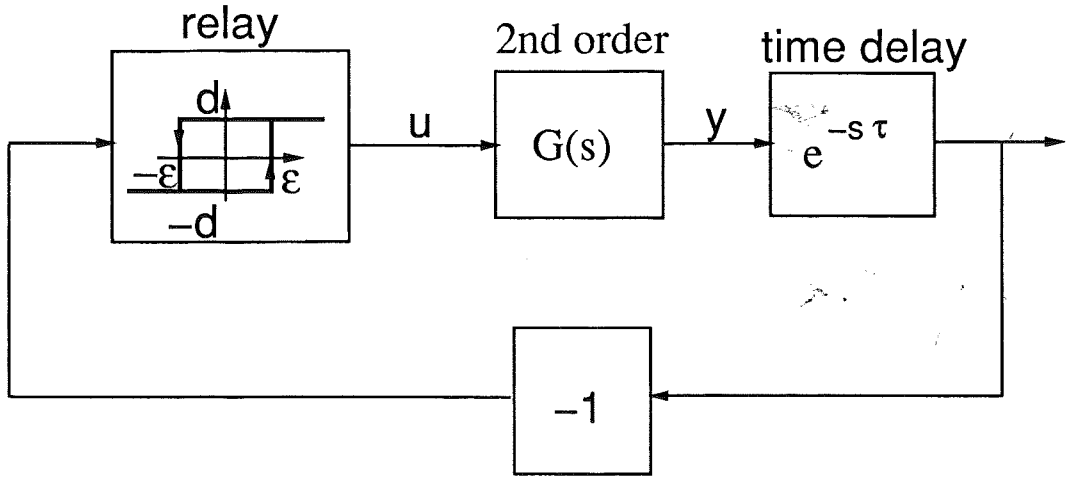

Figure 6.1 A relay feedback system with time delay

Parameterize the second order system with complex poles as

$$G(s) = \frac{\omega^2}{s^2 + 2\zeta\omega s + \omega^2} \tag{6.1}$$

Assume the relay output to be $u = +1$. The step response $y(t)$ is then

$$y(t) = 1 + e^{-\zeta\omega t} A \sin(\omega_1 t + \varphi) \qquad \omega_1 = \omega\sqrt{1-\zeta^2} \tag{6.2}$$

for some constants A and φ depending on initial conditions. The derivative can be written as

$$\begin{aligned} \dot{y}(t) &= -\omega e^{-\zeta\omega t} A(\sin(\omega_1 t + \varphi)\cdot\zeta - \cos(\omega_1 t + \varphi)\cdot\sqrt{1-\zeta^2}) \\ &= -\omega e^{-\zeta\omega t} A \sin(\omega_1 t + \varphi - \theta) \end{aligned} \tag{6.3}$$

where $\zeta = \cos\theta$. Considerable insight into the behaviour can be obtained by observing the remarkable fact that the relay switchings occur at a straight line in the $(y, \dot{y})$ plane. A similar result, but for relay servos, is given in Graham-McRuer (1961). There, it is referred to as the *delayed switching line.*

THEOREM 6.1—The delayed switching line
Consider the relay feedback system in Figure 6.1. Assume the relay output to be $u = +1$ and that y passes the hysteresis ε when $t = 0$, i.e. $y(0) = \varepsilon$. Thus, the relay is switching to $u = -1$ at time $t = \tau$. Then $(y(\tau), \dot{y}(\tau)) \in \mathcal{S}_{+-}$ lies along a straight line in the phase plane for all initials $\dot{y}(0)$. The line is

$$\dot{y}(\tau) = a(y(\tau) - 1) + b \quad \text{where} \quad \begin{cases} a = \omega \dfrac{\sin(\theta - \omega_1\tau)}{\sin\omega_1\tau} \\ b = \dfrac{\omega_1(1-\varepsilon)e^{-\zeta\omega\tau}}{\sin\omega_1\tau} \end{cases}$$

Proof:

$$\begin{aligned} \sin(\omega_1\tau + \varphi - \theta) &= \sin(\omega_1\tau + \varphi)\cos\theta - \cos(\omega_1\tau + \varphi)\sin\theta = \\ &= \sin(\omega_1\tau + \varphi)\cos\theta - \sin\theta(\cos\omega_1\tau\underline{\cos\varphi} - \sin\omega_1\tau\sin\varphi) \end{aligned}$$

Eliminate the underlined $\cos\varphi$-term by use of the following relation

$$\begin{aligned} \sin(\omega_1\tau + \varphi)\frac{\sin\theta\cos\omega_1\tau}{\sin\omega_1\tau} &= (\sin\omega_1\tau\cos\varphi + \cos\omega_1\tau\sin\varphi)\frac{\sin\theta\cos\omega_1\tau}{\sin\omega_1\tau} = \\ &= \sin\theta\cos\omega_1\tau\underline{\cos\varphi} + \frac{\sin\theta\sin\varphi\cos^2\omega_1\tau}{\sin\omega_1\tau} \end{aligned}$$

This gives

$$\begin{aligned} \sin(\omega_1\tau + \varphi - \theta) &= \sin(\omega_1\tau + \varphi)\frac{\sin\omega_1\tau\cos\theta - \cos\omega_1\tau\sin\theta}{\sin\omega_1\tau} + \\ &+ \sin\theta\sin\varphi\frac{\sin^2\omega_1\tau + \cos^2\omega_1\tau}{\sin\omega_1\tau} \\ &= \sin(\omega_1\tau + \varphi)\frac{\sin(\omega_1\tau - \theta)}{\sin\omega_1\tau} + \frac{\sin\theta\sin\varphi}{\sin\omega_1\tau} \end{aligned}$$

Multiply with $-\omega A e^{-\zeta\omega\tau}$ and use that $A\sin\varphi = y(0) - 1 = \varepsilon - 1$ (constant!) and that $\omega\sin\theta = \omega_1$. Then from (6.2) and (6.3) we get

$$\dot{y}(\tau) = \omega\frac{\sin(\theta - \omega_1\tau)}{\sin\omega_1\tau}(y(\tau) - 1) + \frac{\omega_1(1-\varepsilon)e^{-\zeta\omega\tau}}{\sin\omega_1\tau} \quad \blacksquare$$

When having a time delay it is convenient to redefine the stroboscopic Poincaré map such that the Poincaré section is as before. The Poincaré section and the switching line $\mathcal{S}_{+-}$ are then no longer the same.

DEFINITION 6.1—The Poincaré map, $\mathcal{P}$, when having a time delay
Let us define the P-map as before as the map from the half line segment $(y(0) = \varepsilon, \dot{y}(0) > 0)$ to the half line segment $-(y(t^*) = -\varepsilon, \dot{y}(0) < 0)$. Notice, that y is not the output of the system. Therefore the corresponding input u will not switch on the Poincaré section. Instead, $u(t) = d$ when $0 \leq t < \tau$ and $u(t) = -d$ when $\tau \leq t \leq t^*$. Notice, that the switching line $\mathcal{S}_{+-}$ is not our chosen Poincaré section. □

The meaning and use of Theorem 6.1 and the definition of the $\mathcal{P}$-map are illustrated in Figure 6.2a and b. The P-map is taken as $(y(0) = \varepsilon, \dot{y}(0)) \rightarrow -(y(t) = -\varepsilon, \dot{y}(t))$. This map can be seen as first a map *to* the straight line, $\mathcal{S}_{+-}$, according to Theorem 6.1, i.e. $(y(0) = \varepsilon, \dot{y}(0)) \rightarrow (y(\tau), \dot{y}(\tau))$ and then *from* the line, $\mathcal{S}_{+-}$, to the Poincaré section, $(y(\tau), \dot{y}(\tau)) \rightarrow -(y(t), \dot{y}(t))$ where $-y(t) = \varepsilon$. The first part of the map onto the line is always monotone, while that is not necessarily the case for the second part of the map, *from* the line. Define the normal to the line, N, in a clockwise sense as

$$N = \begin{pmatrix} \omega \sin(\theta - \omega_1 \tau) \\ -\sin \omega_1 \tau \end{pmatrix}$$

A monotone map is illustrated in Figure 6.2a, where the flow *from* the line, F, (when $u = -1$) is in the normal direction, i.e. $N^T F \geq 0$. In Figure 6.2b the nonmonotone case is shown when $N^T F < 0$.

EXAMPLE 6.1—Second order system with time delay
Reconsider the system $G(s) = e^{-s}/(s^2 + s + 1)$ in a relay feedback loop with relay gain, $d = 1$, and hysteresis, $\varepsilon = 0.005$. This example was studied in Chapter 2 (Example 2.5) where it was shown that there were 3 different limit cycle solutions for this choice of d and ε. Two of them were, however, constructed by use of the initial time history such that $y(t)$ was passing the hysteresis when $\tau < t < 0$. If we disregard these solutions, e.g. by assuming that $y(t) = 0$, $t \in (-\tau, 0)$, we are left with only one limit cycle solution. This solution was concluded to be locally stable by use of the approximate describing function analysis. Now, we will consider the stability issue by use of the Poincaré map. The solution is shown in the $(y, \dot{y})$ phase plane in Figure 6.3, starting with the initial condition $(y(0), \dot{y}(0)) = (\varepsilon, 0)$. The line $(y(\tau), \dot{y}(\tau))$ is also indicated. The corresponding Poincaré map defined as $\mathcal{P}(\dot{y}(0)) = -\dot{y}(t)$ where $y(0) = \varepsilon$ and $y(t) = -\varepsilon$, is given in Figure 6.4. Global convergence is obtained if $|\mathcal{P}'(\dot{y})| < 1$ and $\mathcal{P}$ is monotone if $\mathcal{P}'(\dot{y}) > 0$.

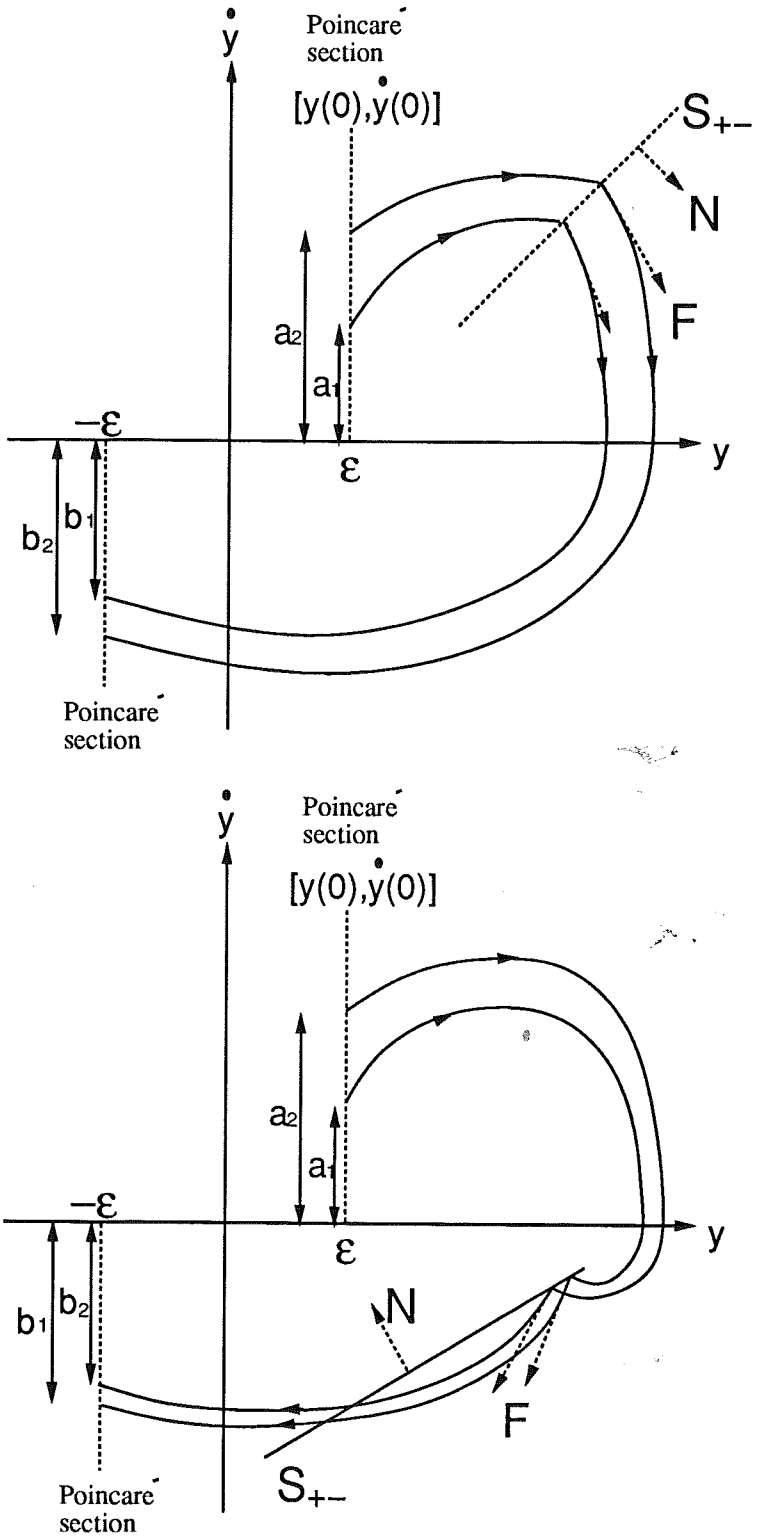

Figure 6.2 The $\mathcal{P}$-map is defined as $b_1 = \mathcal{P}(a_1)$ and $b_2 = \mathcal{P}(a_2)$. a) (above) Monotone $\mathcal{P}$-map when $N^T F > 0$, i.e. $(b_2 - b_1)/(a_2 - a_1) > 0$. b) (below) Nonmonotone $\mathcal{P}$-map when $N^T F < 0$, i.e. $(b_2 - b_1)/(a_2 - a_1) < 0$.

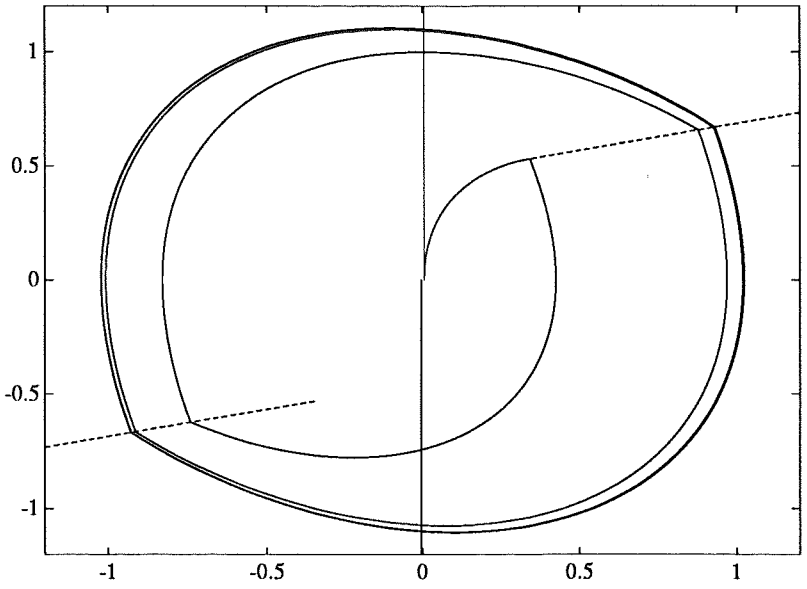

Figure 6.3 Phase plane solution, $(y, \dot{y})$, for the system $G(s) = e^{-s}/(s^2+s+1)$ during relay feedback with $d = 1$ and $\varepsilon = 0.005$. The switch line $\mathcal{S}_{+-}$ is dashed.

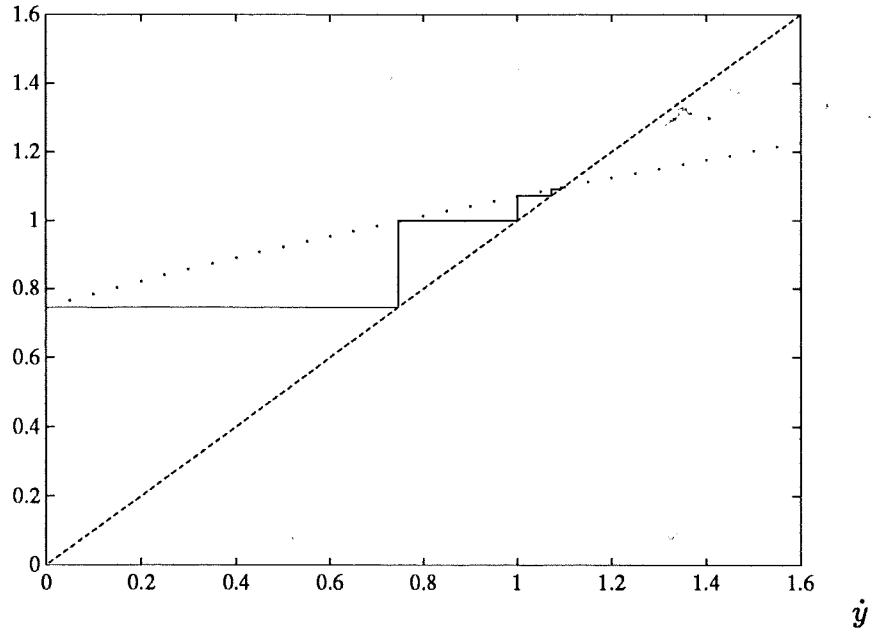

Figure 6.4 The Poincaré map $\mathcal{P}(\dot{y}_i) = \dot{y}_{i+1}$ (dotted curve) and $\dot{y}_{i+1} = \dot{y}_i$ (dashed line) for the relay feedback system with $G(s) = e^{-s}/(s^2+s+1)$, $d = 1$ and $\varepsilon = 0.005$. Successive iterations follows the solid line starting from the initial condition $\dot{y}(0) = \dot{y}_0 = 0$, then $\dot{y}_1 \approx 0.75, \ldots \dot{y}_\infty \approx 1.1$.

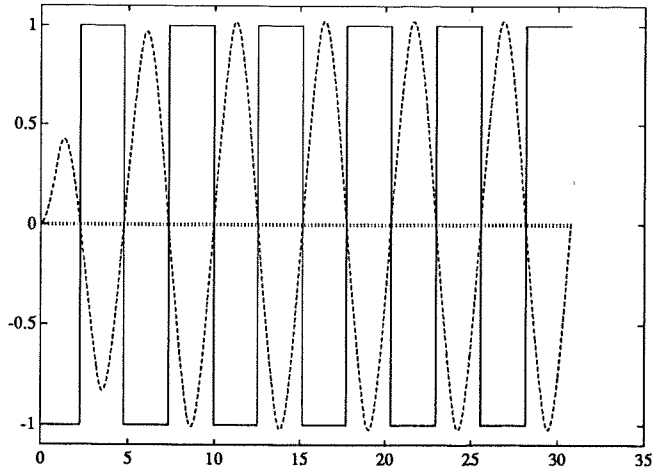

Figure 6.5 The output, $z(t)$, for the system $G(s) = e^{-s}/(s^2+s+1)$ in a relay feedback with $d = 1$ and $\varepsilon = 0.005$.

This seems to be the case, at least in the plotted interval. The corresponding output, $z(t)$, is shown in Figure 6.5. □

6.2 Multi switch limit cycles

From the intuition about the phase plane behaviour gained by Theorem 6.1, we are able to construct peculiar examples. By choosing the time delay longer and longer the switch line $\mathcal{S}_{+-}$ turns clockwise. This can cause contraction of the $\mathcal{P}$-map. Let us consider the unstable case with two complex poles. Then the map *to* $\mathcal{S}_{+-}$ is expanding, but *from* $\mathcal{S}_{+-}$ to the $\mathcal{P}$-section, $y(t) = -\varepsilon$, there could be contraction. Think of when the flow, F, from $\mathcal{S}_{+-}$ is tangential to $\mathcal{S}_{+-}$, i.e. $N^T F = 0$ (compare Figure 6.2). Then different $\dot{y}$ on the $\mathcal{P}$-section are mapped to the same point, i.e. contraction. When the contraction outweights the expansion we have the basic ingredients for *chaos* or *strange behaviour*. We will choose a quite large hysteresis such that some of the rotating phase plane trajectories *miss* the hysteresis at their first revolution. But since they expand they will hit the hysteresis on their next revolution. This will give a discontinuous $\mathcal{P}$-map. We will start with studying *multi switch limit cycles*. In next section the example will be modified to produce a chaotic solution.

DEFINITION 6.2—Multi switch limit cycles
A k-switch limit cycle is defined as points, $\{\dot{y}_1, \dot{y}_2, \ldots \dot{y}_k\}$, at the $\mathcal{P}$-section such that $\mathcal{P}(\dot{y}_1) = \dot{y}_2$, $\mathcal{P}(\dot{y}_2) = \dot{y}_3$, $\ldots \mathcal{P}(\dot{y}_k) = y_1$ where all y_i, $i = 1, \ldots k$, are different. □

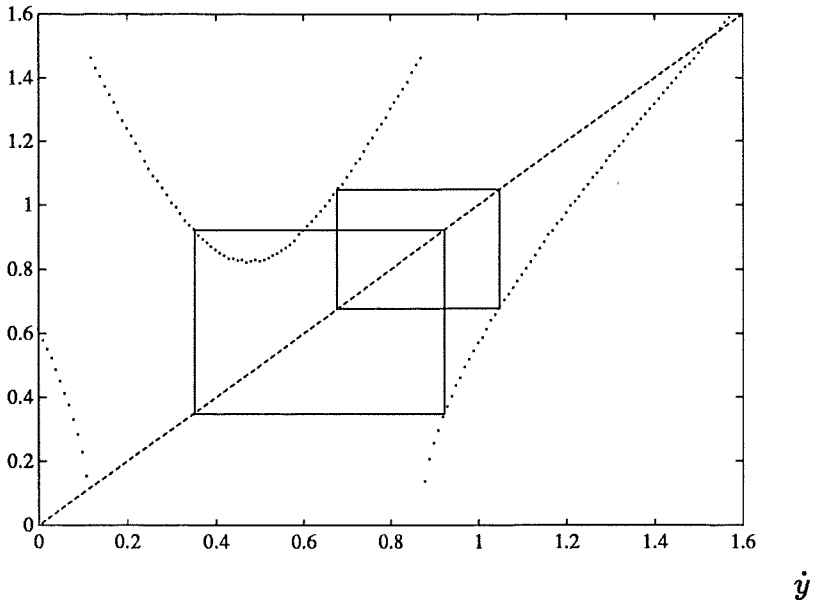

Figure 6.6 The discontinuous map $\mathcal{P}(\dot{y}_0) = \dot{y}_1$ (dotted curve) and $\dot{y}_1 = \dot{y}_0$ (dashed curve) as a function of $\dot{y}_0$. Two 2-switch limit cycles are illustrated as solid lines. The system is $G(s) = \omega^2/(s^2 + 2\zeta\omega s + \omega^2)$ with $\zeta = -0.1$, $\omega = 1$ and the relay characteristics are $d = 1$, $\varepsilon = 2$.

EXAMPLE 6.2—Multi switch limit cycles

Reconsider the system (6.1), but now with unstable poles, $\zeta = -0.1$, $\omega = 1$ and with the relay characteristics $d = 1$, $\varepsilon = 2$. There will be many multi switch limit cycles, some stable, other unstable. Two 2-switch limit cycles are illustrated in Figure 6.6. The right one of them is stable. The left one is unstable and will eventually drift over into a stable 12-switch limit cycle. In Figure 6.7, two 3-switch limit cycles are shown. Both these are unstable. The left one will drift over into a stable 12-switch limit cycle and the right one will drift over into the previous stable 2-switch limit cycle. The stable 12-switch limit cycle is shown in Figure 6.8. It is interesting to notice that for each multi switch limit cycle, described as above by the $\mathcal{P}$-map, there are two corresponding solutions. For example, in the 2-switch case above we have $\mathcal{P}(\dot{y}_1) = \dot{y}_2$, $\mathcal{P}(\dot{y}_2) = \dot{y}_1$, which corresponds to either $y_1 = \varepsilon$, $y_2 = -\varepsilon$ or $y_1 = -\varepsilon$, $y_2 = \varepsilon$. In the 12-switch case we have $\mathcal{P}(\dot{y}_1) = \dot{y}_2$, $\mathcal{P}(\dot{y}_2) = \dot{y}_3$, $\ldots \mathcal{P}(\dot{y}_{12}) = \dot{y}_1$, which corresponds to either $y_i = (-1)^{i-1}\varepsilon$ or $y_i = (-1)^i\varepsilon$, $i = 1, 2, \ldots 12$. In the phase plane these two solutions are each other's reflection. They are both shown in Figure 6.9. Both curves have the same stability property since they correspond to the same $\mathcal{P}$-map. Thus, the interlaced curves indicate the extreme sensitivity to initial conditions. One of the 12-switch limit cycle solutions is plotted versus time in Figure 6.10. □

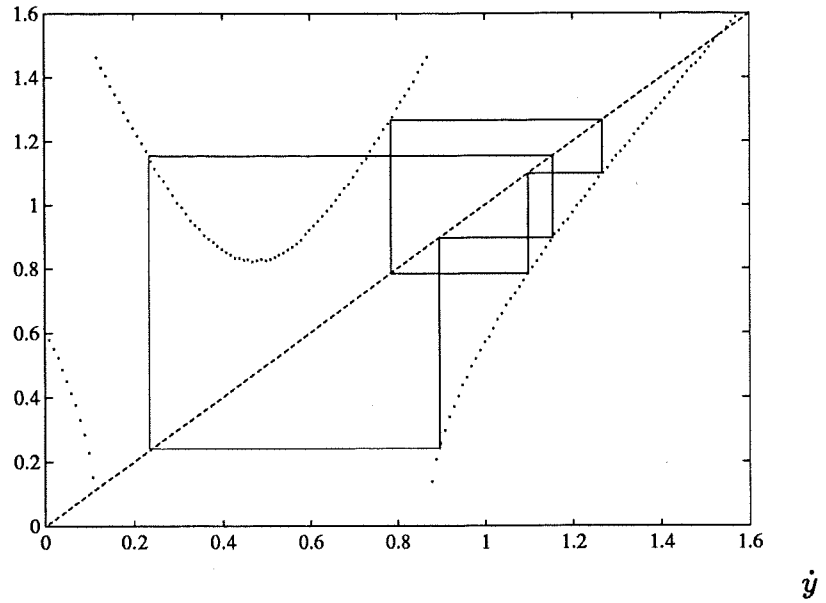

Figure 6.7 The discontinuous map $\mathcal{P}(\dot{y}_0) = \dot{y}_1$ (dotted curve) and $\dot{y}_1 = \dot{y}_0$ (dashed curve) as a function of $\dot{y}_0$. Two 3-switch limit cycles are illustrated as solid lines. The system is $G(s) = \omega^2/(s^2 + 2\zeta\omega s + \omega^2)$ with $\zeta = -0.1$, $\omega = 1$ and the relay characteristics are $d = 1$, $\epsilon = 2$.

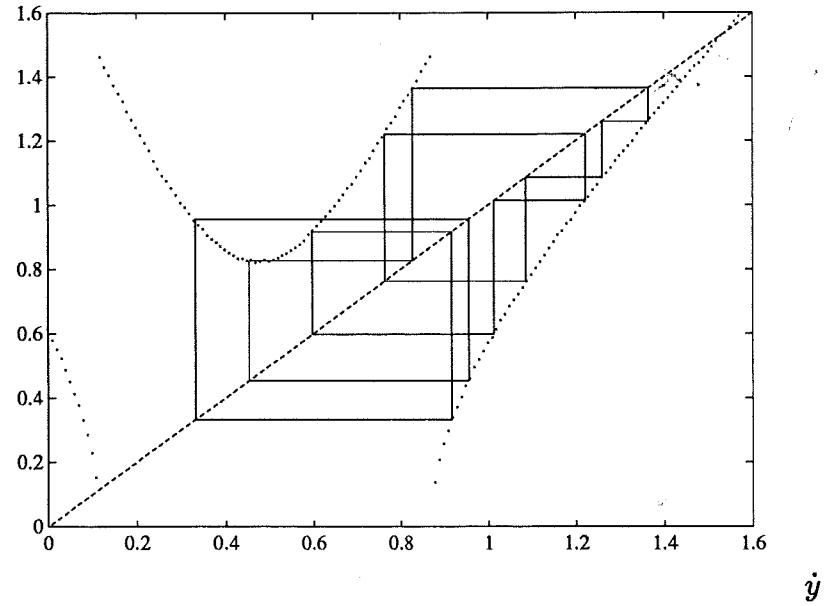

Figure 6.8 The discontinuous map $\mathcal{P}(\dot{y}_0) = \dot{y}_1$ (dotted curve) and $\dot{y}_1 = \dot{y}_0$ (dashed curve) as a function of $\dot{y}_0$. A 12-switch limit cycles is illustrated as solid lines. The system is $G(s) = \omega^2/(s^2 + 2\zeta\omega s + \omega^2)$ with $\zeta = -0.1$, $\omega = 1$ and the relay characteristics are $d = 1$, $\epsilon = 2$.

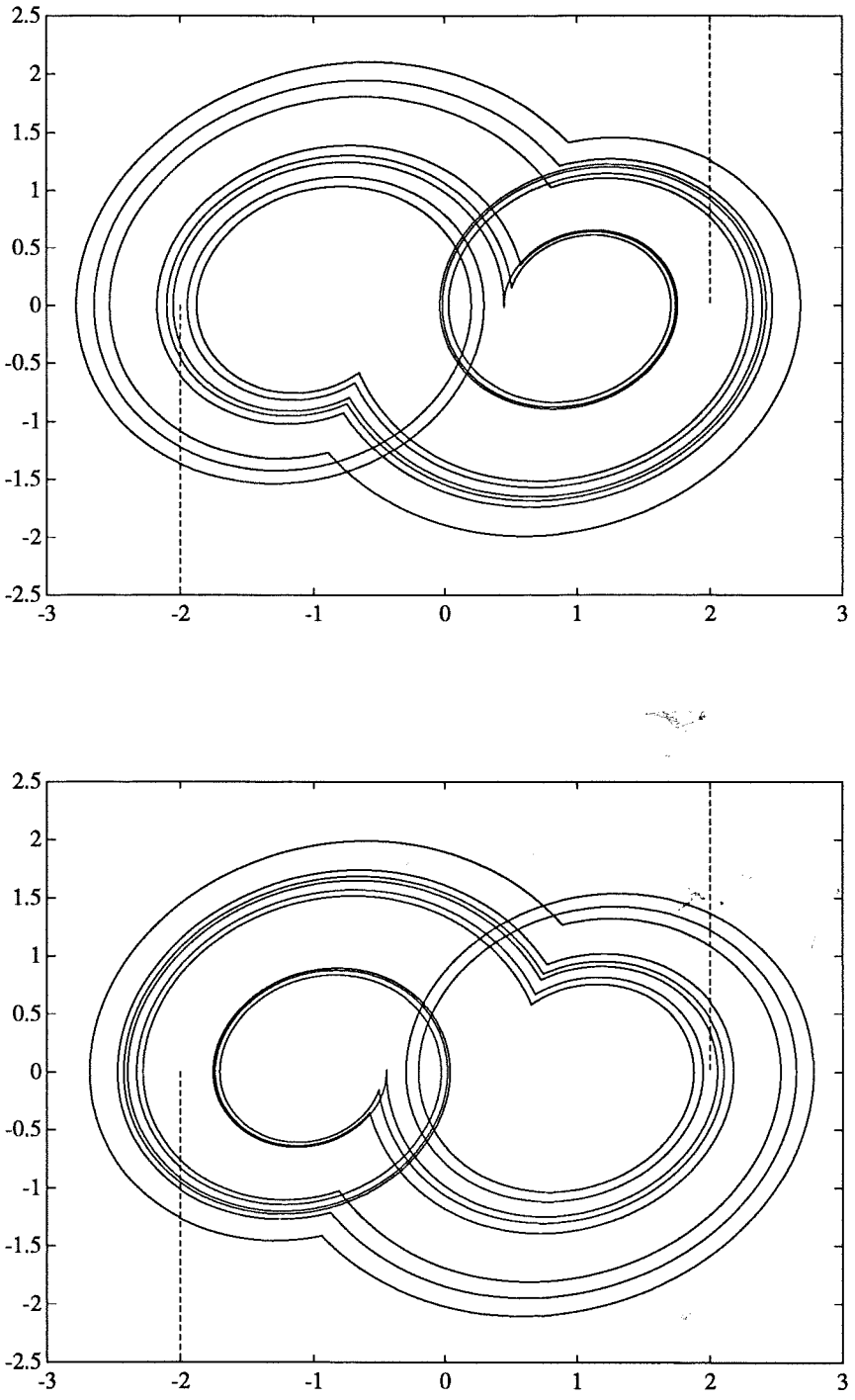

Figure 6.9 Two 12-switch limit cycles (solid closed curves above and below) corresponding to the same $\mathcal{P}$-map. The system is $G(s) = \omega^2/(s^2 + 2\zeta\omega s + \omega^2)$ with $\zeta = -0.1$, $\omega = 1$ and the relay characteristics are $d = 1$, $e = 2$. The Poincaré sections are shown as dashed lines.

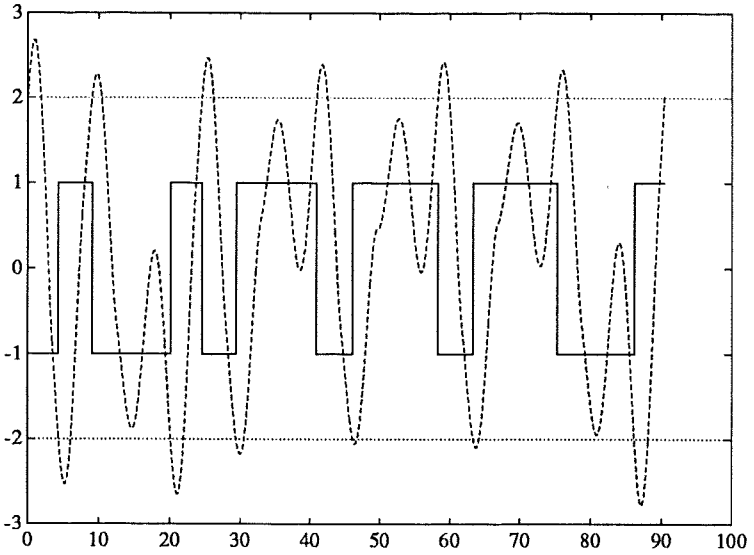

Figure 6.10 One period of a locally stable 12-switch limit cycle. The system is $G(s) = \omega^2/(s^2 + 2\zeta\omega s + \omega^2)$ with $\zeta = -0.1$, $\omega = 1$ and the relay characteristics are $d = 1$, $\epsilon = 2$ (dotted). The output $z(t)$ is dashed and the relay output $u(t)$ is solid.

6.3 Chaos

From a practical point of view chaos can be defined as bounded steady-state behaviour that is not an equilibrium point, not periodic, and not quasi-periodic. One property of chaotic systems is *extreme sensitivity to initial conditions*: given two different initial conditions arbitrary close to one another, the trajectories emanating from these points diverge until, for all practical purposes, they are uncorrelated. Simply put, a chaotic system is a *deterministic* system that exhibits *random* behaviour. Also, the limit set for chaotic behaviour is not a simple geometrical object like a circle or torus, but it has fractal structure. In the previous section, multi switch limit cycles were indeed limit cycles, forming a closed curve in the phase plane, even though the discontinuous $\mathcal{P}$-map gave rise to quite peculiar and complicated behaviour. Yet another property of chaotic systems is the fine structure of the limit set, the *strange attractor*. This means that the attracting limit set is not a closed curve in the phase plane. No matter how much we amplify to reveal details, more and more new details will always show up.

Dimension

Attractors can be classified by using the concept of dimension. An attractor is said to be n-dimensional if, in a neightbourhood of every point, it looks

like an open subset of $\mathbb{R}^n$. For instance, a (multi switch) limit cycle is one-dimensional since it looks locally like an interval. A torus is two-dimensional since, locally, it resembles an open subset of $\mathbb{R}^2$. That is typically for 2-periodic (quasi-periodic) solutions. An equilibrium point is considered to have zero dimension. The neighbourhood of any point of a strange attractor, however, has a fine structure and does not resembles any Euclidean space. Hence, strange attractors are not manifolds and do not have integer dimension. There are several ways to generalize dimension to the fractional case. One is the *correlation dimension*, D_C. This is easily estimated by use of points, sampled from a trajectory, see Parker-Chua (1987).

DEFINITION 6.3—Correlation Dimension, D_C
Suppose N points of a trajectory have been gathered either through simulations or from measurements. Define the correlation as

$$C(\epsilon) = \lim_{N\to\infty} \frac{1}{N^2} \left\{ \begin{matrix} \text{the number of pairs of points} \\ x_i, x_j \quad \text{such that} \quad ||x_i - x_j|| < \epsilon \end{matrix} \right\}$$

Then the correlation dimension is

$$D_C = \lim_{\epsilon\to 0} \frac{\ln C(\epsilon)}{\ln \epsilon}$$

□

EXAMPLE 6.3—Chaos
Once again, consider the system (6.1), but modify slightly the parameters; $\zeta = -0.105$ and $\varepsilon = 2.1$. The idea is to get multi switch solutions to come very close to the unstable limit cycle. The nearer the solution comes the unstable limit cycle the longer it will stay there. Thus, the $\mathcal{P}$-map will scan over a large number of points with high density near the limit cycle. Finally, the solution will diverge far away from the limit cycle in a multi switch like fashion until it once again comes back very close to the limit cycle. However, not to exactly the same point as before. The $\mathcal{P}$-map will once again scan over a large number of points with high density, slightly different points than before, producing a fine structure. The procedure repeats resulting in a strange attractor with fractional dimension. The $\mathcal{P}$-map is shown in Figure 6.11. In order to see that the solution is not a closed curve the $\mathcal{P}$-map is plotted versus iterations in Figure 6.12. The strange attractor is plotted in the phase plane $(y, \dot{y})$ in Figure 6.13. Note the fine structure and the increasing density near the edge of the unstable limit cycle solution. By use of samples of data from the strange attractor the dimension can be estimated. In Figure 6.14, $\ln[C(\epsilon)]$ is plotted versus $\ln[\epsilon]$, where the $\mathcal{P}$-map data are used. For a finite number of data there is an interval where this curve is linear. The slope there, approximately 0.85, will give us an estimate of the dimension of

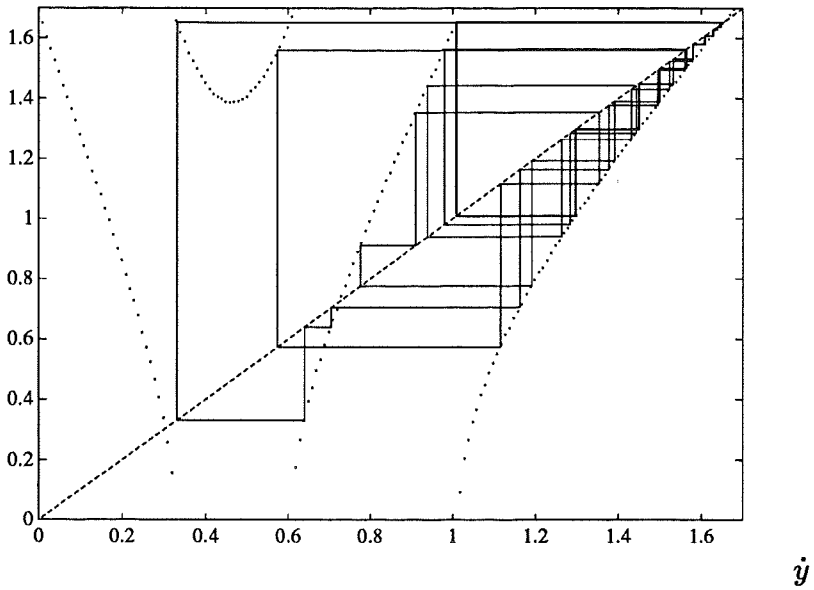

Figure 6.11 The Poincaré map for a strange attractor (the solid lines). The system is $G(s) = \omega^2/(s^2 + 2\zeta\omega s + \omega^2)$ where $\zeta = -0.105$, $\omega = 1$, and the relay characteristics are $d = 1$, $\varepsilon = 2.1$. The discontinuos Poincaré map $\mathcal{P}(\dot{y}_{i+1}) = \dot{y}_i$ (dotted line) and $\dot{y}_{i+1} = \dot{y}_i$ (dashed line) are plotted versus $\dot{y}_i$.

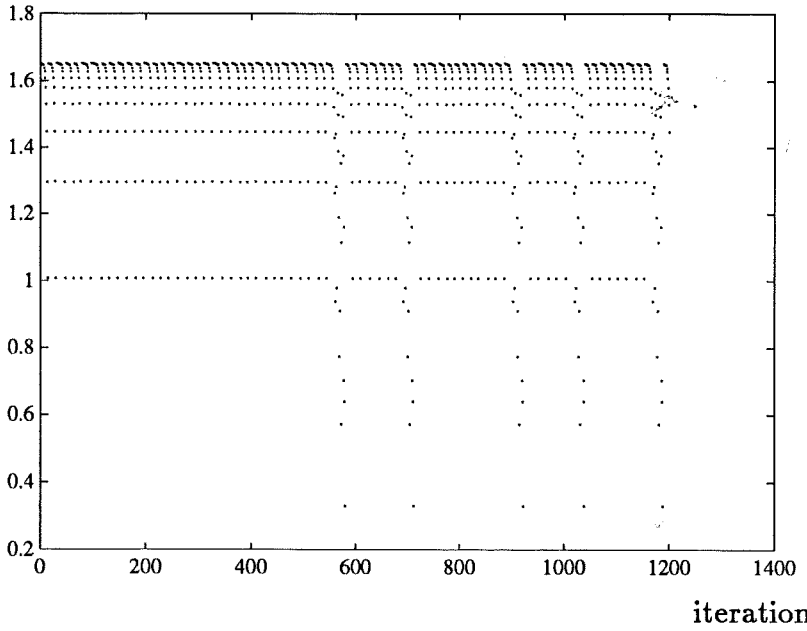

Figure 6.12 The Poincaré map from Figure 6.11, plotted versus iterations. This shows that the solution is not periodic, i.e. not a limit cycle. Also, the increasing density of points near the unstable limit cycle is seen, indicating fractional dimension close to 2.

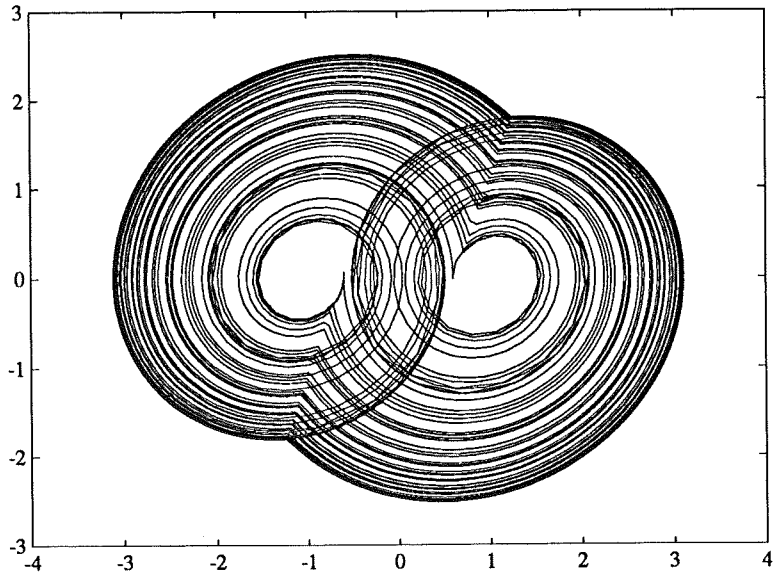

Figure 6.13 A strange attractor in the $(y, \dot{y})$ phase plane. The system is $G(s) = \omega^2/(s^2 + 2\zeta\omega s + \omega^2)$ where $\zeta = -0.105$, $\omega = 1$, and the relay characteristics are $d = 1$, $\varepsilon = 2.1$. The dimension is estimated to $D_C \approx 1.85$.

the $\mathcal{P}$-map. The strange attractor (in the phase plane) will therefore have the dimension, $D_C \approx 1.85$. □

Bifurcation

A bifurcation plot is commonly used to illustrate the complicated behaviour of a system that can exhibit chaos. The stable attractors shown by the $\mathcal{P}$-map are displayed versus one critical parameter. Typically, the plot shows a single curve suddenly splitting up into multiple curves or random like patterns, i.e. a limit cycle that suddenly change into a multi switch limit cycle or a strange attractor. Consider Example 6.3, but let ζ to vary, i.e. let ζ to be our critical parameter in a bifurcation plot. Choose the interval $\zeta \in \{-0.105, -0.100\}$. First, iterate the $\mathcal{P}$-map to find the attractor. Then, store a large number of data in order to reveal all multi switch levels or the pattern of a strange attractor. Note, that just one attractor is found per chosen initial condition, $\dot{y}(0)$. This means that the resulting bifurcation plot will only show one solution for each ζ. There may be many stable solutions as we saw in Example 6.2. The bifurcation plot is given in Figure 6.15. Note that we here did not get chaos when $\zeta = -0.105$ as we got before. Instead there is a stable 5-switch limit cycle. Thus, one and the same system can exhibit chaotic behaviour or limit cycles, depending on the initial condition.

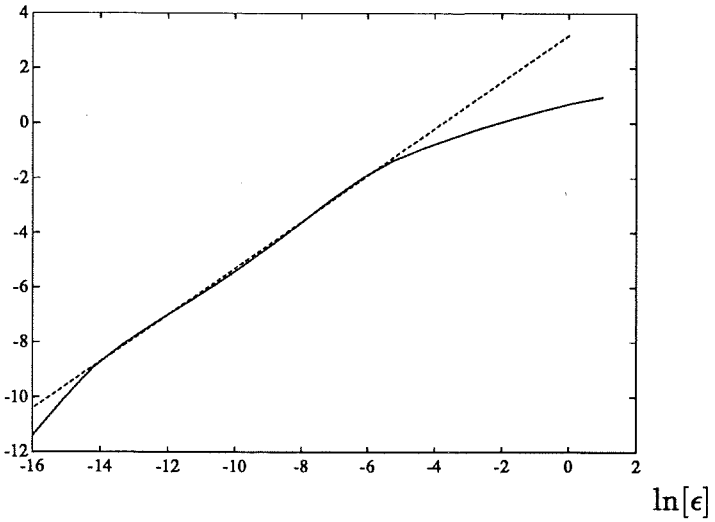

Figure 6.14 Data from the $\mathcal{P}$-map is used to plot the correlation $\ln[C(\epsilon)]$ versus $\ln[\epsilon]$ (solid curve). For a finite number of data there is an interval where this curve is linear. The slope there (the dashed line) will give us an estimate of the dimension of the $\mathcal{P}$-map, approximately 0.85. The strange attractor (in the phase plane) in Figure 6.13 will therefore have the dimension $D_C \approx 1.85$.

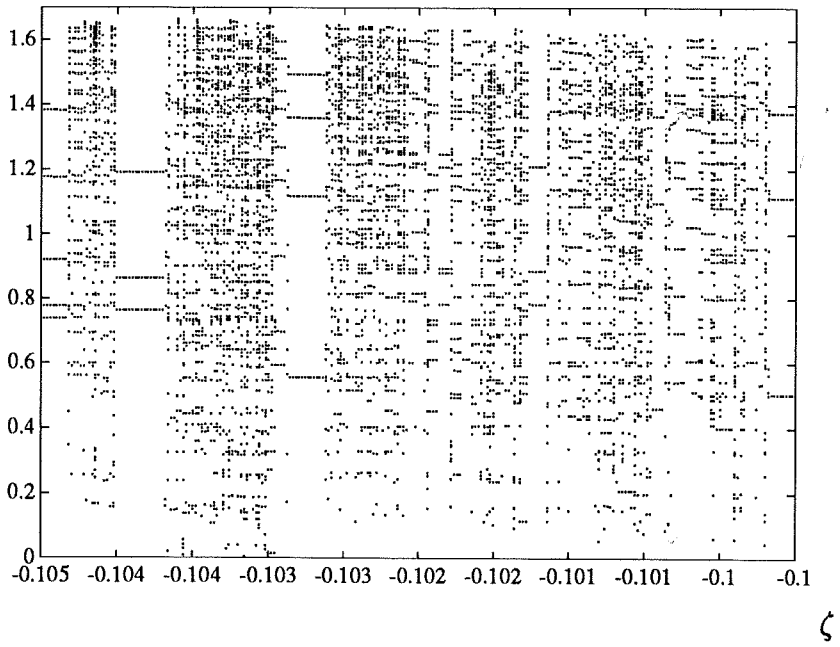

Figure 6.15 Bifurcation plot for the relay feedback system, $G(s) = e^{-3.5s}/(s^2 + 2\zeta s + 1)$ and $d = 1$, $\varepsilon = 2.1$. The $\mathcal{P}$-map attractors are plotted versus ζ. The same $\dot{y}(0)$ is used for all ζ.

6.4 Summary

Relay feedback of a second order system with unstable complex poles can give rise to chaos. This was shown in Cook (1985), who used positive feedback. It was also shown that all limit cycle solutions are unstable. In this chapter we have investigated second order systems with time delays. It has been shown that chaos can then be obtained even with negative feedback. Some of the limit cycle solutions also appear to be stable.

7

Identification of dissolved oxygen concentration dynamics

Relay oscillations can be used in many different ways. In Åström-Hägglund (1984) it is shown how relay oscillations can be used to obtain the dynamics required to tune a PID controller. An unconventional use of relay feedback to determine dynamics is given in this Chapter. The dynamics of dissolved oxygen (DO) concentration in an activated sludge system can be described by a nonlinear, time-varying differential equation. It is characterized by the oxygen transfer rate*, $K_L a$, which is a nonlinear function of the air flow rate, and the respiration rate, R, which is varying with time. The quantities, $K_L a$ and R, are of special interest. It will be shown that a relay-like feedback can be used to cause a self-excitation that reveals information about $K_L a$ and R. They will both, however, contain an undetermined bias that is not identifiable. The relay amplitude is adjusting itself to keep a prescribed oscillation amplitude around a DO setpoint. This makes a tradeoff between estimation and control. It should be noted that the main purpose here is not to regulate the DO concentration but to identify the dynamics. The tradeoff between estimation and control has therefore been made in favour for estimation. However, in spite of the introduced excitation the DO control will

* The notation, $K_L a$, is standard in literature and should be read as one single quantity and not $K_L \cdot a$.

be satisfactory. The idea has been tested in a series of full scale experiments at Malmö Sewage Works in Sweden. Results from one of these experiments are presented in this chapter.

7.1 Introduction

The respiration rate, R, is an essential variable in an activated sludge system. It is the oxygen utilization rate due to the growth and decay of microorganisms and will vary with different loads on the plant. Respiration rate is an indicator of biological degradable load. Toxics may either slow down the growth rate or kill part of the organisms. This also is reflected in R, and can signal for a bypass action to save the organisms. The advantage of knowing R may not be limited to process diagnostics. In Olsson (1985), it was proposed to be used in step feed and sludge inventory control. It was shown in Olsson-Andrews (1978) that the respiration rate profile along the biological reactor is important. Knowledge of the profile can be used to adjust of the air flow rate distribution along the basin. The profile would also suggest an appropriate setpoint for the DO control.

The idea of on-line estimation of R given only DO sensor and air flow signals, was proposed by Brouzes (1968), among others. However, in an open aerator R cannot be calculated from the DO mass balance unless the oxygen transfer rate K_La is known. Different approaches have been suggested for estimation of K_La and R. Certain assumptions have then been made, which have been more or less unrealistic. In a simulation study by Ko *et al* (1982), R was assumed constant. Similar simplifications were assumed by Howell-Sopido (1985). Another approach was taken by Cook *et al* (1981), where deviations of R from an unknown steady state value was estimated. Adaptive control schemes have been applied in Holmberg-Olsson (1985), Holmberg (1986), Holmberg *et al* (1988) and Marsili-Libelli (1990). In these papers K_La was assumed proportional to the air flow rate. In Holmberg (1990) it was shown that this assumption is not correct. The simplification will make any estimates of K_La and R biased.

In section 7.2 the DO model is given. An adaptive control scheme using relay excitation is presented in section 7.3. Identifiability is discussed in section 7.4, where it is shown that K_La and R will be undetermined by a bias. Reconstruction of the nonlinear K_La and the time varying $R(t)$, apart from the undetermined bias, are made in section 7.5. Conclusions are given in section 7.6.

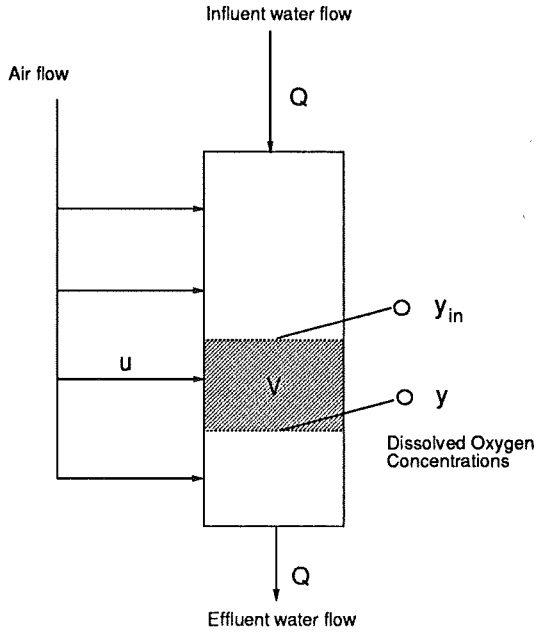

Figure 7.1 The biological reactor—a full scale plant. The dashed zone is regarded as completely mixed.

7.2 The dissolved oxygen concentration dynamics

Full scale experiments have been made at Malmö Sewage Works. The plant is designed to serve 550 000 person equivalents but a normal load is about 400 000. A normal water flow is about 1 300 l/s. The total flow is split between an activated sludge system and a fixed film bed reactor system. The former is divided into three parallel double basins, each one of them having a volume of 3 300 m^3. The outline of one such double basin is shown in Figure 7.1. The influent biodegradable substrate will be removed continuously by the activity of the microorganisms, causing a profile along the reactor of the DO concentration and the respiration rate. We will consider a part of the reactor, the dashed zone in Figure 7.1, as completely mixed. The influent DO concentration, y_{in}, is then measured at the mid point of the reactor and the effluent DO concentration, y, at the 3/4-point. The completely mixed assumption approximate the DO concentration in the whole dashed zone to be equal to y. This simplification gives the model

$$\frac{dy}{dt} = \frac{Q}{V}(y_{in} - y) + K_L a(u) \cdot (c - y) - R \tag{7.1}$$

where

$K_L a(u)$	Oxygen transfer rate
R	Respiration rate
y	DO concentration in the dashed zone

c	DO saturation concentration
y_{in}	Influent DO concentration to the dashed zone
u	Air flow rate to the dashed zone
Q	Water flow rate
V	Volume of the dashed zone

The values of $K_L a(u)$ and R are unknown. Normally, the respiration rate, R, has a daily variation reflecting the activity of the bacteria. It may, however, make rapid changes (within fractions of hours) if toxic disturbances enter the plant. The oxygen transfer rate, $K_L a(u)$, on the other hand is regarded to be a static function of u, the air flow rate. In fact, it will change with time, but rather within weeks than days. This is due to clogging of the diffusers of the air production system.

7.3 Adaptive control by relay excitation

First assume that

$$K_L a(u) = a \cdot u$$

If this is valid, there are two unknown parameters to consider, a and R. Two linearly independent equations are needed in order to calculate the two parameters. Therefore excite the system by forcing it into a limit cycle. The equation is then considered consecutively twice a period, giving two linearly independent equations. The two parameters, a and R, are then calculated and used by an adaptive regulator. It is important to maintain y within some range in order to keep an environment that favour flock forming organisms. The regulator is therefore designed to keep y oscillating around a setpoint y_{sp}. The amplitude is then adjusted to a level that compromise between regulation and estimation. The adaptive controller can be split up into three parts, regulation, excitation and estimation.

Regulation: Let the control error be $e = y_{sp} - y$. Assume perfect estimation, i.e. $\hat{a} = a$ and $\hat{R} = R$. It follows from (7.1) that the control law

$$u(t) = \frac{-\frac{Q(t)}{V}(y_{in}(t) - y(t)) + \hat{R}(t) + e(t)}{\hat{a}(c - y(t))} \quad ; \; t = kh, \; k = 1, 2, \ldots$$

gives a closed loop system such that

$$\frac{de(t)}{dt} = -e(t) \quad ; \quad t = kh, \; k = 1, 2, \ldots$$

at the sample instants. The sampling period is $h = 12$ minutes. This choice is considered appropriate for describing the dynamics in (7.1). If a too short

sampling interval is used higher order dynamics from e.g. the air production system makes the simplified model (7.1) unappropriate. The control signal u will be kept constant over the sampling period. This will both reduce the effect of unmodelled dynamics and have a practical benefit since it is easy to accomplish. It is also useful for the identification procedure.

Excitation: Since the parameters are unknown excitation is needed in order to receive information about the parameters. Therefore, a relay is introduced to get self-excitation, i.e. the control law is modified to

$$u(t) = \frac{-\frac{Q(t)}{V}(y_{in}(t) - y(t)) + \hat{R}(t) + e(t) + d \cdot \text{sign}[e(t)]}{\hat{a}(c - y(t))} \quad ; t = kh, k = 1, 2, \ldots$$

giving, at sampling instants, the closed loop

$$\frac{de(t)}{dt} = -e(t) - d \cdot \text{sign}[e(t)] \quad ; \quad t = kh, \; k = 1, 2, \ldots$$

A compromise between parameter tracking and accurate control is made by tuning of the relay amplitude, d, once the system has started to oscillate. The relay amplitude is tuned such that the amplitude of the oscillation becomes e_{sp}, which is a design parameter. The oscillation is considered to has started when $|e(kh) + e(kh - h)| < e_{sp}$. The relay amplitude tuning is

$$d(kh + h) = d(kh) + k_d(e_{sp} - |e(kh)|)$$

$$k_d = \begin{cases} k_d^0 & \text{when } |e(kh) + e(kh - h)| < e_{sp} \\ 0 & \text{otherwise} \end{cases}$$

The parameter k_d^0 determines the tuning rate of the relay amplitude once the oscillation has started.

Estimation: Rewrite the system (7.1) as

$$\frac{dy}{dt} = Ay + B \qquad \begin{cases} A = -(K_L a + \frac{Q}{V}) \\ B = -R + \frac{Q}{V} y_{in} + K_L a \cdot c \end{cases}$$

Assume that all parameters are constant during the sampling period h and introduce the notation

$$h^* = \frac{1}{A}(e^{Ah} - 1)$$

Then the zero order hold sampled system is

$$y(kh + h) = e^{Ah} y(kh) + \frac{B}{A}(e^{Ah} - 1) =$$
$$= (Ah^* + 1)y(kh) + Bh^*$$

Thus,

$$\frac{y(kh+h)-y(kh)}{h^*} = Ay(kh)+B = \frac{dy(kh)}{dt}$$

If an old estimate of a is used in the calculation of $h^* = h^*(\hat{a}_{old})$, the derivative can be approximated by

$$\frac{\widehat{dy(kh)}}{dt} = \frac{y(kh+h)-y(kh)}{h^*(\hat{a}_{old})}$$

Starting from scratch with $\hat{a} = 0$, we get the Euler approximation since $h^*(0) = h$. Now, use the estimator model

$$(\widehat{\frac{dy}{dt}} - \frac{Q}{V}(y_{in}-y)) = \begin{pmatrix} u(c-y) & -1 \end{pmatrix} \begin{pmatrix} \hat{a} \\ \hat{R} \end{pmatrix}$$

This equation is now considered at two time instants. Between these instants the system is excited by the relay such that the two considered equations become linearly independent. It is then straightforward to solve for $\hat{a}$ and $\hat{R}$.

Simulation

The behaviour of the proposed controller is illustrated in Figure 7.2. No noise is present in this simulation and the parameters are constants, $a = 0.005$ and $R = 10$. The tank dilution is constant, $Q/V = 1$, and $y_{in} = 0$. The DO setpoint is $y_{sp} = 2$ mg/l and the oscillation setpoint is $e_{sp} = 0.2$ mg/l. The intention here, is to illustrate the control/excitation part of the algorithm. The control input affects the time constant of the system through $K_L a$. A step response upwards is therefore different form a step response downwards. This has the effect that the mean value of y during the oscillation is becoming slightly different from y_{sp}. This is not compensated for. Thus, instead of oscillating between $y_{sp} + e_{sp} = 2.2$ and $y_{sp} - e_{sp} = 1.8$ the results are 2.16 and 1.76 respectively. The relay amplitude is initialized to $d = 1$. When the oscillation starts, the relay amplitude is adjusted to give an oscillation amplitude e_{sp}. The tuning gain is $k_d = 1$. The adjusted relay amplitude d is shown below in Figure 7.2. The parameters converge quickly and are already after 3 sampling periods $\hat{a} = 0.0051$ and $\hat{R} = 10.2$.

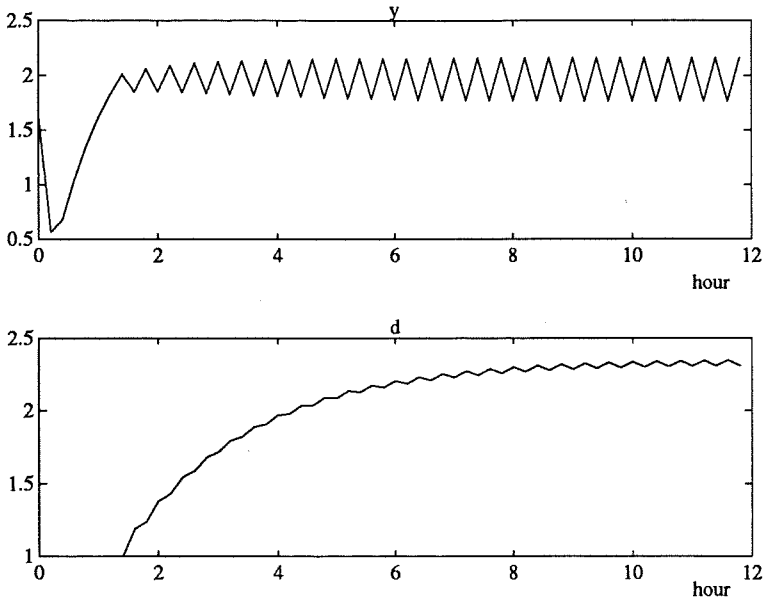

Figure 7.2 Simulation to illustrate the control/excitation part of the algorithm. All parameters are constants, $a = 0.005$, $R = 10$, $Q/V = 1$ and $y_{in} = 0$. The control parameters are $y_{sp} = 2\ mg/l$ and $e_{sp} = 0.2\ mg/l$. The relay tuning gain is $k_d = 1$ and the relay amplitude is initialized to $d = 1$. Above, the tuned oscillation, y, and below, the tuned relay amplitude, d, are shown.

Experiment

The above adaptive control scheme was tried during a 3 day experiment at Malmö Sewage Works. The resulting y and u are shown in Figure 7.3. The dotted lines indicate $y_{sp} \pm 2e_{sp}$, where $y_{sp} = 2$ mg/l and $e_{sp} = 0.2$ mg/l. The output y is supposed to oscillate between $y_{sp} \pm e_{sp}$. Due to disturbance the amplitude of the oscillation will be larger. Figure 7.3 shows that it is increased roughly with a factor of 2, except for two occasions where the input u is saturated. A square wave is used when u is saturated. Then at least the estimation can continue during the saturation. The control is not much worse than with conventional control although we introduce the excitation to be able to estimate the parameters. The tradeoff between regulation and estimation is made to benefit the estimation. On the other hand the regulation we get is considered to be quite satisfactory.

Model mismatch could lead to large estimation errors. In order not to propagate an occasionally large error in the estimate $\hat{a}$ into the calculation of $\widehat{\frac{dy}{dt}}$, the estimate $\hat{a}$ was filtered. The estimate was limited to non-negative values. The unfiltered $\hat{a}$ is shown in Figure 7.4 together with the input u. Note that $\hat{a}$ and u are changing in opposite phase to each other. The model assumption $K_L a(u) = a \cdot u$ is therefore inappropriate. When u is large the

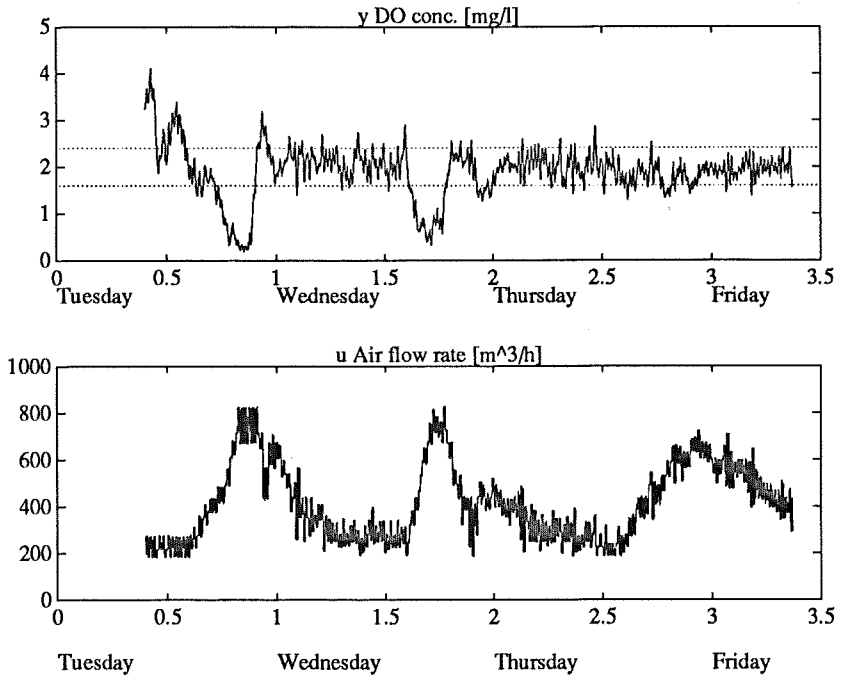

Figure 7.3 A three day experiment at Malmö Sewage Works. Above, the DO concentration, y, and below the air flow rate, u. The dotted lines show twice the oscillation setpoints, i.e. $y_{sp} \pm 2e_{sp}$, where $y_{sp} = 2$ mg/l and $e_{sp} = 0.2$ mg/l.

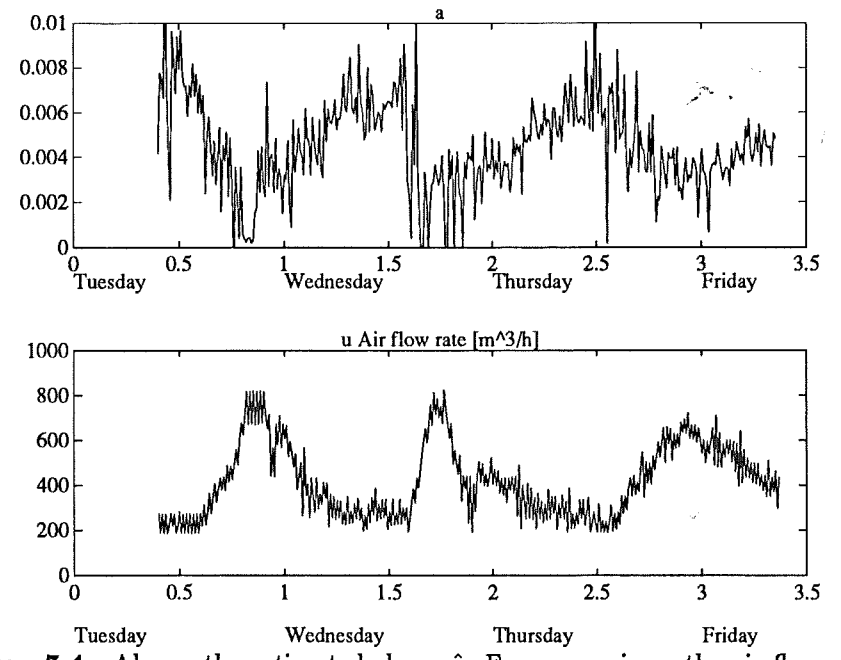

Figure 7.4 Above, the estimated slope, $\hat{a}$. For comparison, the air flow rate u is shown below. Notice that $\hat{a}$ and u are changing in opposite phase. This is an indication of a nonlinear relation between $K_L a$ and u.

slope a is small and vise versa. The relation between K_La and u can thus be expected to be nonlinear. Such a character of K_La can be observed by independent aeration efficiency experiments. A proposed qualitative shape of such a nonlinearity is sketched in Figure 7.5. Thus, a local approximation

$$K_La(u) = a \cdot u + b$$

would be an appropriate model. The problem is that, during control of y, u is varying quite rapidly to outweigh the influence from R. The parameters a and b are therefore constant only during short intervals where u is not changing too much.

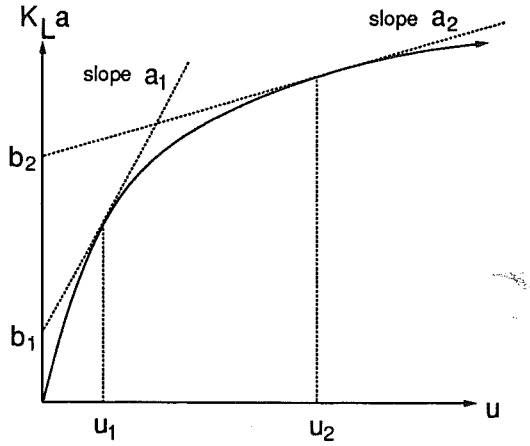

Figure 7.5 A sketch, illustrated the assumed shape of $K_La(u)$. When $u \approx u_1$, the K_La model is approximately $K_La(u) \approx a_1 \cdot u + b_1$, with a large a_1 and a small b_1, while when $u \approx u_2$, the model is $K_La(u) = a_2 \cdot u + b_2$, with instead a small a_2 and a large b_2.

The errors made by not having the parameter b in the estimator model is investigated below. Suppose for simplicity that $\widehat{\frac{dy}{dt}} = \frac{dy}{dt}$. Then, consider the DO equation at two consecutive sampling instants (indexed 1 and 2)

$$\begin{pmatrix} u_1(c-y_1) & -1 \\ u_2(c-y_2) & -1 \end{pmatrix} \begin{pmatrix} \hat{a} \\ \hat{R} \end{pmatrix} = \begin{pmatrix} u_1(c-y_1) & -1 \\ u_2(c-y_2) & -1 \end{pmatrix} \begin{pmatrix} a \\ R \end{pmatrix} + b \begin{pmatrix} c-y_1 \\ c-y_2 \end{pmatrix}$$

Solving for $\hat{a}$ and $\hat{R}$ gives

$$\begin{cases} \hat{a} = a + \dfrac{y_1 - y_2}{u_2(c-y_2) - u_1(c-y_1)} \approx a \\ \hat{R} = R + b\dfrac{u_1(c-y_1)(c-y_2) - u_2(c-y_2)(c-y_1)}{u_2(c-y_2) - u_1(c-y_1)} \approx R - b(c-y_{sp}) \end{cases}$$

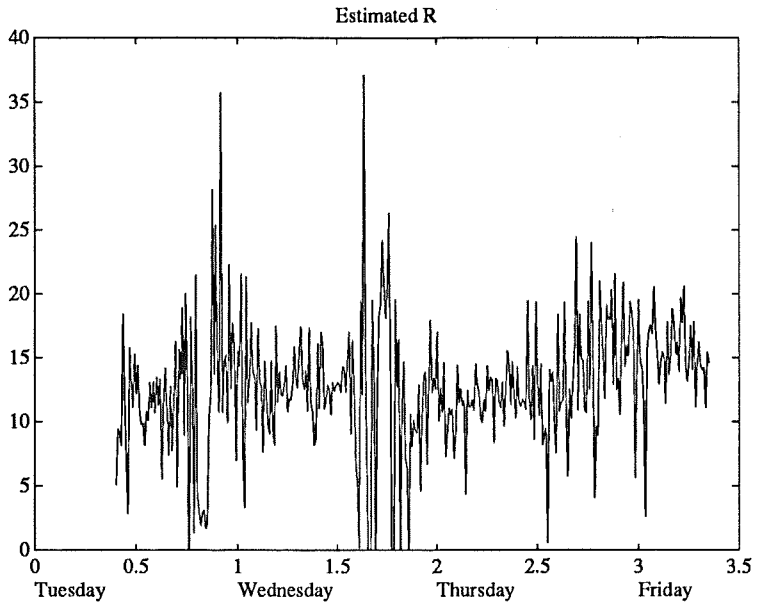

Figure 7.6 The estimated respiration rate, $\hat{R}$. The true R is expected to vary together with u during control to keep y constant. This is not seen here. The reason is that $\hat{R} \approx R - b(c - y_{sp})$ where b is changing together with u (see Figure 7.5). The variations in $\hat{R}$ is therefore suppressed.

since $y_1 \approx y_2 \approx y_{sp}$ during control. Thus, the estimate $\hat{a}$ is expected to be accurate while $\hat{R}$ will be biased. Moreover, u is changing together with R during control to keep y constant. It follows from the graph of $K_L a(u)$ in Figure 7.5 that the bias, b, increases with increasing u. The daily variations of R would therefore be suppressed in $\hat{R}$, if seen at all. The estimated $\hat{R}$, in Figure 7.6, supports this. Hardly no dayly variations are seen, just noise around a fairly constant level.

The following conclusions can be drawn from the experiment. The relay adaptive controller succeeds fairly well to keep y within the prescribed limits. This was, however, not the primary goal. The main purpose was to find $K_L a$ and R. This was not succeeded. The reason was that the $K_L a$ model was inappropriate. A nonlinear relation between $K_L a$ and u should be used. On parts of the data where u is fairly constant the nonlinear model can be approximated by

$$K_L a(u) = a \cdot u + b \tag{7.2}$$

Different estimates $\hat{a}$ and $\hat{b}$ associated with different levels of u are then forming the nonlinear $K_L a$ model. However, next section shows that the parameter b is not identifiable, leaving any estimated $K_L a$ and R undetermined by a bias.

7.4 Identifiability

Consider a part of the data where u is fairly constant such that the linearized K_La model (7.2) is appropriate. Let the true system be defined by

$$\begin{cases} R_1(t) \\ K_La_1(u) = a \cdot u + b \end{cases} \rightarrow y_1(t)$$

Then

$$\begin{cases} R_2(t) = R_1(t) - b[c - y_1(t)] \\ K_La_2(u) = a \cdot u \end{cases} \rightarrow y_2(t)$$

will give the same result, $y_2(t) = y_1(t)$. No identification algorithm can therefore distinguish whether the data $y_1(t)$ have been generated by K_La_1 and R_1 or by K_La_2 and R_2, i.e. the bias parameter b is not identifiable. If $R(t)$ and $y(t)$ could be assumed uncorrelated there would be a chance for identification of b. Such an assumption can, however, not be justified. The identification is therefore focused on the parameter a for different levels of u. Biases on any estimation of R and K_La are something that have to be accepted. This will be illustrated later (Figure 6.9) where two different choices of the bias parameter b give rise to very similar $\hat{y}$ that can be made arbitrarily close to the true y by letting $\widehat{R}$ vary.

7.5 Reconstruction of $K_La(u)$ and $R(t)$

The local K_La model was found to give parameters that were depending on the air flow rate, i.e.

$$K_La(u) = a(u) \cdot u + b(u)$$

In Figure 7.4 the dependence between a and u was recognized and in Figure 7.6 the expected load peaks in $\hat{R}$ were missing due to variations of b together with u. A more appropriate model is therefore a nonlinear relation like

$$\widehat{K_La}(u) = p_0u^2 + p_1u + p_2 \tag{7.3}$$

with presumably constant parameters p_0, p_1 and p_2. The parameters p_0 and p_1 are then used to model the relation $a(u)$. The parameter p_2, on the other hand, will be unknown like b. But unlike b it will be constant for all u. The global model (7.3) is associated to the local model (7.2) around a given air flow rate, u_0, as

$$\widehat{K_La}(u) \approx \widehat{K_La}(u_0) + \frac{d\widehat{K_La}(u_0)}{du}(u - u_0) = a \cdot u + b$$

where

$$\begin{cases} a = \dfrac{d\widehat{K_L a}(u_0)}{du} = 2u_0 p_0 + p_1 \\ b = \widehat{K_L a}(u_0) - \dfrac{d\widehat{K_L a}(u_0)}{du} u_0 = p_2 - p_0 u_0^2 \end{cases}$$

By using the estimated slope $\hat{a}$, the parameters p_0 and p_1 can be calculated by the least squares method from the equation system

$$\begin{pmatrix} \hat{a}_1 \\ \hat{a}_2 \\ \cdot \\ \cdot \\ \hat{a}_n \end{pmatrix} = \begin{pmatrix} 2u_1 & 1 \\ 2u_2 & 1 \\ \cdot & \cdot \\ \cdot & \cdot \\ 2u_n & 1 \end{pmatrix} \begin{pmatrix} p_0 \\ p_1 \end{pmatrix} \quad \rightarrow \quad \begin{cases} p_0 \\ p_1 \end{cases}$$

where n is the number of data used with the sampling interval $h = 12$ minutes. Note that, the parameter p_2 will be undetermined, giving a bias in $\widehat{K_L a}$. In order to see if the estimation of p_0 and p_1 gives reproducible constant values we split the data series into two halves. The resulting least squares estimated parameters are

$$\begin{cases} p_0 = -4.6 \cdot 10^{-6} \\ p_1 = 8.5 \cdot 10^{-3} \end{cases} \quad \text{Thuesday} - \text{Wednesday night}$$

and

$$\begin{cases} p_0 = -3.3 \cdot 10^{-6} \\ p_1 = 7.1 \cdot 10^{-3} \end{cases} \quad \text{Wednesday night} - \text{Friday}$$

respectively, while the whole data series gives

$$\begin{cases} p_0 = -4.0 \cdot 10^{-6} \\ p_1 = 7.9 \cdot 10^{-3} \end{cases} \quad \text{Thuesday} - \text{Friday}$$

The estimated slopes $\hat{a}$ are plotted against the air flow rate u in Figure 7.7. The estimates $\hat{a}$ are marked 'x' and 'o' in the first and second half of the data series respectively. Corresponding data are used in least squares fitting of straight lines $a = 2p_0 \cdot u + p_1$. These are dashed and dotted respectively. The solid line is the least squares fitting using the whole data series. Notice the negative slope of the lines, $p_0 < 0$, which makes $\hat{a}$ and u to vary in opposite phase as was seen in Figure 7.4. Compared to the large noise level of $\hat{a}(u)$ the least squares fitting of a straight line is surprisingly reproducible. The small change of the parameters p_0 and p_1 during the experiment is considered to

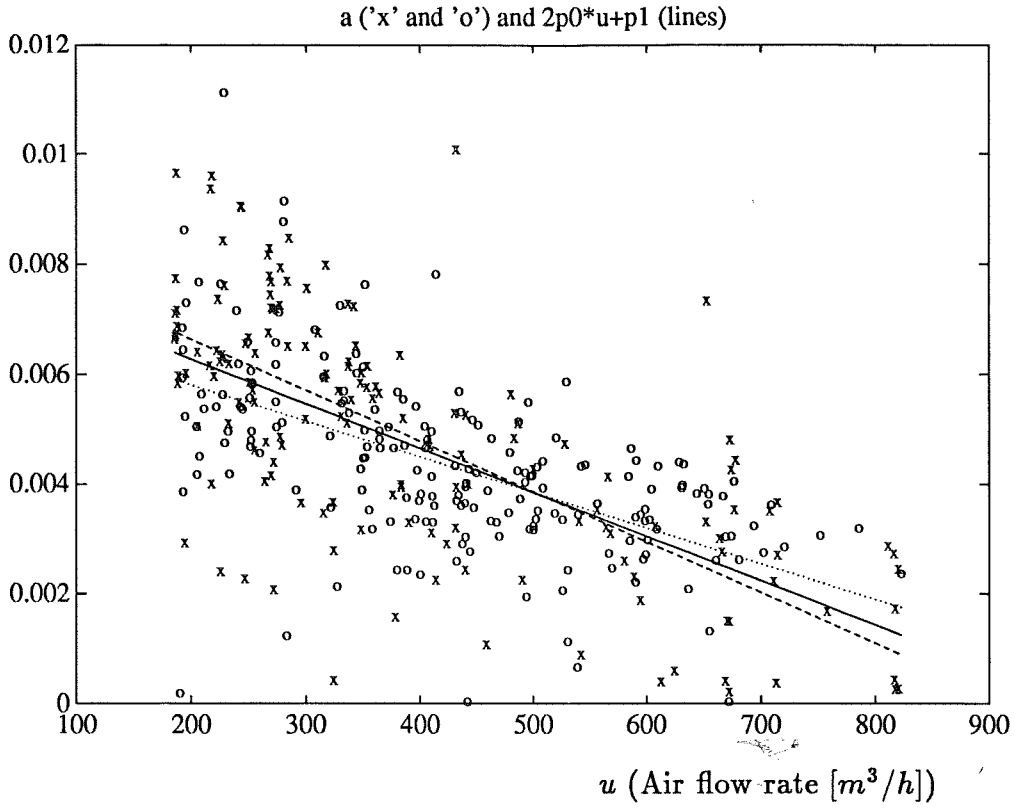

Figure 7.7 The estimated slopes $\hat{a}$ plotted against u, compare Figure 7.4. The estimates $\hat{a}$ are marked *'x'* and *'o'* in the first and second half of the data series respectively. Corresponding data are used in least squares fitting of straight lines $a = 2p_0 \cdot u + p_1$. These are dashed and dotted respectively. The solid line is the least squares fitting using the whole data series. Notice the negative slope of the lines, $p_0 < 0$, which makes $\hat{a}$ and u to vary in opposite phase as was seen in Figure 7.4.

be unsignificant. We therefore take the estimated p_0 and p_1 corresponding to the whole data series as our estimates. The unknown p_2 will be put to zero.

Once $\widehat{K_L a}(u)$ is estimated, it can be used in the DO mass balance equation for calculation of $\hat{R}(t)$. Since $\widehat{K_L a}$ is biased, so is $\hat{R}$. The estimated function $\widehat{K_L a}(u)$ and the corresponding $\hat{R}(t)$ are shown in Figure 7.8. Compare the result of Figure 7.8 with Figure 7.6.

To show the influence of the bias parameter p_2 (or b), a smaller part of the data will be considered, see Figure 7.9. Now, the sampling interval, $h = 2$ minutes will be used in order to reveal more details. The estimated $\widehat{K_L a}$ function, from Figure 7.8 above, is used with $p_2 = 0$ and $p_2 = 1$ respectively. Corresponding estimates for the respiration rate are calculated via the balance equation. These estimates are quite noisy due to the shorter sampling interval. They are therefore filtered through a low pass filter. In

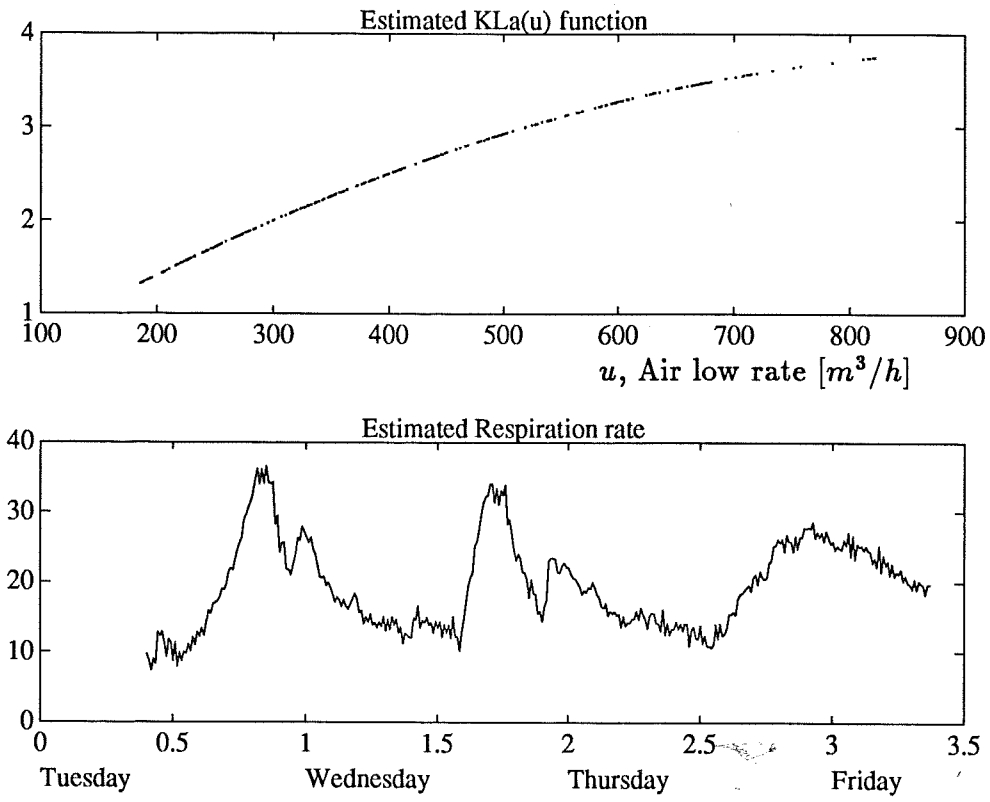

Figure 7.8 Above, the estimated function $\widehat{K_La}(u) = p_0u^2 + p_1u + p_2$, where $p_0 = -4.0 \cdot 10^{-6}$, $p_1 = 7.9 \cdot 10^{-3}$ and the undetermined p_2 is made zero. Below, the corresponding estimated $\widehat{R}(t)$.

Figure 7.9, these filtered $\widehat{R}(t)$ are shown. The curve corresponding to $p_2 = 0$ is plotted with $'o'$ and the curve corresponding to $p_2 = 1$ is plotted with $'x'$. Corresponding $\hat{y}$ calculated through the DO mass balance equation are also shown together with the true y. The error $y - \hat{y}$ can be made arbitrarily small by less filtering on $\widehat{R}$.

7.6 Conclusions

Identification of the dissolved oxygen (DO) concentration dynamics can be made during DO control. The system is self-excited by a relay-like feedback that forces the system into an oscillation around the DO setpoint. The oscillation gives information about the oxygen transfer rate, K_La, and the respiration rate, R. A nonlinear model relating the air flow rate, u, to K_La can be estimated. The respiration rate, $R(t)$, can also be reconstructed as a function of time. However, there will remain biases in the estimated K_La and R. The bias of R can be measured by independent measurements. It

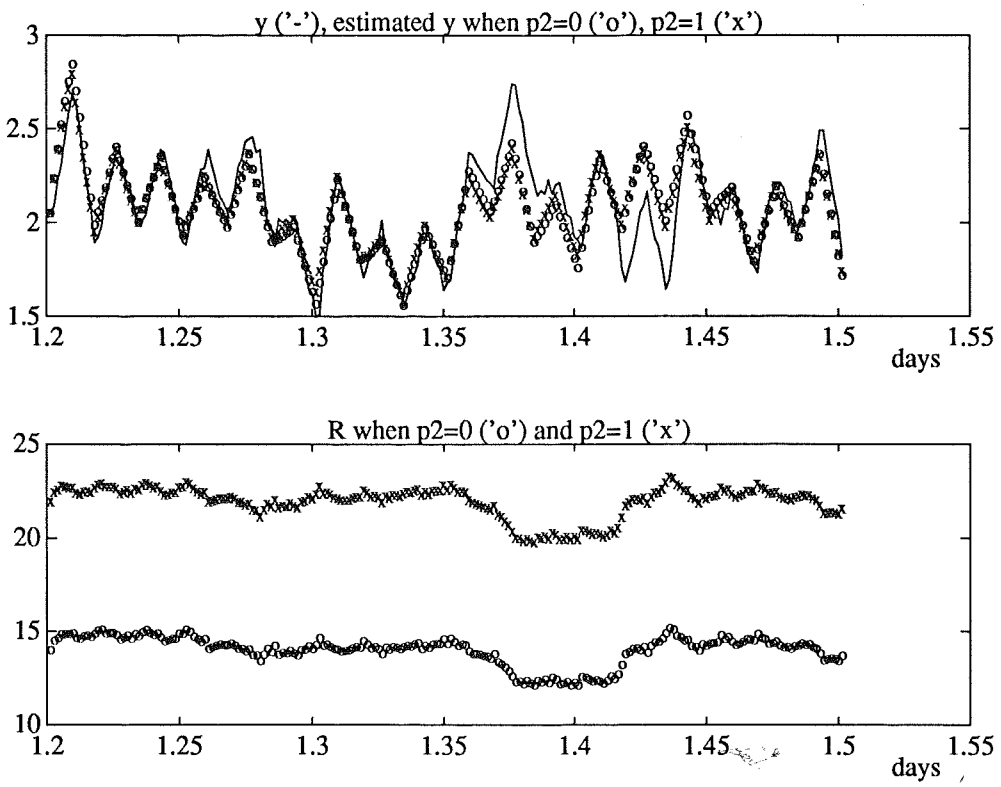

Figure 7.9 Below, estimated $\widehat{R}(t)$ corresponding to the estimated $\widehat{K_L a}(u)$ with $p_2 = 0$ (marked 'o') and $p_2 = 1$ (marked 'x') respectively. Above, the corresponding $\hat{y}$ with similar marking and the true y (solid). The deviation between the $\hat{y}$'s and y are due to filtering on $\widehat{R}(t)$.

is physically reasonable to assume that the bias is fairly constant over quite long periods ($\sim$ weeks). This means that the estimation technique is a useful operational tool.

8

Conclusions

Relay feedback of dynamical systems are common configurations in control systems. Automatic tuning is one recent area of application. The idea is to force a dynamical system into a limit cycle by use of a relay feedback. Information for tuning simple PID controllers or pretuning more sophisticated controllers is then obtained from the oscillation. All controllers, also adaptive controllers, need prior information for their initialization. A relay experiment is appealing since it is simple and often gives the required information. The problem, however, is that even though it usually works for many processes the behaviour is not fully understood. It is therefore not clear for what class of systems the relay experiment is applicable. Strange behaviour of systems with relay feedback has also been observed. The aim of this thesis has been to develop an understanding of the behaviour of systems with relay feedback. This is done by analysing simple systems. These simple systems are, however, often used as models in process industry where pre-tuning is most popular.

The behaviour of a relay feedback system is complicated. The describing function method is a simple approximate technique. A brief overview of the describing function analysis technique has been presented in Chapter 2. In Chapter 3, it has been demonstrated that a relay with a variable hysteresis can act as a nonlinearity with a specified phase shift. This can be of particular interest in pre-tuning applications since the Nyquist curve can be scanned in phase rather than in frequency. For the purpose of design of simple controllers it is of interest to know the transfer function where the phase lag is in the range of $45^o - 180^o$, while the interesting frequency range usually is unknown. In process industry many processes can be approximated by a first or second order system with a time delay. Relay feedback of such systems

have been investigated in Chapter 4–6. The mechanisms behind the oscillations are quite complicated. In Chapter 4, it was shown that relay feedback of a first order system with a time delay can exhibit a large variety of different types of limit cycles with different stability and convergence properties. The first order system includes a direct term. This can be regarded as an approximation of a second order system with one fast and one slow mode. Necessary and sufficient conditions for reaching the different types of limit cycles have been given. Relay feedback of stable as well as unstable systems can have stable limit cycle solutions. Also, peculiar behaviour with different types of stable asymmetrical limit cycles were found. Relay feedback of second order systems were analyzed in Chapter 5. It was noticed that a stable system without a zero in the transfer function had a unique limit cycle solution. However, a zero can give two limit cycle solutions, even for nice systems which are stable and minimum phase. It has also been investigated how a phase plane trajectory approaches a stable limit cycle. This analysis gives automatically an understanding both for the existence of a limit cycle solution and for the convergence mechanisms. When one eigenvalue is much larger than the other, then the convergence is extremely fast. This is in agreement with the results in Chapter 4, where relay feedback of first order systems reach the limit cycle solution directly after *one* switch. The results explain why automatic tuning with the relay method is so fast. In Chapter 6 it is shown that strange behaviour can be found by relay feedback of an unstable second order system with complex poles and with a time delay. This could lead to multi switch limit cycles and chaotic motions. The difference to other works is the introduction of the time delay, which makes it possible to construct chaos also with negative feedback. Another difference is that some of the limit cycle solutions appear to be stable.

Identification of the dissolved oxygen concentration dynamics in a biological reactor has been made in Chapter 7. A relay feedback excite the dynamics in order to get identifiability. The idea has been tried successfully in a series of full scale experiment at Malmö Sewage Works. The dynamics are described by the oxygen transfer rate, $K_L a$, and the respiration rate, R, both valuable for diagnoses and operation of the waste water treatment plant. It was found that both $K_L a$ and R will be undetermined by a bias. However, the daily variation of R can be estimated. Also, $K_L a$ can be modelled as a nonlinear function of the air flow rate. The bias of R can be measured by independent measurements. The estimation technique is therefore still a useful operational tool.

The main new results were given in Chapter 4, where different types of limit cycles were found and classified. Future research can be made on relay feedback of second order systems with a time delay. The estimation technique

described in Chapter 7 is also considered to be original and successful. A future research how to use the estimated respiration rate in other control loops is suggested. Also, the influence of the respiration rate profile along the basin would be interesting to investigate.

9

References

AMRANI, D. and D. P. ATHERTON (1989): "Designing Autonomous Relay Systems with Chaotic Motion," *Proc. 28th IEEE Conf. on Decision and Control*, Tampa (FL), pp. 512–517.

ATHERTON, D. P. (1975): *Nonlinear Control Engineering—describing function anaylysis and design*, Van Nostrand Reinhold Company Limited, Molly Millar's Lane, Workingham, Berks.

BROUZES, P. (1968): "Automated Activated Sludge Plants with Respiratory Metabolism Control," *4th Int. Conf. on Water Pollution Control Res., Prague*, Advances in Water Pollution Research (1969).

COOK, P. A. (1985): "Simple Feedback Systems With Chaotic Behaviour," *Systems and Control Letters*, **6**, 223–227.

COOK, S. and S. MARSILI-LIBELLI (1981): "Estimation and Control Problems in Activated Sludge Processes," *Water Sci. and Tech.*, **13**, 737–742.

GRAHAM, D. and D. MCRUER (1961): *Analysis of Nonlinear Control Systems*, John Wiley & Sons, Inc..

HOLMBERG, U. and G. OLSSON (1985): "Simultaneous On-line Estimation of Oxygen Transfer Rate and Respiration Rate," in A. Johnson (Ed.): *Modelling and Control of Biotechnological Processes*, Pergamon Press, Oxford, pp. 185–189.

HOLMBERG, U. (1986): "Adaptive Dissolved Oxygen Control and On-line Estimation of Oxygen Transfer and Respiration Rates," *AIChE's Annual*

Meeting, Miami Beach.

HOLMBERG, U. (1987): "Adaptive Dissolved Oxygen Control and On-line Estimation of Oxygen Transfer and Respiration Rates," Licentiate Thesis, TFRT-3189, Department of Automatic Control, Lund Institute of Technology, Lund, Sweden.

HOLMBERG, U., G. OLSSON and B. ANDERSSON (1988): "Simultaneous DO Control and Respiration Estimation," *Water Sci. and Tech.*, **21**, 1185–1195.

HOLMBERG, U. (1990): "On Identifiability of Dissolved Oxygen Concentration Dynamics," *IAWPRC's* 25^{th} *Anniversary Conference and Exhibition*, Kyoto, Japan.

HOWELL, J. A. and B. O. SOPIDO (1985): "On-line Respirometry and Estimation of Aeration Efficiences in an Activated Sludge Aeration Basin from Dissolved Oxygen Measurements," in A. Johnson (Ed.): *Modelling and Control of Biotechnological Processes*, Pergamon Press, Oxford, pp. 191–198.

KO, K. Y., B. C. MCINNIS and G. C. GOODWIN (1982): "Adaptive Control and Identification of the Dissolved Oxygen Process," *Automatica*, **18**, 727–730.

LILJA, M. (1989): "Controller Design by Frequency Domain Approximation," PhD Thesis, TFRT-1031, Department of Automatic Control, Lund Institute of Technology, Lund, Sweden.

LJUNG, L. (1987): *System Identification—Theory for the user*, Prentice-Hall, Englewood Cliffs, N. J..

LJUNG, L. (1988): *System Identification Toolbox, for use with Matlab*, The MathWorks, Inc..

MARSILI-LIBELLI (1990): "Adaptive Estimation of Bioactivities in the Activated Sludge Process," *IEE Proceedings*, **137**, Pt. D., No. 6.

OLSSON, G. and J. F. ANDREWS (1978): "The Dissolved Oxygen Profile—a Valuable Tool for Control of the Activated Sludge Process," *Water Research*, **vol. 12**, Pergamon Press Ltd, Printed in Great Britain, pp. 985–1004.

OLSSON, G (1985): "Control Strategies for the Activated Sludge Process," *Comprehensive Biotechnology*, Pergamon Press, pp. 1107–1119.

PARKER, T. and L. O. CHUA (1987): "Chaos: A Tutorial for Engineers," *Proceedings of the IEEE*, **75**, no. 8.

TSYPKIN, Y. Z. (1984): *Relay Control Systems*, Cambridge University Press, Cambridge, UK..

ÅRZÉN, K. E. (1987): "Realization of Expert System Based Feedback Control," Report TFRT-1029, Department of Automatic Control, Lund Institute of Technology, Lund, Sweden.

ÅSTRÖM, K. J. and J. ANTON (1984): "Expert Control," Report TFRT-7271, Department of Automatic Control, Lund Institute of Technology, Lund, Sweden.

ÅSTRÖM, K. J. and T. HÄGGLUND (1984a): "Automatic tuning of simple regulators with specifications on phase and amplitude margins," *Automatica*, **20**, 645–651.

ÅSTRÖM, K. J. and T. HÄGGLUND (1984b): "Automatic tuning of simple regulators," *Proceedings IFAC 9th Word Congress*, Budapest.

ÅSTRÖM, K. J. and B. WITTENMARK (1989): *Adaptive Control*, Addison-Wesley Publishing Company.

ZIEGLER, J. G. and N. B. NICHOLS (1942): "Optimum settings for automatic controllers," *Trans. ASME*, **64**, 759–768.